U.S. DEPARTMENT OF COMMERCE
National Technical Information Service

PB-246 188

A MATHEMATICAL MODEL OF ELECTROSTATIC PRECIPITATION

Southern Research Institute

Prepared for
National Environmental Research Center

April 1975

KEEP UP TO DATE

Between the time you ordered this report—which is only one of the hundreds of thousands in the NTIS information collection available to you—and the time you are reading this message, several *new* reports relevant to your interests probably have entered the collection.

Subscribe to the **Weekly Government Abstracts** series that will bring you summaries of new reports *as soon as they are received by NTIS* from the originators of the research. The WGA's are an NTIS weekly newsletter service covering the most recent research findings in 25 areas of industrial, technological, and sociological interest—invaluable information for executives and professionals who must keep up to date.

The executive and professional information service provided by NTIS in the **Weekly Government Abstracts** newsletters will give you thorough and comprehensive coverage of government-conducted or sponsored research activities. And you'll get this important information within two weeks of the time it's released by originating agencies.

WGA newsletters are computer produced and electronically photocomposed to slash the time gap between the release of a report and its availability. You can learn about technical innovations immediately—and use them in the most meaningful and productive ways possible for your organization. Please request NTIS-PR-205/PCW for more information.

The weekly newsletter series will keep you current. But *learn what you have missed in the past* by ordering a computer **NTISearch** of all the research reports in your area of interest, dating as far back as 1964, if you wish. Please request NTIS-PR-186/PCN for more information.

WRITE: Managing Editor
5285 Port Royal Road
Springfield, VA 22161

Keep Up To Date With SRIM

SRIM (Selected Research in Microfiche) provides you with regular, automatic distribution of the complete texts of NTIS research reports *only* in the subject areas you select. SRIM covers almost all Government research reports by subject area and/or the originating Federal or local government agency. You may subscribe by any category or subcategory of our WGA **(Weekly Government Abstracts)** or **Government Reports Announcements and Index** categories, or to the reports issued by a particular agency such as the Department of Defense, Federal Energy Administration, or Environmental Protection Agency. Other options that will give you greater selectivity are available on request.

The cost of SRIM service is only 45¢ domestic (60¢ foreign) for each complete microfiched report. Your SRIM service begins as soon as your order is received and processed and you will receive biweekly shipments thereafter. If you wish, your service will be backdated to furnish you microfiche of reports issued earlier.

Because of contractual arrangements with several Special Technology Groups, not all NTIS reports are distributed in the SRIM program. You will receive a notice in your microfiche shipments identifying the exceptionally priced reports not available through SRIM.

A deposit account with NTIS is required before this service can be initiated. If you have specific questions concerning this service, please call (703) 451-1558, or write NTIS, attention SRIM Product Manager.

This information product distributed by

NTIS U.S. DEPARTMENT OF COMMERCE
National Technical Information Service
5285 Port Royal Road
Springfield, Virginia 22161

304103

PB 246 188

EPA-650/2-75-037

April 1975

Environmental Protection Technology Series

A MATHEMATICAL MODEL OF ELECTROSTATIC PRECIPITATION

Reproduced by
NATIONAL TECHNICAL
INFORMATION SERVICE
US Department of Commerce
Springfield, VA. 22151

U.S. Environmental Protection Agency
Office of Research and Development
Washington, DC 20460

TECHNICAL REPORT DATA

(Please read Instructions on the reverse before completing)

1. REPORT NO. EPA-650/2-75-037	2.	3. RECIPIENT'S ACCESSION NO. PB 246 188
4. TITLE AND SUBTITLE A Mathematical Model of Electrostatic Precipitation		5. REPORT DATE April 1975
		6. PERFORMING ORGANIZATION CODE
7. AUTHOR(S) J. P. Gooch, J. R. McDonald, and S. Oglesby Jr.		8. PERFORMING ORGANIZATION REPORT NO. SORI-EAS-75-171 2887-XXVI
9. PERFORMING ORGANIZATION NAME AND ADDRESS Southern Research Institute 2000 Ninth Avenue, South Birmingham, Alabama 35205		10. PROGRAM ELEMENT NO. 1AB012; ROAP 21ADJ-026
		11. CONTRACT/GRANT NO. 68-02-0265
12. SPONSORING AGENCY NAME AND ADDRESS EPA, Office of Research and Development NERC-RTP, Control Systems Laboratory Research Triangle Park, NC 27711		13. TYPE OF REPORT AND PERIOD COVERED Final
		14. SPONSORING AGENCY CODE

15. SUPPLEMENTARY NOTES

16. ABSTRACT

The report describes a mathematical model which relates collection efficiency to electrostatic precipitator (ESP) size and operating parameters. It gives procedures for calculating particle charging rates, electric field as a function of position in wire-plate geometry, and the theoretically expected collection efficiencies for various particle sizes and ESP operating conditions. It proposes methods for empirically representing collection efficiency losses caused by non-uniform gas velocity distributions, gas bypassing the electrified regions, and particle reentrainment due to rapping of the collection electrodes. Incorporating these proposed techniques into a mathematical model of ESP performance reduces the theoretically calculated overall collection efficiencies. It compares the reduced efficiencies with those obtained from measurements on ESPs treating flue gas from coal-fired generating stations. It also presents the effects of changes in particle size distributions on calculated collection efficiencies obtained from the mathematical model.

PRICES SUBJECT TO CHANGE

17. KEY WORDS AND DOCUMENT ANALYSIS

a. DESCRIPTORS	b. IDENTIFIERS/OPEN ENDED TERMS	c. COSATI Field/Group
Air Pollution	Air Pollution Control	13B
Electrostatic Precipitation	Stationary Sources	13H
Mathematical Models		
Collection		14B
Efficiency		

18. DISTRIBUTION STATEMENT Unlimited	19. SECURITY CLASS (This Report) Unclassified	21. NO. OF PAGES 162
	20. SECURITY CLASS (This page) Unclassified	22. PRICE 6.25

EPA Form 2220-1 (9-73)

ATTENTION

AS NOTED IN THE NTIS ANNOUNCEMENT,
PORTIONS OF THIS REPORT ARE NOT LEGIBLE.
HOWEVER, IT IS THE BEST REPRODUCTION
AVAILABLE FROM THE COPY SENT TO NTIS.

EPA-650/2-75-037

A MATHEMATICAL MODEL OF ELECTROSTATIC PRECIPITATION

by

John P. Gooch, Jack R. McDonald,
and Sabert Oglesby Jr.

Southern Research Institute
2000 Ninth Avenue South
Birmingham, Alabama 35205

Contract No. 68-02-0265
ROAP No. 21ADJ-026
Program Element No. 1AB012

EPA Project Officer: Leslie E. Sparks

Control Systems Laboratory
National Environmental Research Center
Research Triangle Park, North Carolina 27711

Prepared for

U. S. ENVIRONMENTAL PROTECTION AGENCY
OFFICE OF RESEARCH AND DEVELOPMENT
WASHINGTON, D.C. 20460

April 1975

1a

EPA REVIEW NOTICE

This report has been reviewed by the National Environmental Research Center - Research Triangle Park, Office of Research and Development, EPA, and approved for publication. Approval does not signify that the contents necessarily reflect the views and policies of the Environmental Protection Agency, nor does mention of trade names or commercial products constitute endorsement or recommendation for use.

RESEARCH REPORTING SERIES

Research reports of the Office of Research and Development, U.S. Environmental Protection Agency, have been grouped into series. These broad categories were established to facilitate further development and application of environmental technology. Elimination of traditional grouping was consciously planned to foster technology transfer and maximum interface in related fields. These series are:

1. ENVIRONMENTAL HEALTH EFFECTS RESEARCH
2. ENVIRONMENTAL PROTECTION TECHNOLCGY
3. ECOLOGICAL RESEARCH
4. ENVIRONMENTAL MONITORING
5. SOCIOECONOMIC ENVIRONMENTAL STUDIES
6. SCIENTIFIC AND TECHNICAL ASSESSMENT REPORTS
9. MISCELLANEOUS

This report has been assigned to the ENVIRONMENTAL PROTECTION TECHNOLOGY series. This series describes research performed to develop and demonstrate instrumentation, equipment and methodology to repair or prevent environmental degradation from point and non-point sources of pollution. This work provides the new or improved technology required for the control and treatment of pollution sources to meet environmental quality standards.

This document is available to the public for sale through the National Technical Information Service, Springfield, Virginia 22161.

Publication No. EPA-650/2-75-037

ABSTRACT

This report describes a mathematical model which relates collection efficiency to electrostatic precipitator (ESP) size and operating parameters. It gives procedures for calculating particle charging rates, electric field as a function of position in wire-plate geometry, and the theoretically expected collection efficiencies for various particle sizes and ESP operating conditions. It proposes methods for empirically representing collection efficiency losses caused by non-uniform gas velocity distributions, gas bypassing the electrified regions, and particle reentrainment due to rapping of the collection electrodes. Incorporating these proposed techniques into a mathematical model of ESP performance reduces the theoretically calculated overall collection efficiencies. It compares the reduced efficiencies with those obtained from measurements on ESPs treating flue gas from coal-fired generating stations. It also presents the effects of changes in particle size distributions on calculated collection efficiencies obtained from the mathematical model. A procedure for estimating the program output by hand calculation is given, and a complete listing of the FORTRAN computer program is contained in an Appendix.

TABLE OF CONTENTS

Page

Abstract iii

List of Figures v

List of Tables vii

Conclusions viii

Sections

I Introduction 1

II Description of Calculations 8

III Input Data and Program Output 63

IV Results 88

V Collection of High Resistivity Dust 105

VI Estimation of Program Output 108

VII Acknowledgements 115

VIII References 116

IX Appendices 119

FIGURES

No.		Page
1	Simplified flow diagram of precipitator model computer program	6
2	Partial grid showing nomenclature used in the numerical analysis	13
3	Nomenclature used in the numerical analysis	15
4	Potential profiles in a wire plate precipitator	18
5	Current density and electric field at the plates as a function of displacement	19
6	Two dimensional physical model for developing a charging theory	26
7	Model for mathematical treatment of charging rate	28
8	Comparison of charge values for 0.18 μm diameter particle	38
9	Comparison of charge values for 0.28 μm diameter particle	39
10	Comparison of charge values for 0.56 μm diameter particle	40
11	Comparison of charge values for 0.92 μm diameter particle	41
12	"F" as a function of ideal efficiency and gas flow standard deviation	52
13	Degradation from 99.9% efficiency with sneakage	56
14	Correction factor for sneakage when $N_S=5$	57
15	Effect of reentrainment on the efficiency of a four-section precipitator designed for a no reentrainment efficiency as indicated for a monodisperse particulate	60
16	Inlet size distribution obtained from modified Brink impactor from power station burning an Eastern coal	68

FIGURES
(Continued)

17 Size data from Brink impactor measurements at inlet of precipitator collecting a low sulfur Western coal 69

18 Current density as a function of resistivity 74

19 Comparison between the voltage vs current characteristics for cold side and hot side precipitators 78

20 Voltage vs current characteristic for second field clean electrode and 1 cm layer of 1×10^{11}ohm-cm dust 79

21 Typical output information from computer model 85

22 Effective migration velocity as a function of current density and particle size 91

23 Effective migration velocities for a full-scale precipitator on a coal-fired boiler 93

24 Fractional collection efficiencies for a full-scale precipitator on a coal-fired power boiler 95

25 Computed performance curves at 5 nA/cm^2 96

26 Computed performance curves at 20 nA/cm^2 97

27 Computed performance curves at 40 nA/cm^2 98

28 Computed performance curves for "hot" precipitator 99

29 Effect of mass median diameter on computed performance 102

30 Effect of particle size distribution standard deviation on computed performance 103

TABLES

No.		Page
1	Input data and data card format	64
2	Size fractionating points of some commercial cascade impactors for unit density spheres	67
3	Input data for Figures 22 through 28	89
4	Theoretical effective migration velocities as a function of current density, temperature, and particle diameter	111
5	Example of manual calculation of overall collection efficiency	112

CONCLUSIONS

Calculation of overall collection efficiency of polydisperse particulate in an electrostatic precipitator from theoretical relationships gives results higher than those obtained from performance measurements on coal-fired power boilers. Corrections to the idealized or theoretical collection efficiency to estimate the effects of non-uniform gas flow, rapping reentrainment, and gas by-passing the electrified sections reduce the overall values of calculated efficiency to the range of values obtained from field measurements. These calculations suggest that the theoretical model may be used as a basis for quantifying performance under field conditions if sufficient data on the major non-idealities become available. The computer model in its present state of development is useful for qualitatively indicating performance trends caused by changes in specific collecting area, electrical conditions, and particle size distributions, provided that back corona does not exist. Current density, applied voltage, and the particle size distribution are the most important variables in the calculation of overall mass collection efficiency for a given specific collection area.

A MATHEMATICAL MODEL OF ELECTROSTATIC PRECIPITATION

SECTION I
INTRODUCTION

Because of the complexity of the factors which influence collection efficiency in electrostatic precipitators, it is necessary to use a high speed computer to predict precipitator performance from the applicable theoretical relationships. A computer model of electrostatic precipitation has been developed by Southern Research Institute as part of a research program sponsored by the Environmental Protection Agency with the objective of improving the understanding of the factors which influence precipitator performance. The computer model predicts particulate collection efficiency under ideal conditions as a function of the dust properties and the operating parameters and includes relationships for estimating the effect of gas velocity distribution, particle reentrainment, and gas sneakage.

In general, a comparison of the overall mass efficiency predicted from the theoretical model with measured efficiencies obtained under field conditions indicates that the theoretical projections are higher than the field measurements. Corrections to the idealized or theoretical collection efficiency to include estimated effects of the previously mentioned non-idealities reduce the theoretical values to the range obtained from field measurements. These calculations and comparisons suggest that the theoretical model may be used as a basis for quantifying performance under field conditions, if sufficient data on the major non-idealities become available.

The Southern Research Institute mathematical model uses the Deutsch equation to predict the collection fraction η_{ij} for the i-th particle size in the j-th incremental length of the precipitator. Thus, the Deutsch equation is applied in the form

$$\eta_{i,j} = 1 - e^{-w_{i,j} A_j/Q} , \qquad (1)$$

where

$w_{i,j}$ = migration velocity of the i-th particle size in the j-th increment

A_j = collection plate area in the j-th increment

Q = volumetric flow rate.

Since the Deutsch equation is based on the assumption that the migration velocity is constant over the collection area of the precipitator, it is necessary to make the incremental lengths sufficiently small so that the electric field at the plate and the charge accumulated by a given particle size remain essentially constant over the increment.

The collection fraction (fractional efficiency) η_i for a given particle size over the entire length of the precipitator is determined from

$$\eta_i = \frac{\sum_j \eta_{i,j} N_{i,j}}{N_{i,1}} = \frac{\sum_j (1-e^{-w_{i,j} A_j/Q}) N_{i,j}}{N_{i,1}}, \quad (2)$$

where $N_{i,j}$ is the number of particles of the i-th particle size per cubic meter of gas entering the j-th increment. The quantity $N_{i,j}$ can be written in the form

$$N_{i,j} = N_{i,j-1} - (1-e^{-w_{i,j-1} A_{j-1}/Q}) N_{i,j-1} = N_{i,j-1} e^{-w_{i,j-1} A_{j-1}/Q}, \quad (3)$$

where $N_{i,1} = N_{i,0}$, the number of particles of the i-th particle size per cubic meter of gas in the inlet size distribution.

The overall collection efficiency η for the entire polydisperse aerosol is obtained from

$$\eta = \sum_i \eta_i P_i , \qquad (4)$$

where P_i is the percentage by mass of the i-th particle size in the inlet size distribution.

The following list gives the major operations which are performed by the computer program in evaluating equations 2 and 4:

1) Read input data, which include the particle size distribution in the form of a histogram, applied voltage, total current, total plate area, plate to plate and wire to wire spacing, gas volume flow, precipitator length, gas temperature and pressure, average density of dust particles, corona wire radius, the standard deviation of the gas velocity distribution, the percentage reentrainment and gas sneakage per stage, the number of stages over which reentrainment and sneakage are assumed to occur, and an estimated efficiency. Those data which are dependent on a given electrical section of the precipitator are inputed in the sectionalized form.

2) Compute the number of particles in each size band of the input mass histogram.

3) Divide the precipitator into .305 meter (1 foot) length increments and compute the amount of material removed per increment from the estimated efficiency.

4) Calculate space charge due to particulate in each increment based on the estimated efficiency per increment, and calculate the reduced free ion density in each increment for use in the calculation of particle charge.

5) Compute the electric field at the plate and calculate the average charging field from the electrode spacing and applied voltage.

6) Calculate the charge on each size particle at the end of each increment of length.

7) Calculate a migration velocity for each size particle at the end of each length increment.

8) Compute the number of particles removed in each size band after each length increment of travel from the Deutsch equation.

9) Calculate the mass median diameter and the weight of the collected dust for each increment.

10) After the required calculations have been performed in all length increments, calculate an overall mass efficiency, and compare this value with the input estimated efficiency. If the difference is greater than 0.05%, the program returns to the first length increment, and repeats all calculations using the newly computed overall efficiency as the input value of efficiency. Usually, only one iteration is required.

11) After convergence on overall efficiency has been obtained, print the collection efficiency and compute the effective migration velocity for each size range. Calculate a precipitation rate parameter from the overall efficiency.

The above operations complete the calculation of theoretical or ideal performance that would be expected under a given set of input conditions. Corrections to these theoretical projections are obtained by operating on the effective migration velocities for each particle size as follows:

12) For a given value of gas velocity standard deviation, calculate a correction factor for the effective migration velocities, using the theoretical efficiency for each particle size.

13) Calculate a correction factor for the effective migration velocities, using assumed values of number of stages and the percent loss per stage from reentrainment and/or sneakage.

14) Obtain an "apparent" effective migration velocity for each particle size by dividing the theoretical values by the product of the two correction factors described above, and calculate a corrected efficiency for each particle size from the Deutsch equation.

15) Calculate a corrected overall efficiency and precipitation rate parameter.

The fundamental steps in the precipitation process are particle charging, particle collection, and the removal and disposal of the collected material. Therefore, in order to calculate the efficiency of particle collection, it is necessary to mathematically model the electric field, the particle charging process, the mechanism by which charged particles are transported to the collection electrode from the gas stream, and efficiency losses caused by reentrainment or other non-idealities.

Figure 1 gives a simplified block diagram of the precipitator model computer program. The program is structured around three major loops, the outermost of which is a direct iteration that converges on the overall mass efficiency. An initial estimate of the overall mass efficiency is required because the space charge on the particulate at any point in the precipitator is a function of the particle charge and the number and size of particles remaining in the gas. The program contains a calculation procedure which estimates the effect of particulate space charge on the average free ion density and the electric field near the collecting electrode.

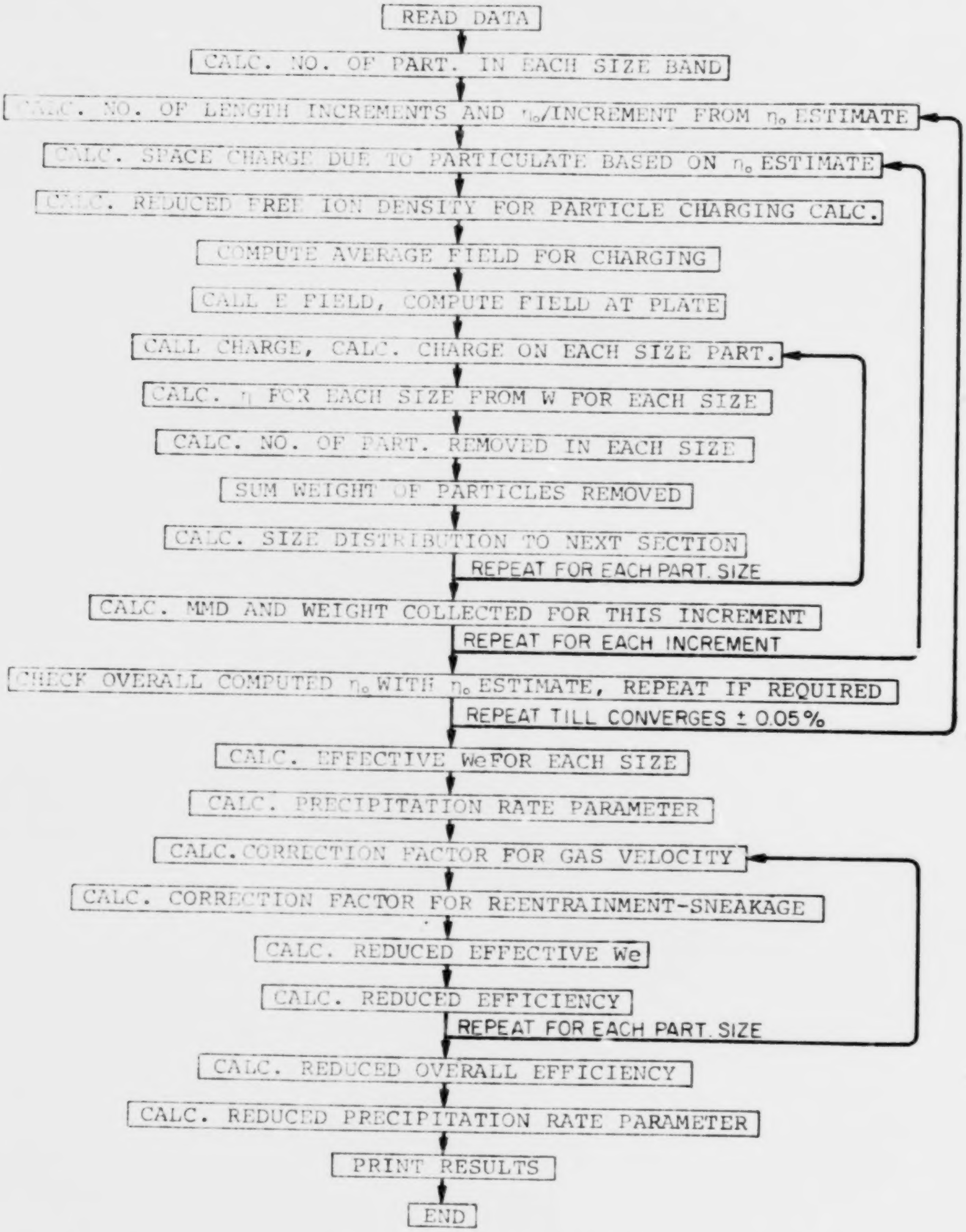
READ DATA
CALC. NO. OF PART. IN EACH SIZE BAND
CALC. NO. OF LENGTH INCREMENTS AND η_o/INCREMENT FROM η_o ESTIMATE
CALC. SPACE CHARGE DUE TO PARTICULATE BASED ON η_o ESTIMATE
CALC. REDUCED FREE ION DENSITY FOR PARTICLE CHARGING CALC.
COMPUTE AVERAGE FIELD FOR CHARGING
CALL E FIELD, COMPUTE FIELD AT PLATE
CALL CHARGE, CALC. CHARGE ON EACH SIZE PART.
CALC. η FOR EACH SIZE FROM W FOR EACH SIZE
CALC. NO. OF PART. REMOVED IN EACH SIZE
SUM WEIGHT OF PARTICLES REMOVED
CALC. SIZE DISTRIBUTION TO NEXT SECTION
REPEAT FOR EACH PART. SIZE
CALC. MMD AND WEIGHT COLLECTED FOR THIS INCREMENT
REPEAT FOR EACH INCREMENT
CHECK OVERALL COMPUTED η_o WITH η_o ESTIMATE, REPEAT IF REQUIRED
REPEAT TILL CONVERGES ± 0.05%
CALC. EFFECTIVE We FOR EACH SIZE
CALC. PRECIPITATION RATE PARAMETER
CALC. CORRECTION FACTOR FOR GAS VELOCITY
CALC. CORRECTION FACTOR FOR REENTRAINMENT-SNEAKAGE
CALC. REDUCED EFFECTIVE We
CALC. REDUCED EFFICIENCY
REPEAT FOR EACH PART. SIZE
CALC. REDUCED OVERALL EFFICIENCY
CALC. REDUCED PRECIPITATION RATE PARAMETER
PRINT RESULTS
END

Figure 1. Simplified flow diagram of precipitator model computer program

The second major loop includes the calculations which must be performed in each incremental length, and the inner-most loop contains the calculations dependent upon particle size.

The following sections present the mathematical relationships used to calculate particulate space charge, electric fields, particle charging rates, collection efficiency, and the degradation of collection efficiency caused by non-ideal effects. The calculation of particle charging rates is given in considerable detail because the charging model was developed under contract with EPA's Control Systems Laboratory and the detailed mathematical development has not been published prior to the date of this report. Input data format and a typical example of the program output are also presented, as well as a discussion of the determination of the input parameters, and examples of typical results obtained from the program. The Appendix contains a listing of the FORTRAN variables used in the program and a listing of the main program with all of the subroutines.

SECTION II
DESCRIPTION OF CALCULATIONS

ELECTRICAL CONDITIONS

Space Charge Calculations

It is well known that the introduction of a significant number of fine dust particles into an electrostatic precipitator significantly influences the voltage-current characteristics of the interelectrode space. Qualitatively, the effect is seen by an increased voltage for a given current compared to a dust-free situation. The increased voltage results from the lowered mobility of the charge carriers which occurs as the highly mobile gas ions are bound to the relatively slow dust particles, thus creating a "space charge". It is desirable to determine the space charge resulting from dust particles because this quantity influences the electric field near the collecting electrode as well as the charging dynamics. Also, the space charge is a function of location along the length of a precipitator and must be determined on an incremental basis along this length.

If we ignore the presence of free electrons, the current density at the collecting electrode results from charge transported by both ions and particulate in accordance with the relationship

$$j_T = E_0\rho_i b_i + E_0\rho_p b_p = E_0\rho_T b_e \qquad (5)$$

where

j_T = total current density, amps/m^2
E_0 = average electric field, volts/m
ρ_i = charge on ions, coul/m^3
b_i = ion mobility, m^2/(volt-sec)
ρ_p = charge on particles, coul/m^3
b_p = particle mobility, m^2/(volt-sec)
$\rho_T = \rho_i + \rho_p$
b_e = effective mobility of ions and particulate, m^2/(volt-sec) .

Thus, an effective mobility may be defined as

$$b_e = \frac{\rho_i b_i + \rho_p b_p}{\rho_T} \quad . \tag{6}$$

The values of b_e are estimated as follows. First,

$$\frac{j_p}{j_T} = \frac{E_0 \rho_p b_p}{E_0 \rho_p b_p + E_0 \rho_i b_i} = \frac{j_p}{j_p + j_i} \quad . \tag{7}$$

The quantity j_p is estimated by (a) calculating the total charge on all particulate present in the inner-electrode space in a given length increment using the saturation charge from field charging, and (b) multiplying this value of charge by an estimated removal rate for the length increment under consideration to obtain the coul/sec, or current, transported by the particulate. If it is assumed that the current density due to the particulate is only a small fraction of the total current density ($j_i >> j_p$) and that the mobility of the ion charge carriers is, on the average, 200 times that of the particulate, then

$$\frac{\rho_p b_p}{\rho_i b_i} << 1 \tag{8}$$

and

$$\frac{J_p}{J_T} = \frac{\rho_p b_p/\rho_i b_i}{\rho_p b_p/\rho_i b_i + 1} \cong \frac{\rho_p b_p}{\rho_i b_i} \cong \frac{\rho_p b_p}{\rho_i (200 b_p)} = \frac{\rho_p}{200 \rho_i} \quad . \tag{9}$$

Oglesby and Nichols[1] have shown that equation 6 can be re-arranged to yield

$$b_e = [\rho_i + \rho_p - \rho_p \; (1 - \frac{b_p}{b_i} \;)] \; \frac{b_i}{\rho_T} \quad . \tag{10}$$

Now, since we have assumed that $b_i = 200\ b_p$,

$$b_e = [\rho_i + \rho_p - \rho_p \; (1 - 0.005)] \; \frac{b_i}{\rho_T} \cong (\frac{\rho_i}{\rho_T}) \; b_i \quad . \tag{11}$$

The value b_e can therefore be estimated from a knowledge of carrier ion mobility and the ratio of ionic space charge to total space charge. The space charge ratio can be obtained by manipulation of equation 9:

$$\frac{\rho_p}{\rho_i} = 200 \; \frac{J_p}{J_T} \; ,$$

$$\frac{\rho_p}{\rho_i} + 1.0 = \frac{\rho_p + \rho_i}{\rho_i} = \frac{\rho_T}{\rho_i} = \frac{200 \; J_p}{J_T} + 1.0 \quad . \tag{12}$$

Substitution of equation (12) into equation (11) gives

$$b_e = b_i \; (\frac{J_T}{200 \; J_p + J_T}) \quad . \tag{13}$$

Although the foregoing procedure provides a basis for estimating the effect of particulate space charge, several of the assumptions are of questionable accuracy. Specifically,

- The current carried by the particulate may be significant.
- Particle mobility varies with size, and the assumption that $b_i = 200\ b_p$ on the average

may be considerably in error.

- For small particles, the saturation field charge is not an appropriate value of charge to use for estimation of the particle contribution to current.

As a result of these problem areas, additional work on developing a more accurate space charge calculation procedure is planned.

Electric Field Calculations

Since the particle migration velocity is a function of the electric field at the plate, it is necessary to calculate the electric field adjacent to the collection electrode. The method employed for this calculation is a numerical technique introduced by Leutert and Böhlen.[2] The equations which must be solved are written in discrete form in two dimensions as

$$\frac{\Delta^2 V}{\Delta x^2} + \frac{\Delta^2 V}{\Delta y^2} = -\frac{\rho}{\varepsilon_0}\text{, and} \qquad (14)$$

$$\rho^2 = \varepsilon_0 \left(\frac{\Delta V}{\Delta x}\frac{\Delta \rho}{\Delta x} + \frac{\Delta V}{\Delta y}\frac{\Delta \rho}{\Delta y}\right)\text{,} \qquad (15)$$

where ρ = space charge, coul/m^3

y = distance parallel to gas flow from wire to wire, m

x = distance perpendicular to gas flow from wire to plate, m

ε_0 = permittivity of free space, coul^2/(N-m^2).

Figure 2 shows a partial grid illustrating the nomenclature used in the numerical solution to the above equations. The initial point for which a solution is obtained is designated point "0". As the calculation progresses to neighboring points, each point in the grid becomes point "0". Using the relationships

$$\frac{\Delta V_0}{\Delta x} = \frac{1}{2a}(V_4 - V_2),\quad \frac{\Delta^2 V_0}{\Delta x^2} = \frac{1}{a}\left(\frac{V_4 - V_0}{a} - \frac{V_0 - V_2}{a}\right) \qquad (16)$$

and

$$\frac{\Delta^2 V_0}{\Delta y^2} = \frac{1}{a}\left(\frac{V_1 - V_0}{a} - \frac{V_0 - V_3}{a}\right),$$

equation 14 becomes, in terms of the grid points on figure 2,

$$V_0 = \frac{1}{4}\left(V_1 + V_2 + V_3 + V_4 + \frac{a^2 \rho_0}{\varepsilon_0}\right) \qquad (17)$$

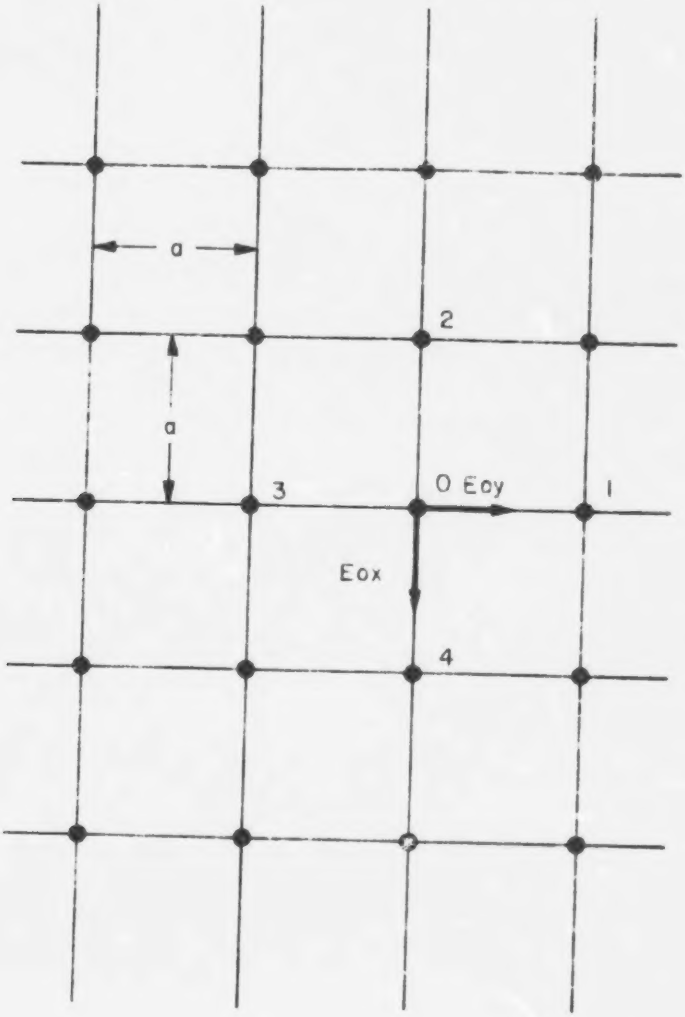
a
2
a
3
O Eoy
1
Eox
4

Figure 2. Partial grid showing nomenclature used in the numerical analysis.

From the relationships

$$-\frac{\Delta V}{\Delta x} = E_{ox}, -\frac{\Delta V}{\Delta y} = E_{oy} \quad ,$$

$\Delta\rho$ in x direction = $\rho_0 - \rho_2$,

$\Delta\rho$ in y direction = $\rho_0 - \rho_3$,

and $\Delta x = \Delta y = a$,

equation 15 may be transformed into a function of the space charge at the surrounding points and E_{ox} and E_{oy}. Solving the resulting equation for the space charge at the point "0" gives

$$\rho_0 = \frac{-\varepsilon_0}{2a}(E_{ox} + E_{oy}) - 1/2 \ [\{\frac{\varepsilon_0}{a}(E_{ox} + E_{oy})\}^2 + 4\{\frac{\varepsilon_0}{a}(E_{ox}\rho_2 + E_{oy}\rho_3)\}]^{\frac{1}{2}} . \quad (18)$$

Figure 3 shows additional nomenclature used in the numerical analysis. The boundary conditions are:

$V = V_0$ on the wire,

$V = 0$ on the plate,

$\frac{\Delta V}{\Delta x} = 0$ along line AB,

$\frac{\Delta V}{\Delta y} = 0$ along lines BC, CD, and AD, and

$\rho = j/[\frac{\Delta V}{\Delta x}\ (b)]$ near the plate.

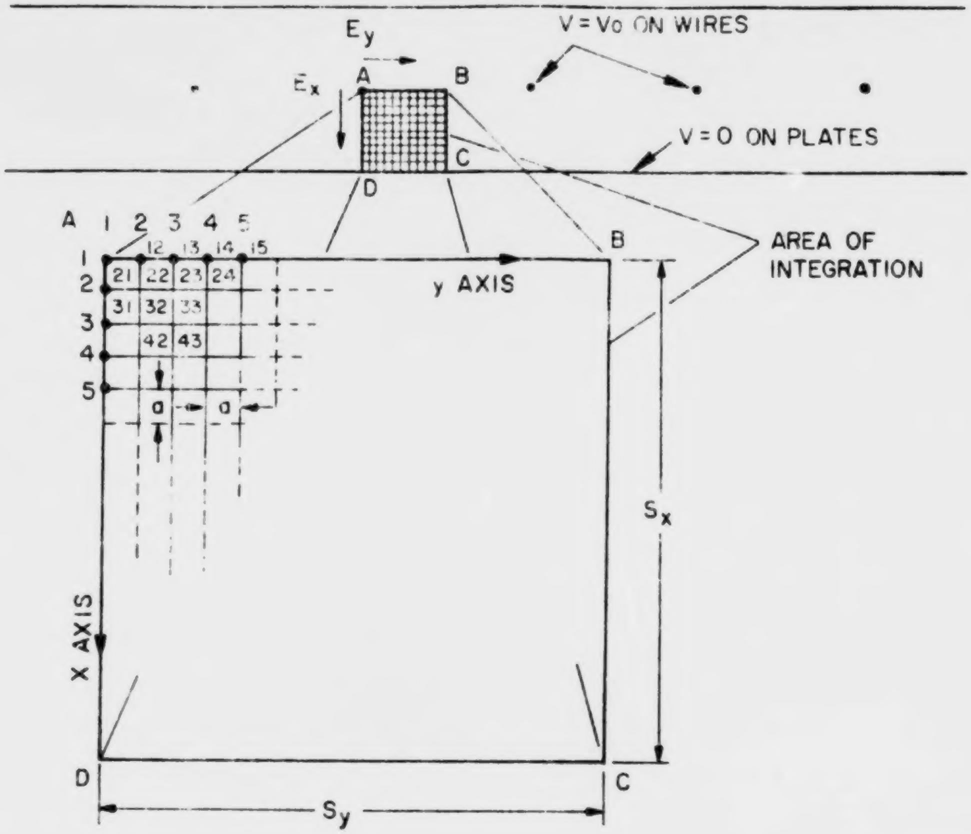
V = Vo ON WIRES
E_y
E_x
A
B
C
D
V = 0 ON PLATES
AREA OF INTEGRATION
A 1 2 3 4 5
12 13 14 15
21 22 23 24
31 32 33
42 43
1
2
3
4
5
a
a
y AXIS
X AXIS
B
S_x
D
C
S_y

S_y = ONE HALF WIRE TO WIRE SPACING
S_x = WIRE TO PLATE SPACING
a = INCREMENT SIZE FOR INTEGRATION
V_0 = APPLIED VOLTAGE
E_x = COMPONENT OF ELECTRIC FIELD PERPENDICULAR TO PLATE
E_y = LONGITUDINAL COMPONENT OF ELECTRIC FIELD
j = AVERAGE CURRENT DENSITY

Figure 3. Nomenclature used in the numerical analysis. The problem is considered two-dimensional so that edge effects and variations in E, V, and ρ parallel to the wires are ignored.

In order to begin the iteration, it is necessary to establish an initial estimate of the potential grid in the interelectrode region and to estimate a space charge for the corona region. The initial estimate of the potential grid is obtained from an expression developed by Cooperman[3] which describes the electric field for wire-plate geometry at voltages less than that required for initiation of the corona. A computer program was written which obtains a numerical solution to equations 14 and 15 by the following steps:

1. V is computed at every point in the integration grid using Cooperman's expression.
2. ρ is computed at every point in the integration grid from equation 18.
3. V is recomputed at every point in the integration grid using equation 17.
4. Steps 2) and 3) are repeated alternately until convergence occurs. Convergence on the potential grid is obtained when the value of the potential at each point in the grid is within one volt of the value calculated at that point in the previous iteration.
5. The computed current density [obtained using the relationship $j = \rho \left(\frac{\Delta V}{\Delta x}\right) b$] is compared with the measured current density. If the computed and measured current densities do not agree within .1% then the space charge representing the corona region is adjusted and steps 1) through 5) are repeated until agreement is obtained.

This procedure iterates on a grid of electric field and space charge density until convergence is obtained. The major approximation, and one that is seemingly unavoidable in practice, is the assumption that the motion of all charge carriers can, on the average, be described by a single effective mobility. The space charge introduced by the particulate present in flue gas would reduce the effective mobility. The program estimates the effect of reduced mobility by using equation 13 of Section II. However, it is necessary to limit the mobility reduction in order to prevent nonconvergence of the grid under certain conditions.

In order to check the accuracy of the calculation procedure, the computer program has been used to calculate potential profiles and electric fields based on the geometry and operating conditions for electric field measurements reported in the literature. Figure 4 shows calculations based on the geometry and operating conditions reported by Penney and Matick [illegible] and their experimental results. Reasonable agreement is found for the potential profiles from the wire to the plate and from a point midway between wires to the plate. Also, excellent agreement is found for the field near the plate (the slope of the potential curve).

Tassicker[5] performed a series of experiments to measure the field and current density at the plate in precipitators of different geometry. Figure 5 shows some of his data on a wire-plate precipitator. Corona wires were adjacent to the points x = -10 and x = +10 cm. Thus, the positions x = +5, x = -5 correspond to positions at the plate midway between the corona wires, and the position x = 0 corresponds to a position at the plate adjacent to a corona wire. The general shape and magnitude of the electric field at the plate show good agreement. Notice that, although the field is fairly uniform along the plate, there is a maximum opposite the corona wire. Since the calculated results appear to match the available data rather well, it may be concluded that Leutert and Böhlen's technique provides a basis for computing electric fields in the region of interest adjacent to the collecting electrode.

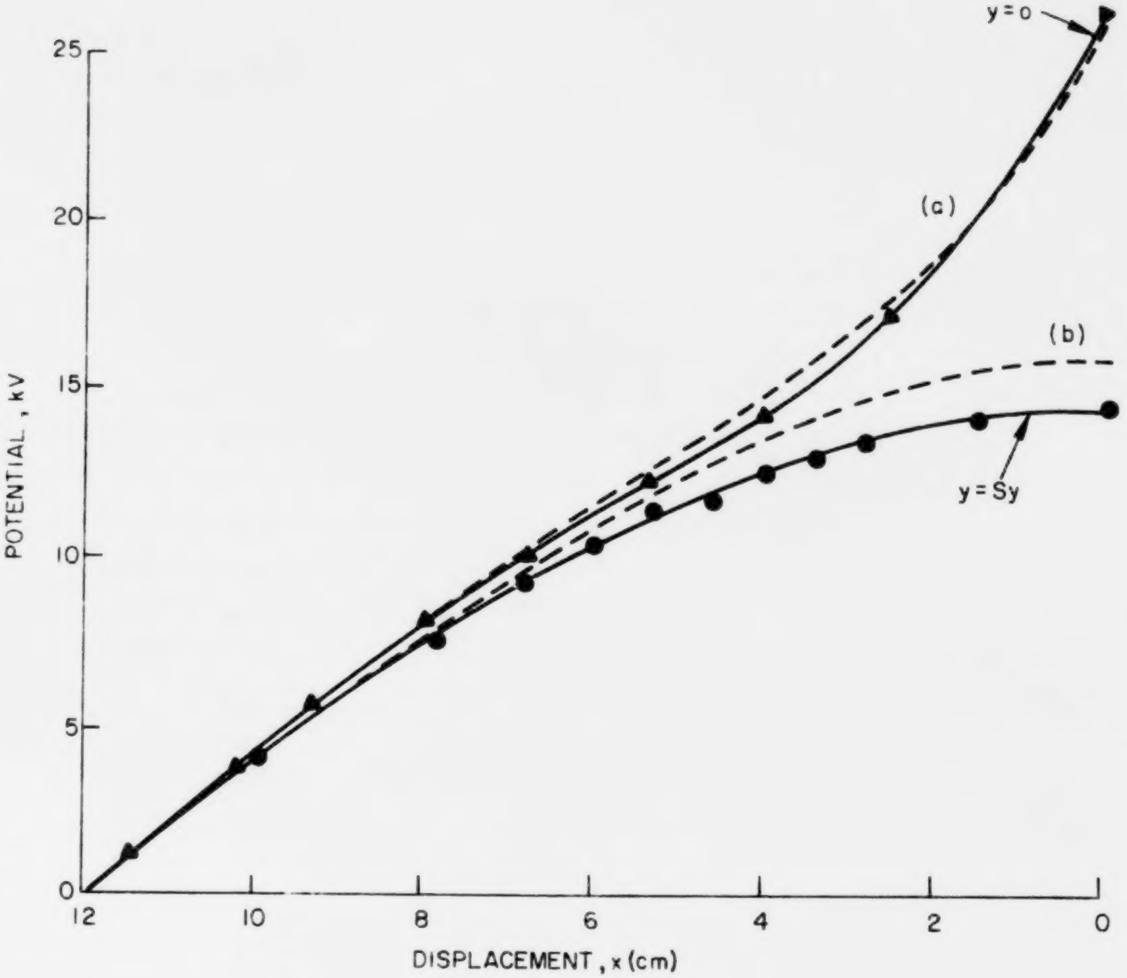

Figure 4. Potential profiles in a wire plate precipitator.

(a) x=0 corresponds to the wire, x=12 cm the plate. Solid line, Penney and Matick (experimental). Dashed line, SRI (calculated).

(b) x=0 corresponds to a point midway between wires, x=12 cm the plate. Solid line Penney and Matick (experimental). Dashed line, SRI (calculated).

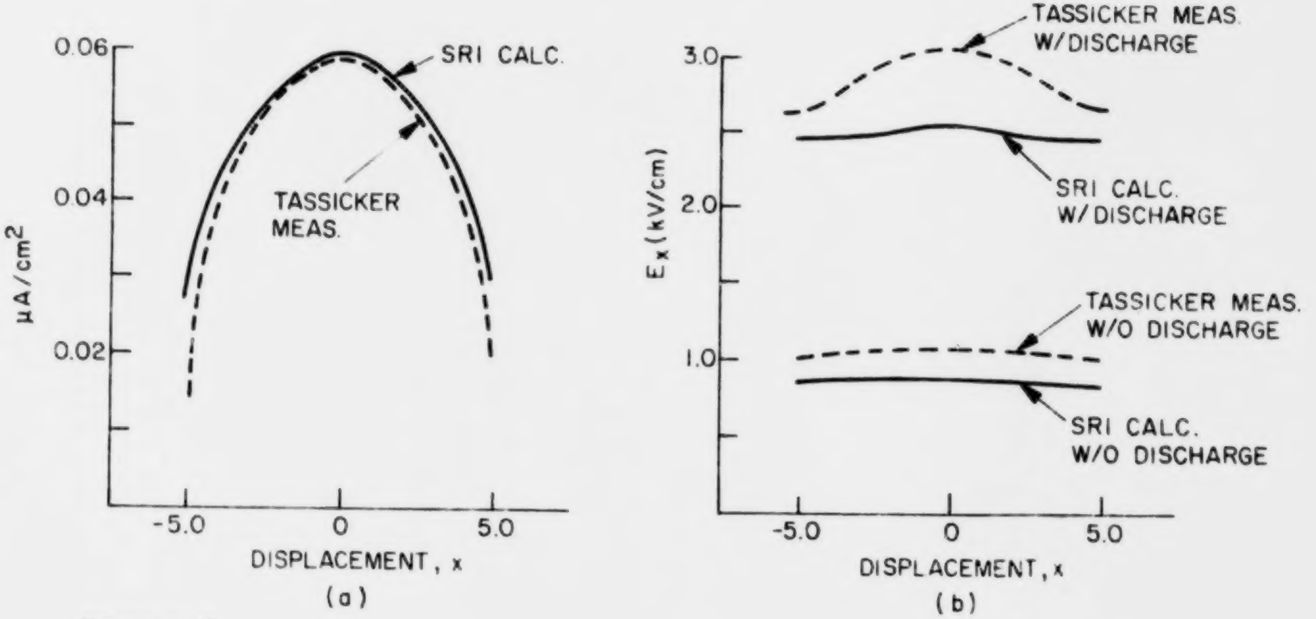

Figure 5.

(a) Current density at the plate as a function of displacement. Only the shape of the curves is significant. The peak values were matched by adjusting parameters. (Positive corona).

(b) Electric field at the plates as a function of displacement, with and without discharge. Although the shape of the field agrees fairly well, the magnitude is slightly low. A change in the effective mobility might correct this. The mobility for oxygen was used. (Positive corona).

CHARGING RATE CALCULATIONS

Particle charging in industrial electrostatic precipitators is performed by electrons and negatively charged gas ions which originate from a negative corona discharge. Although the gases present in stack gases are ordinarily good electrical insulators, processes such as naturally occurring radiation and flame ionization continuously produce a small number of ion-electron pairs in each cubic centimeter of gas. These sources of ionization provide initiating electrons for the corona process. If an electric field is applied to these gases, positive ions and free electrons will be driven by the electrical force, and the electrons, because of their greater mobility, will move at a higher velocity than the relatively sluggish positive ions. When the electric field reaches some critical value, the free electrons will acquire sufficient energy to remove a valence electron from some of the neutral gas molecules through collisions. The newly freed electrons, together with the ionizing electrons, will again accelerate and ionize other neutral gas molecules. This process, termed avalanche multiplication, will continue as long as the localized electric field exceeds the critical value for electron avalanche. Peek[6] has studied this phenomenon in detail and has derived a semi-empirical relationship that relates the field strength required for electrical breakdown to electrode geometry, temperature, and pressure.

For the case of industrial electrostatic precipitators with negative corona electrodes, the corona process will produce negative charge carriers in the region between the corona and the collecting electrodes. The electrons will flow toward the collecting electrode, and the positive ions will travel toward and strike the corona electrode. The free electrons flowing from the corona region will travel toward the collection electrode and attach to electronegative gases such as oxygen, water vapor, and sulfur dioxide. The ionized electronegative gases are the major carriers of the corona current and thus predominate in the particle charging process.

When a stable corona current has been established under typical flue gas conditions, two particle charging mechanisms are active in moving the ions to the dust particles: field charging and diffusion charging. For the purposes of this discussion, it will be assumed that, with both mechanisms, negatively charged ions are the exclusive carriers of charge in the space between the corona region immediately surrounding the discharge electrode and the collecting electrode.

The mathematical relationships describing field charging and diffusion charging have been derived in the literature and are summarized by White.[7] The charging rates predicted by the field charging equations are in good agreement with experimental data for large particles ($r > 2\ \mu m$) and moderate to high external electric fields;[8,9] and the charging rates predicted by the diffusion charging equations are in good agreement with experimental data over a fairly broad range of particle sizes where the external electric is low.[8,10] Neither the field nor the diffusion charging equations are adequate for predicting charging rates for particles with radii in the .8 μm to 2 μm region[11] when an electric field is applied.

The computer program described in this report employs two different models to account for the charging process. The program user specifies which model should be employed, based upon the specific objectives for using the program. The following is a discussion of the two particle charging models and their intended uses.

Sum of the Classical Field and Diffusional Charging Rates

The classical field charging rate [7] is given by

$$\left(\frac{dq}{dt}\right)_{\text{field}} = \frac{N_0 e b_i q_s}{4\epsilon_0} \left(1 - \frac{q}{q_s}\right)^2 \quad , \qquad (19)$$

where N_0 = undisturbed ion concentration, #/m^3
e = electronic charge, coulombs
b_i = ion mobility, m^2/(volt-sec)
ϵ_0 = permittivity constant, $coul^2/(N\text{-}m^2)$
q = instantaneous charge on the particle, coulombs
q_s = saturation charge, coulombs

The conventional saturation charge q_s does not take into account the persistence of the momentum of the ions due to the external electric field and the transient behavior of the field. Thus, a modified saturation charge q_s' is used to account for these factors. It is given by

$$q_s' = 4\pi\epsilon_0 \, (a+\lambda_m)^2 \, (1.2\ E_0) \left(1 + 2\,\frac{K-1}{K+2}\,\frac{a^3}{(a+\lambda_m)^3}\right) , \qquad (20)$$

where a = particle radius, m

λ_m = an adjustable parameter = $m\lambda$, where

λ = ion mean free path, m

m = number of mean free paths

E_0 = average charging field, volts/m

K = relative dielectric constant of the particle.

The effect of the modified saturation charge is to allow a greater charge to accumulate on the particle than the conventional saturation charge before the field charging mechanism ceases.

The classical diffusional charging rate[7] is given by

$$\left(\frac{dq}{dt}\right)_{\text{diffusion}} = N_0 e \pi a^2 \tilde{v} \exp \quad (-eV/kT) \quad , \qquad (21)$$

where $\tilde{v}$ = ion mean thermal speed, m/sec

V = potential near the surface of the charged particle, volts

k = Boltzmann's constant, joules/°K

T = absolute temperature, °K .

The potential near the surface of the charged particle is approximated by

$$V = \frac{1}{4\pi\varepsilon_0} \frac{q}{a} \quad . \qquad (22)$$

The total charging rate can be estimated by adding the rates given by equations 19 and 21. Then,

$$\frac{dq}{dt} = \left(\frac{dq}{dt}\right)_{\text{field}} + \left(\frac{dq}{dt}\right)_{\text{diffusion}} \qquad (23)$$

$$= \frac{N_0 e b_i q_s'}{4\varepsilon_0}\left(1 - \frac{q}{q_s'}\right)^2 + N_0 e \pi a^2 \bar{v} \exp\left(-eV/kT\right)$$

Equation 23 reduces to the classical diffusional equation in the absence of an applied electric field and approaches the results obtained from the classical field charging equation for large particles and high fields. The charging rates predicted are lower than those found experimentally. The disagreement is largest in the particle size range where both field and diffusional charging are important. The disagreement is due mainly to the fact that the effects of the external electric field on the diffusional charging process have been neglected.

Equation 23 is solved by summing up incremental amounts of charge Δq acquired in successive time intervals Δt, where initially $q = 0$ and $t = 0$. This procedure is straightforward and the computer program runs relatively fast when it utilizes this charging model. Thus, if the user is interested in an approximate precipitator performance or wants to examine trends under certain conditions, employment of this charging model would save significant amounts of computer time. This charging model is selected for use by the computer program when a certain indicator (NCALC) is read into the program as 1 in the input data. This indicator is the third piece of information of data card set 7 as described in the section which discusses data card format.

Southern Research Institute Model

Figure 6 shows the two dimensional physical model which is used as the basis for the theoretical development of the charging process. The particle shown in this sketch, and its environment, are considered to be representative of the average of a large number of similar systems which make up the aerosol under investigation. Because the ion concentration may only be 10 times as large as the particle concentration, and because of the screening effect of neighboring charged particles, macroscopic theories based on diffusion due to ion concentration gradients may not be applicable. The approach used in the SRI model is to apply some ideas from kinetic theory in order to calculate the charging rate in terms of the probability of collisions between ions and the particle of interest.

In this theory particle charging is largely attributed to the thermal motion of the ions and the electric field acts as a perturbation on the thermal charging process. Although in practical situations the thermal kinetic energy of the ions is always much greater than the kinetic energy gained from the external electric field, experiments show that the charging rate is greatly enhanced by the application of a field.[8] The effect of the applied electric field is to modify the ion distribution near the particle in such a way that the average ion concentration is increased. Murphy et al[12] estimated an increase in ion concentration by a factor up to 440 times as large as the normal Maxwell Boltzmann distribution would predict when the particle field and applied field are antiparallel, depending on the amplitude of the applied field. When the two fields are parallel, however, the decrease was less than a factor of 3. Thus, the changes in ion concentration do not cancel and there is a large net increase in ion concentration near the particle.

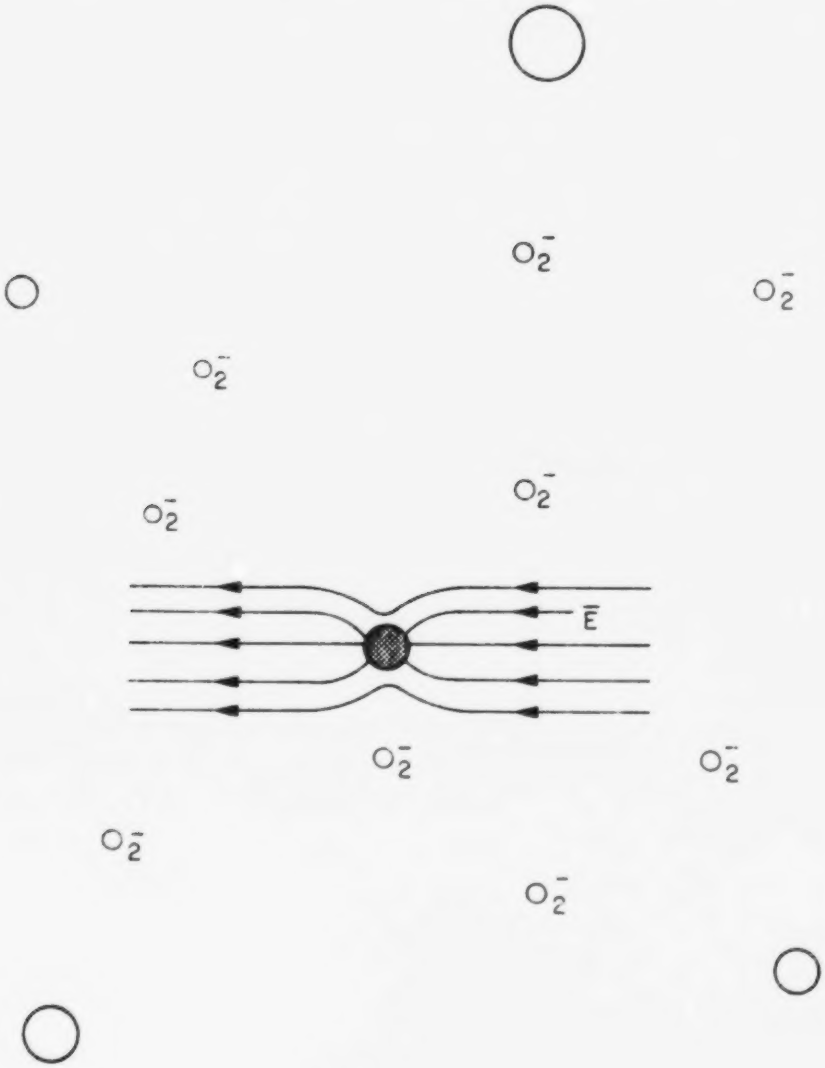
O_2^-
O_2^-
O_2^-
O_2^-
O_2^-
$\bar{E}$
O_2^-
O_2^-
O_2^-
O_2^-

Figure 6. Two dimensional physical model for developing a charging theory

Figure 7 is a simplified diagram which is used to define the nomenclature used in the theoretical development. The physical description, however, is based on the conceptual representation shown in Figure 6, where the particle of interest is surrounded by gas molecules, ions, and other charged particles. The particle is assumed to be spherical and only components of electric field due to charge on the particle and the applied field are considered. The external electric field is taken to be uniform and directed along the negative z axis. The dashed line in Figure 7 labeled r_0 corresponds to points in space where the radial component of the total electric field is equal to zero. The angle θ_0 corresponds to the azimuthal angle at which r_0 is equal to the particle radius, a. The point of intersection between r_0 and the particle surface will always lie on the hemisphere defined by $\theta_0 \leq \pi/2$. As the charge on the particle increases, θ_0 will go to zero and r_0 will exceed "a" for all angles.

If the space charge in the region outside the volume of interest is homogeneous, we can write an expression for the radial component of the electric field very near the particle as follows:[13]

$$E_r = E_0 \cos \theta \left(1 + 2 \frac{K-1}{K+2} \frac{a^3}{r^3}\right) - \frac{ne}{4\pi \varepsilon_0 r^2} , \qquad (24)$$

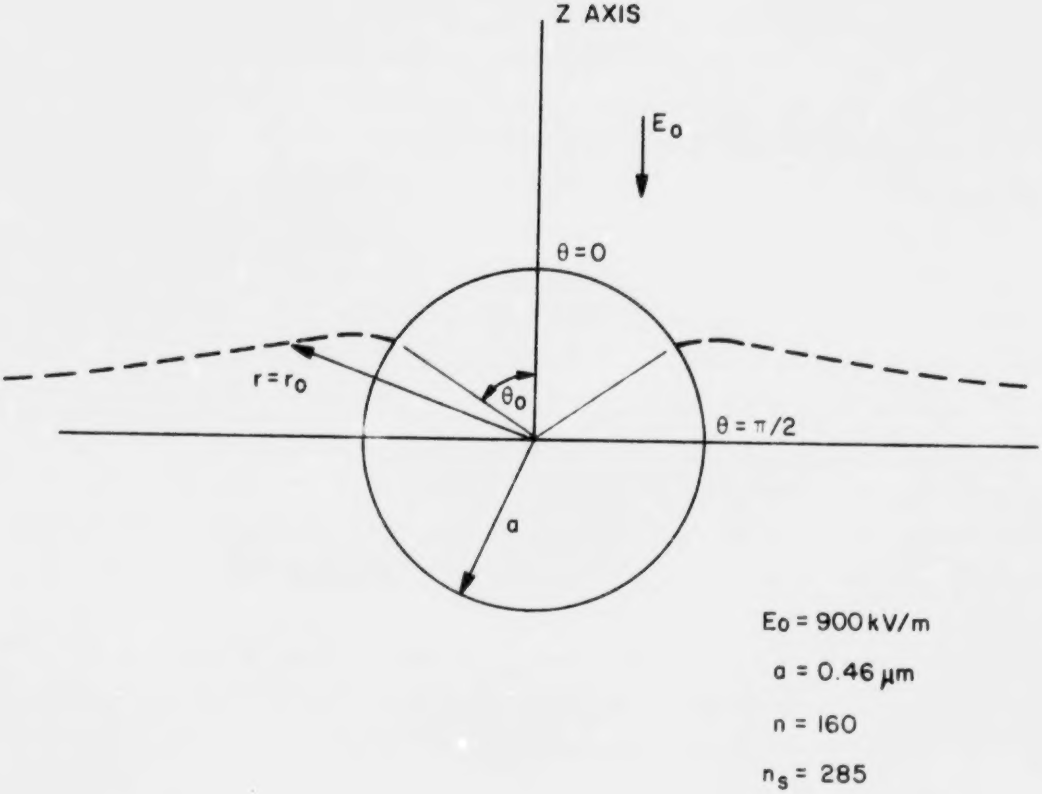
Z AXIS
E_0
$\theta = 0$
$r = r_0$
θ_0
$\theta = \pi/2$
a
$E_0 = 900$ kV/m
$a = 0.46$ μm
n = 160
$n_s = 285$

Figure 7. Model for Mathematical Treatment of Charging Rate. Along the line $r = r_0(\theta)$, the radial component of the electric field is equal to zero.

where

E_r = radial component of electric field (V/m),
E_o = external field (V/m),
K = particle dielectric constant,
a = particle radius (m),
r = radial distance to point of interest (m),
n = number of charges on particle,
e = electronic charge (1.6×10^{-19} coul.),
ε_o = the permittivity of the gas ($\sim 8.85 \times 10^{-12}$ coul^2/N-m^2), and
θ = the azimuthal angle measured from the z axis (radians).

For the purposes of discussion, we will define three areas of interest on the particle surface. One area, designated by Region I, is that bounded by $\theta = 0$ and $\theta = \theta_o$; a second region, Region II, is bounded by $\theta = \theta_o$ and $\theta = \pi/2$; and the third region of interest, Region III, is the "dark side" of the particle where $\theta > \pi/2$. Our approach to arriving at an equation for the charging rate, dq/dt, is to quantify the probability that ions can reach the particle surface in each of these three regions.

The rate at which ions reach the particle surface is

$$\frac{dn}{dt} = \frac{1}{e}\frac{dq}{dt} = P \cdot N_s(E_o, a, \theta). \tag{25}$$

P = the probability that a given ion will move towards the particle. From kinetic theory, $P = 1/4\ \tilde{v}A$, where $\tilde{v}$ is the mean thermal speed of the ions given by

$$\tilde{v} = \left(\sqrt{\frac{8kT}{\pi m}}\right) \tag{26}$$

and A is the surface area of the particle on which the ions may impinge.

$N_s(E_o,a,\theta)$ = the ion concentration near the particle surface. From classical kinetic theory, $N_s(E_o,a,\theta)$ can be related to the equilibrium ion concentration, N_o, by the expression

$$N_s(E_o,a,\theta) = N_o e^{-\Delta V(E_o,a,\theta)/kT} .$$

$\Delta V(E_o,a,\theta)$ = the energy difference between the particle surface (r=a) and some larger distance (r=r') where the equilibrium ion distribution is undisturbed.

Thus, for diffusion to the entire surface of a spherical particle, we write

$$\frac{dq}{dt} = N_o e\pi\ a^2 \tilde{v} e^{-\Delta V(E_o,a,\theta)/kT} . \tag{27}$$

Up to this point, the derivation is similar to that given by White[14] for the classical diffusional charging rate. For diffusional charging, ΔV is set equal to $ne^2/4\pi\varepsilon_o a$, the potential energy at the particle surface, and the influence of the applied field is not taken into account. (In this case, $r' = \infty$.)

Because of collisions with neutral molecules, the energy of the ions is not conserved, and hence, there is no potential energy function associated with the electric field given by equation 24. However, a minimum amount of work must be done in moving an ion from some point in space (defined by $r = r'$) to the particle surface. This minimum work is given by

$$\Delta V(E_o,a,\theta) = \int_{r'}^{a} \bar{F}\cdot\overline{dr} = \int_{r'}^{a} qE_r dr = \frac{ne^2}{4\pi\varepsilon_o r} + eE_o r \cos\theta \tag{28}$$

$$\times \left[1 - \frac{K-1}{K+2}\frac{a^3}{r^3}\right]\Bigg|_{r=r'}^{r=a} .$$

If expression (28) is used for ΔV, $N_s(E_o,a,\theta)$ becomes

$$N_s(E_o,a,\theta) = N_o \exp - \left[\left\{\frac{ne^2(r'-a)}{4\pi\varepsilon_o kTar'} + \frac{\left[3ar'^2 - r'^3(K+2) + a^3(K-1)\right]eE_o\cos\theta}{kT(r')^2(K+2)}\right\}\right] . \tag{29}$$

If θ is set equal to zero in equation (29) and the resulting equation is used for $\bar{N}_s$, equation 25 becomes identical to that given by Liu and Yeh[15] as a solution to the diffusional equation. Our approach to the solution of this differential equation for the charge as a function of time is quite different, however, and yields a smaller charging rate.

Ideally, we would like to apply equation (29) to the entire particle surface by averaging over the angle θ. To do this, it is necessary to choose some radial distance $r'(\theta)$ where the ion density is undisturbed. If we choose $r' = r_o$, the point at which the radial component of the electric field (E_r) is zero, we can only apply equation 27 in its present form to Region II, as defined in Figure 5. In Region I, $r_o < a$ and the argument of the exponential becomes positive. This can be interpreted from energy considerations to mean that any ion which is near the particle surface in Region I and moving toward the particle has a 100% probability of impacting on the particle surface. In charging Region III, no finite r_o exists. Thus, the charging rate in each region must be calculated separately and the rates added to yield the total charging rate:

$$\frac{dq}{dt} = \left(\frac{dq}{dt}\right)_{I} + \left(\frac{dq}{dt}\right)_{II} + \left(\frac{dq}{dt}\right)_{III} . \tag{30}$$

Equation 27 was developed using expressions from kinetic theory which, in turn, are based on the assumption that the system is in equilibrium. In solving equation 27 for the charge as a function of time, we will assume that the charging dynamics can be approximated by a series of steady states so that the expressions in equation (30) may be applied. Nevertheless, in reaching the ultimate expression for

$q(N_o t)$, we will consider the motion of the ions due to the applied field.

In Region I, the argument of the exponential in equation 27 becomes positive. In this case, equation 27 predicts charging rates which are too large to be approximated by steady state solutions. In fact, the charging rate is limited to the rate at which ions are brought into the system by the external field. This rate is given by the product of the current density and the surface area (A_I) of Region I:

$$\left(\frac{dq}{dt}\right)_I = \int_{A_I} \bar{j}\cdot\overline{dA}_I = b_i e N_o \int_{A_I} E_r dA_I \; . \tag{31}$$

This is identical to the charging equation developed by Pauthenier[16] which we refer to as the classical field charging equation. We may write this equation in a more conventional and useful form,

$$\left(\frac{dq}{dt}\right)_I = N_o b_i \pi n_s e(1 - \frac{n}{n_s})^2 \; , \tag{32}$$

where

$$n_s = (1 + 2\,\frac{K-1}{K+2})E_o a^2/e, \tag{33}$$

$$\theta_o = \text{arc cos } (n/n_s), \text{ and} \tag{34}$$

the other symbols have been previously defined.

When $n > n_s$, r_o is greater than "a" for all values of the angle θ, and this charging mechanism ceases ($A_I \to 0$).

In Region II charge is acquired by the particle due to ion diffusion which is enhanced by the presence of the applied electric field. In this case, equations 25 and 29 apply, and the charging rate is

$$\left(\frac{dq}{dt}\right)_{II} = \frac{e\tilde{v}\bar{N}_s A_{II}}{4} \quad , \qquad \text{where} \tag{35}$$

$\bar{N}_s$ is the magnitude of the ion density at the particle surface averaged over Region II. Explicitly,

$$\bar{N}_s = \frac{\int_0^{2\pi} \int_{\theta_o}^{\pi/2} N_s(E_o,a,\theta)\sin\theta d\theta d\phi}{\int_0^{2\pi} \int_{\theta_o}^{\pi/2} \sin\theta d\theta d\phi} \quad , \quad \text{where} \tag{36}$$

$N_s(E_o,a,\theta)$ is given by equation 29. Using this expression for $\bar{N}_s$ and writing A_{II} in terms of "a" and θ, we find

$$\left(\frac{dq}{dt}\right)_{II} = \frac{e\bar{N}_s\tilde{v}}{4}\left[\int_0^{2\pi} \int_{\theta_o}^{\pi/2} a^2\sin\theta d\theta d\phi\right] \qquad \text{or}$$

$$\left(\frac{dq}{dt}\right)_{II} = \frac{e\pi a^2 N_o\tilde{v}}{2}\int_{\theta_o}^{\pi/2} \exp\left[-\left\{\frac{ne^2(r_o-a)}{4\pi\varepsilon_o kTar_o} + \frac{[3ar_o^2-r_o^3(K+2) + a^3(K-1)]eE_o\cos\theta}{kTr_o^2(K+2)}\right\}\right]\sin\theta d\theta \quad . \tag{37}$$

For each value of the particle charge , a value of θ_o is calculated using equation (34) and the integration of equation (37) is performed. The integration is complicated by the dependence of r_o on the angle θ. Thus for each value of θ, a value of r_o must be calculated. The magnitude of r_o is found from the condition that $E_r(E_o,a,\theta) = 0$, where $E_r(E_o,a,\theta)$ is given by equation 24. We find that r_o varies by factors of 20-60, depending on a and E_o, as θ varies from 0 to $\pi/2$.

In Region III, the particle surface between the angles $\theta = \pi/2$ and $\theta = \pi$, the electric fields due to the particle charge and the external field are in the same direction and there is no radial point r_o for which the total electric field is equal to zero. In this case, equations 27 and 29 would predict that no charging could occur on this side of the particle. This is a result of our application of equilibrium thermodynamics to a dynamic problem. Physically, this means that the ions move in the direction of the electric force and are swept from the system. In reality, additional ions are swept into the system by the same electric field. As Murphy et al pointed out,[12] the change in the ion density (and hence, charging rate) near the particle surface is much greater for small values of θ than for the region $\theta > \pi/2$ when an electric field is applied. Our calculations also indicate that this is true. As an approximation, the effects of the applied field are neglected in Region III and the classical diffusional equation is used:

$$\left(\frac{dq}{dt}\right)_{III} = \frac{\pi a^2 \hat{v} e N_o}{2} \exp\left(-ne^2/4\pi\varepsilon_o akT\right) . \qquad (38)$$

In the preceding paragraphs, we have developed equations for the charging rate for each of three charging regions on the surface of the particles. The charging rate of the particle is the sum of these rates:

$$\frac{dq}{dt} = \left(\frac{dq}{dt}\right)_I + \left(\frac{dq}{dt}\right)_{II} + \left(\frac{dq}{dt}\right)_{III} \qquad \text{or}$$

$$\frac{dq}{dt} = N_o b_i \pi n_s e\left(1-\frac{n}{n_s}\right)^2 + \frac{\pi a^2 \tilde{v} N_o e}{2} \int_{\theta_o}^{\pi/2} \exp-\left[\left\{\frac{ne(r_o-a)}{4\pi\varepsilon_o kTar_o} + \frac{\left[3ar_o^2-r_o^3(K+2)+a^3(K-1)\right] eE_o \cos\theta}{kT\, r_o^2(K+2)}\right\}\right] \sin\theta d\theta$$

$$+ \frac{\pi a^2 \tilde{v} N_o e}{2} \exp(-ne^2/4\pi\varepsilon_o akT) \qquad (39)$$

Equation (39) is integrated numerically using the quartic Runge-Kutta method[17] in the following procedure:

The initial conditions are taken to be n=o at t=0.

n_s is calculated using equation (33).

For each increment in the Runge-Kutta scheme, a value of θ_o is calculated from equation (34).

The integral over θ in equation (39) is performed using Simpson's Rule, and for each value of θ which is chosen for this integration, r_o is calculated.

The three individual charging rates are calculated and then added to give the total instantaneous charging rate for a particular value of n.

The charging model described by equation (39) reduces to the classical diffusional equation in the absence of an applied electric field and approaches the results obtained from the classical field charging equation for large particles and high fields. As is discussed below, the charging rates predicted by equation (39) agree within 25% of Hewitt's data over all particle sizes, electric field strengths, and charging times. For practical charging times in electrostatic precipitators, the agreement is within 15%. The model also gives a good description of particle charging in the range of particle sizes where both field and diffusional charging are important.

Figures 8, 9, 10, and 11 give comparisons of charge values as a function of N_0t for particle sizes of 0.18, 0.28, 0.56, and 0.92 μm diameter. The calculated charge values shown were obtained with the SRI model and the sum of the field and diffusion rates model for the indicated multiples of mean free path. These comparisons indicate that λ_m has no appreciable effect on the results obtained for m values of 0, 1, and 2, with the SRI model, but considerable variation in charge with λ_m occurs with the sum of the rates model. These comparisons also demonstrate close agreement obtained between Hewitt's data and the results obtained with the SRI model.

Since the numerical method of finding the particle charge as a function of time is extensive, the program runs slowly when it utilizes this charging model. The user would want to employ this model when he needs the best charging mechanism available in order to compare with experimental results or for actual precipitator sizing where time is not a factor. This charging model is selected for use by the computer program when the indicator NCALC is read into the program as 0 in the input data.

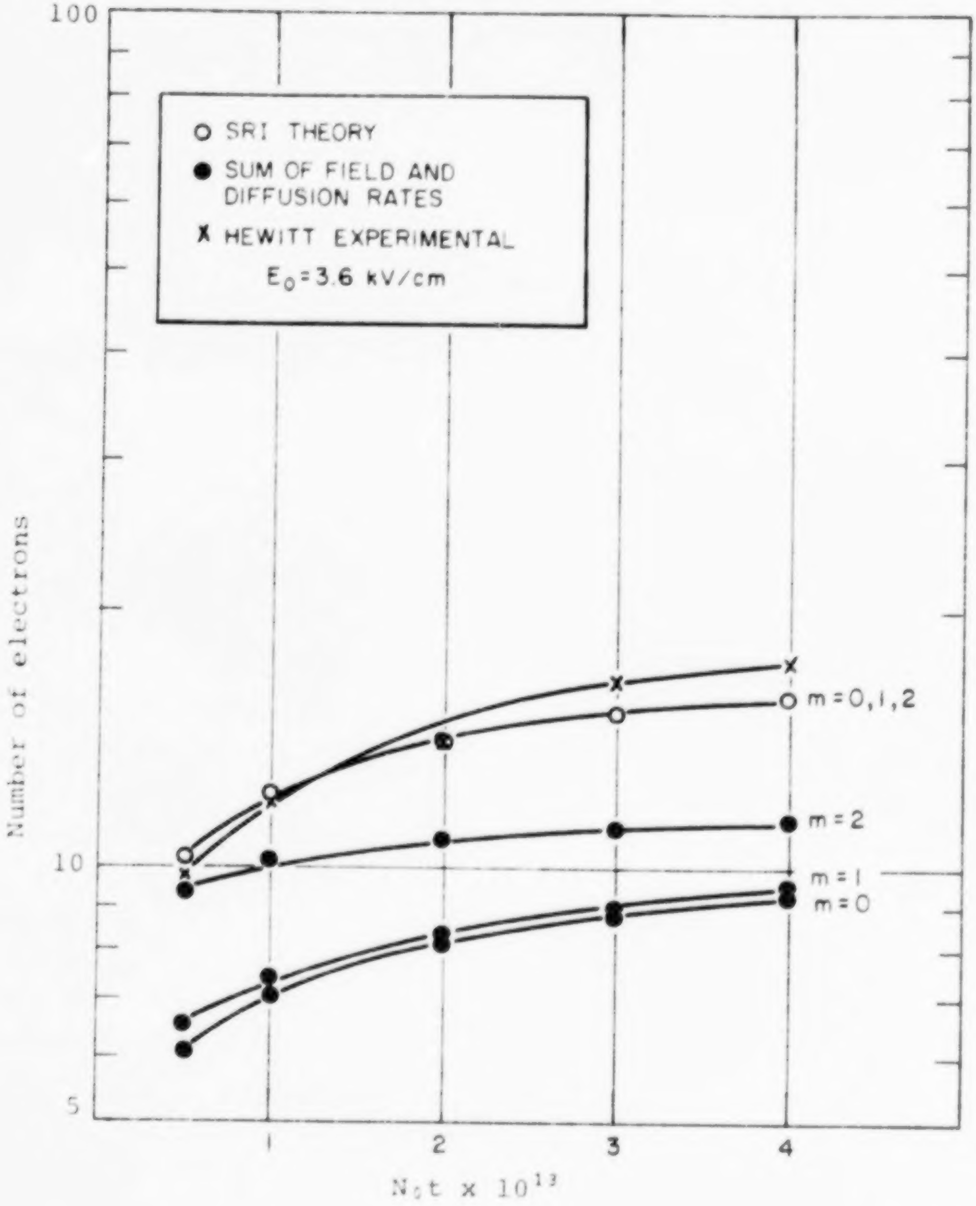

Figure 8. Comparison of charge values for 0.18 μm diameter particle

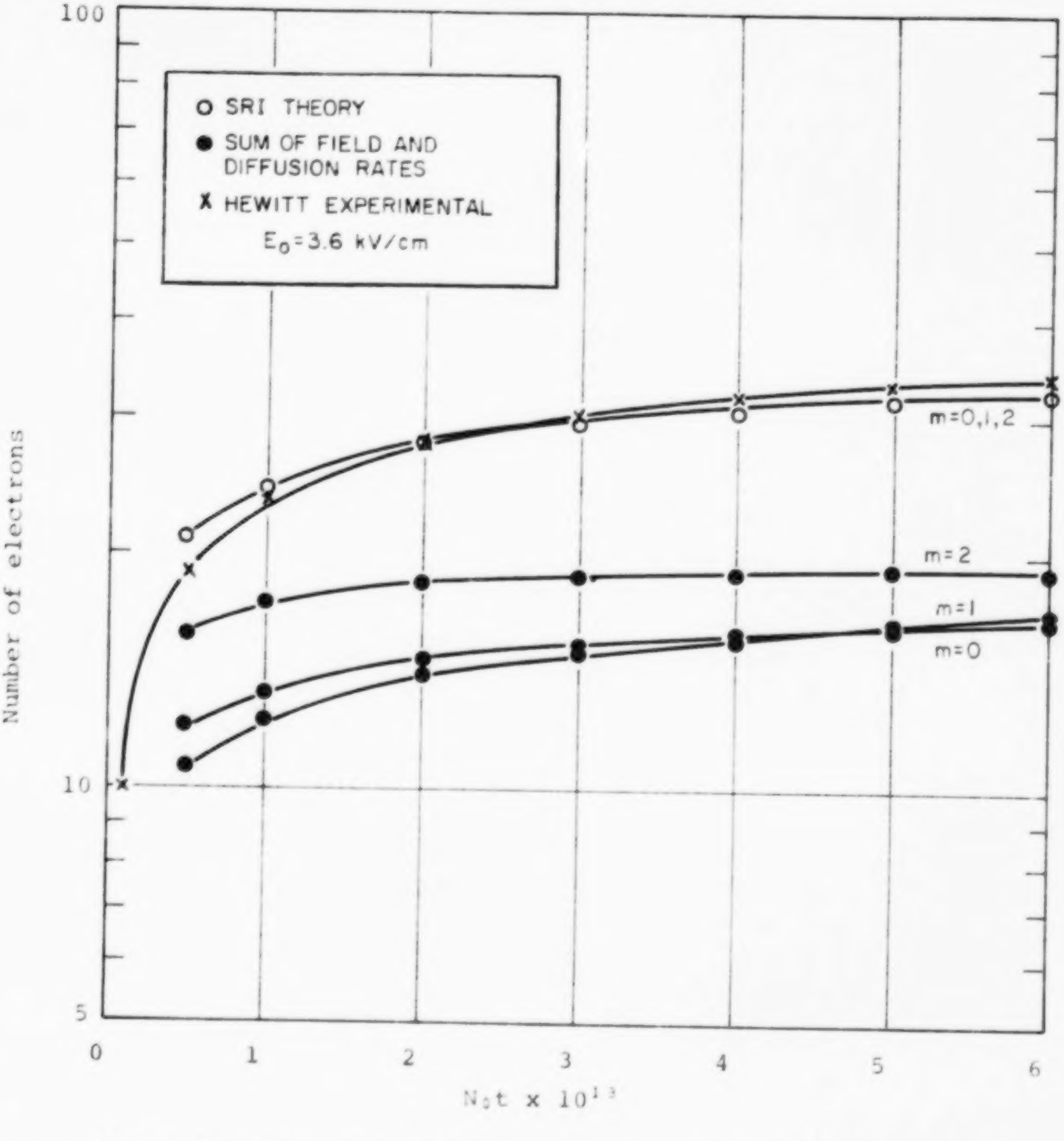

Figure 9. Comparison of charge values for 0.28 μm diameter particle

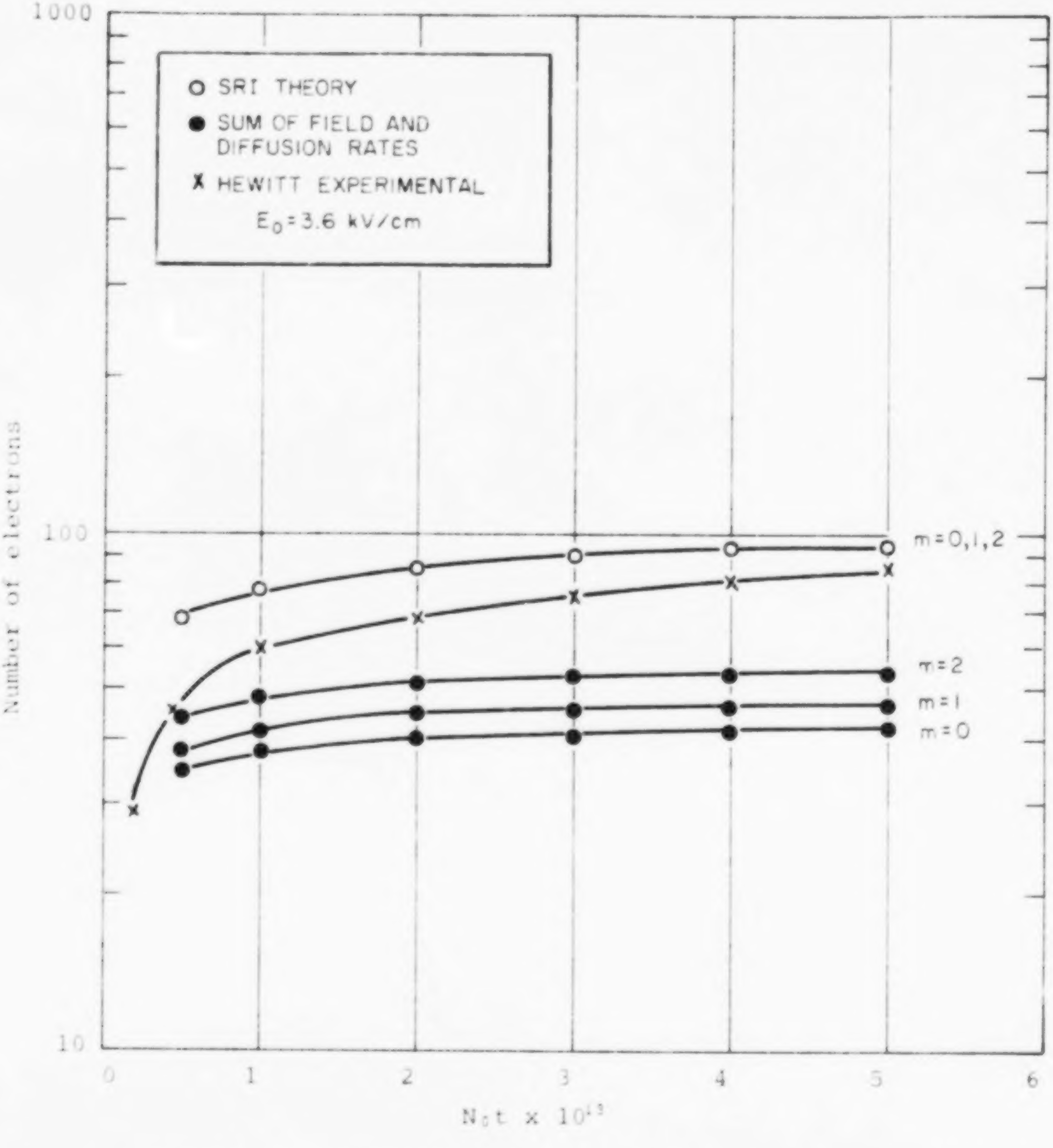

Figure 10. Comparison of charge values for 0.56 μm diameter particle

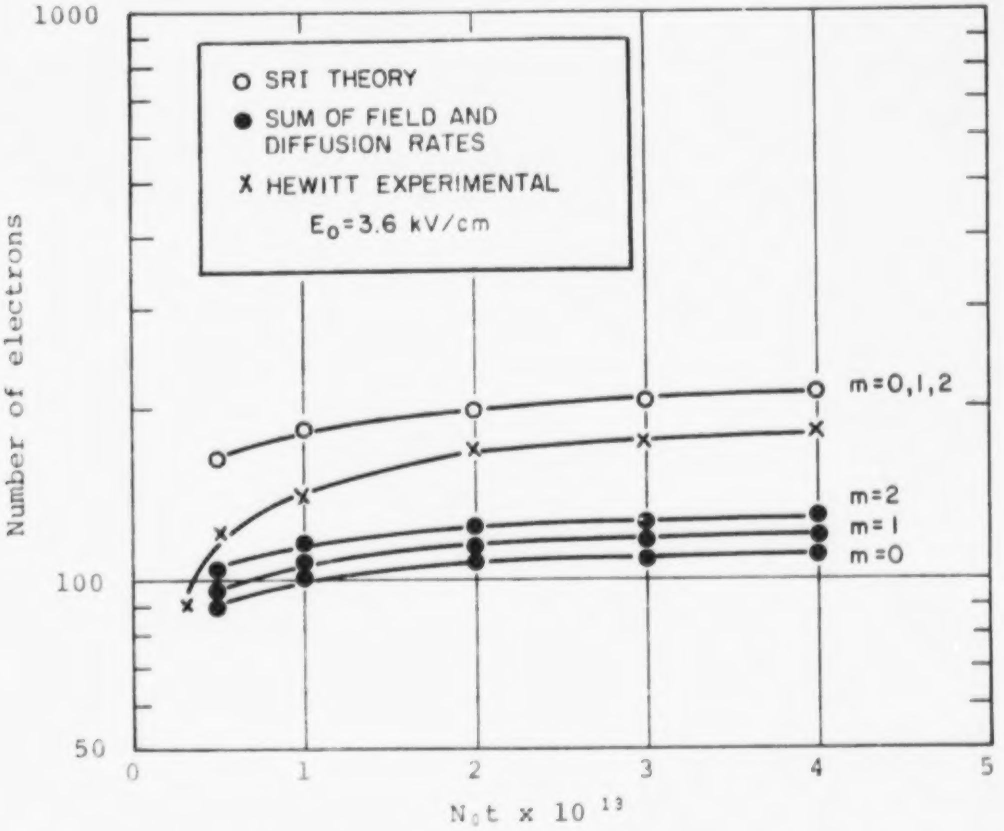

Figure 11. Comparison of charge values for 0.92 μm diameter particle

PARTICLE COLLECTION

Migration Velocity

Once the particle charge and electric field values have been computed, the next step in calculating theoretical collection efficiency is the calculation of the electrical drift velocity, or migration velocity, resulting from the coulomb and viscous drag forces acting upon a suspended particle. For particle sizes and electrical conditions of practical interest, the time required for the particle to achieve the steady-state value of velocity is negligible, and the migration velocity is given by:[18]

$$w = \frac{qE_p\,C}{6\pi a\mu}\,, \tag{40}$$

where w = migration velocity of a particle of radius a, m/sec

q = charge on particle, coul

E_p = electric field near the collection electrode, volt/m

a = particle radius, m

μ = gas viscosity, kg/m-sec

C = Cunningham correction factor, or slip correction factor[19]

$= (1 + A\lambda/a)$,

where $A = 1.257 + 0.400 \exp(-1.10\ a/\lambda)$

and λ = mean free path of gas molecules.

Particle Collection Fractions

For the idealized case of laminar flow, the collection length required for 100% collection of a particle with a known migration velocity is easily calculated. However, laminar flow never occurs in industrial precipitators, so the calculation is of academic interest only. Consideration will therefore be limited to turbulent flow conditions.

Gas flow velocities in most cases of practical interest are between 0.60 and 2.0 m/sec, while theoretical migration velocities for particles smaller than 6.0 μm are usually less than 0.30 m/sec. The path of these smaller particles therefore tends to be dominated by the turbulent motion of the gas stream in the interelectrode region. Under these conditions, the path of the particles is random, and the determination of the collection efficiency of a given particle becomes, in effect, the problem of determining the probability that a particle will enter a laminar boundary zone adjacent to the collection electrode in which capture is assured. The classical equation for describing collection of monodisperse particles in electrostatic precipitators under turbulent flow conditions was derived by Deutsch:[20]

$$\eta = 1.0 - \exp\left(-A_p w/Q\right), \tag{41}$$

where η = collection fraction of the particle size under consideration

A_p = collection area, m^2

w = migration velocity of particle of radius a, m/sec

Q = gas volume flow rate, m^3/sec.

The assumptions on which the derivation of this equation is based are:

a) Gas turbulence provides sufficient mixing to establish a uniform particle concentration at any cross section of the precipitator.

b) The gas velocity through and across the precipitator is uniform except for a boundary layer near the wall.

c) The particle migration velocity near the collecting surface is constant for all particles and small compared with the average gas velocity. This implies that the equation is strictly applicable only to a monodisperse aerosol with particle diameters less than about 6 to 10 μm, under conditions such that the migration velocity and hence the electric field at the plate and the charge accumulated on a particle do not vary over the length of collection area.

d) There are no disturbing effects, such as reentrainment, back corona, etc.[21]

In order to use equation (41) in the precipitator model and approximate assumption c) it is necessary to use the incremental length approach. White[22] reports a series of experiments using nearly monodisperse oil fumes under experimental conditions that were consistent with all of the above assumptions. The results demonstrated convincingly that equation (41) adequately describes the collection of monodisperse aerosols in an electrostatic precipitator under idealized conditions.

It has been common practice to correlate data from field electrostatic precipitators with an equation with the same functional form as equation 41:

$$\eta_0 = 1 - \exp\left(-A_p w_p / Q\right) , \tag{42}$$

where η_0 = overall mass collection fraction
w_p = an empirical parameter (precipitation rate parameter).

The parameter w_p characterizes the performance of a given precipitator under a specified set of operating conditions, and often varies widely, even among installations treating a similar flue gas. Equation 42 is inadequate for design purposes because it is a gross over-simplification in which particle size effects and variations in electrical conditions are lumped into the quantity w_p.

Program Calculations

The computer program calculates a migration velocity for each representative particle size at the end of each length increment using equation 40. Particle charge and electric field values employed in the calculation are calculated in the electric field and particle charge subroutines from the residence time and electrical conditions pertaining to the length increment under consideration. The fraction of particles collected for each representative particle size in each length increment is obtained from the Deutsch equation as follows:

$$\eta_j = 1.0 - \exp\ (-A_j w/Q)\ , \tag{43}$$

where η_j = collection fraction for length increment
A_j = collection area for length increment, m^2
Q = gas volume flow, $m^3/sec.$,

The number of particles removed in each size band is obtained from

$$X_{jc} = X_{jo} \times \eta_j\ . \tag{44}$$

where X_{jc} = the number of particles of radius a per m^3 of gas collected in a given length increment
X_{jo} = the number of particles of radius a per m^3 of gas at the beginning of each length increment.

The total number of particles collected, the mass of particles collected, and the number of particles entering the next length increment are obtained from the quantity X_{jc} and the entering size distribution. All the calculations are performed on the basis of a cubic meter of gas. After these operations have been completed for all representative particle sizes, the program calculates the mass median diameter and the total mass of the particulate collected in the length increment under consideration, and then returns to the beginning of the length increment loop to repeat the calculations for the following length increment.

When the program has completed the required calculations for all length increments, the overall mass efficiency is computed and compared with the estimated value which was used for the space charge calculations. If the disagreement is greater than

±.05%, the computed overall mass efficiency is used for a new estimate, and the program returns to the beginning of the length increment loop and repeats the calculations for the entire precipitator length. Usually, less than three iterations are required to obtain agreement within the specified limits.

The next operation performed by the program, after convergence on the overall mass efficiency has been obtained, is the calculation of effective or length averaged migration velocities for the different particle sizes from the Deutsch equation:

$$w_e = \frac{Q}{A_T} \ln \left(\frac{1}{1-\eta}\right) \quad , \tag{45}$$

where w_e = effective migration velocity of particle of radius a, m/sec

A_T = total collecting area

η = collection fraction for given particle size over total length.

The values obtained for w_e in this manner are in effect an average of the values of w obtained in the incremental length sections. A precipitation rate parameter, w_p, is computed by the program from equation 42 after the individual efficiencies and effective migration velocities have been obtained for all particle sizes.

The calculation procedure described here in effect consists of assuming that the Deutsch equation adequately describes the mechanism by which monodisperse particles are transported to the collection electrode. For particles larger than 10 μm diameter, the assumption is invalid because the motion of these particles is not dominated by turbulence due to their relatively high migration velocities. Under these conditions, the Deutsch model would be expected to under-predict efficiencies. The practical effect in modelling precipitator performance will be slight, however, since even the Deutsch equation predicts ideal collection efficiencies greater than 99.6% for 10.0 μm diameter particles at relatively low values of current density and collection area [i.e., a current density of 10×10^{-9} amps/cm^2 and a collection area to volume flow ratio of 39.4 m^2/(m^3/sec) or 200 ft^2/(1000 ft^3/min)].

A more serious objection to the assumption of uniform turbulent mixing of the particulate may be found in experimental measurements obtained with a laser obscurometer which suggest that, under certain conditions, a concentration of the fine fraction of the particulate occurs in the space adjacent to the collection electrode.[23] The causes for such a gradient and its effect on predicted collection rates have not been determined as of the date of this report.

METHODS FOR REPRESENTING NON-IDEAL EFFECTS

In the preceding sections, a basis for calculating theoretical collection efficiencies has been described. This section will discuss the non-idealities which exist in full-scale electrostatic precipitators and describe calculation procedures for estimating the effects on predicted collection efficiencies. The factors of major importance are:

(1) Gas velocity distribution
(2) Gas sneakage
(3) Rapping reentrainment.

These non-idealities will reduce the collection efficiency that may be achieved for a precipitator operating with a given specific collecting area. Since the model is structured around the Deutsch equation for individual particle sizes, it is convenient to represent the effect of the non-idealities in the model as correction factors which apply to the exponential argument of the Deutsch equation. In the subsequent discussions, these correction factors will be used as divisors for the theoretical migration velocities. The resulting "apparent" migration velocities are empirical quantities only and should not be thought of as an actual reduction in the migration velocity in the region of space adjacent to the collecting electrode.

Effect of Gas Velocity Distribution

Although it is widely known that a poor velocity distribution gives a lower than anticipated efficiency, it is difficult to apply a numerical description for gas flow quality. White[24] discusses non-uniform gas flow and suggests corrective actions. Prezler and Lajos[25] assign a figure-of-merit based upon the relative kinetic energy of the actual velocity distribution compared to the kinetic energy of a uniform velocity. This figure of merit will be a measure of how difficult it may be to rectify the velocity distribution but not necessarily a measure of how much the precipitator performance would be degraded. The following discussion will describe an approach to the calculation of degradation of performance based upon the velocity distribution, the theoretical or ideal efficiency, and the Deutsch equation.

It will be assumed that the Deutsch equation as written applies to each particle size with a known migration velocity, w, and that the specific collection area and size of precipitator are fixed.

Given:

$$\eta = 1 - e^{-\frac{A_p w}{Q}} \quad .$$

It can be seen that

$$1 - \eta = e^{-\frac{A_p}{A_1} \frac{w}{u_a}} , \qquad (46)$$

and

$$\ln \left(\frac{1}{1-\eta}\right) = \frac{A_p}{A_1} \frac{w}{u_a} = \frac{k}{u_a} \quad , \qquad (47)$$

where

A_p = plate area
A_1 = inlet cross sectional area
Q = inlet volume flow rate
w = migration velocity for a given particle size
u_a = average inlet velocity
$k = \frac{A_p w}{A_1}$
η = ideal collection fraction .

From this form of the Deutsch equation it can be seen that the logarithm of the inverse of the penetration is proportional to the inverse of the velocity (and thus the transit time). The precipitator can now be divided into a number of imaginery channels corresponding to pitot traverse points. Using the altered form of the Deutsch equation, the losses for all the channels can be summed and averaged to obtain the mean loss in the precipitator using an actual velocity distribution instead of an assumed uniform distribution. This can be accomplished as follows:

(1) Calculate constant k from the efficiency predicted under ideal conditions:

$$k = u_a \ln \frac{1}{1-\eta}$$

(2) Calculate the mean penetration:

$$p = \frac{1}{Nu_a} \sum_{i=1}^{N} u_i(1-\eta_i) , \qquad (48)$$

or

$$p = \frac{1}{Nu_a} \sum_{i=1}^{N} u_i e^{-\frac{k}{u_i}} , \qquad (49)$$

where

N = number of points for velocity traverse

u_i = point values of velocity

η_i = point values of collection fraction for the particle size under consideration.

Note that the average penetration is a weighted average to include the effect of higher velocities carrying more particles per unit time than lower velocities.

For any practical velocity distribution and efficiency, the mean penetration obtained by summation over the velocity traverse will be higher than the calculated penetration based on an average velocity. If an apparent migration velocity for a given particle size is computed based upon the mean penetration and the Deutsch equation, the result will be a value lower than the value used for calculation of the single point values of penetration. The ratio of the original migration velocity to the reduced "apparent" migration velocity is a numerical measure of the performance degradation caused by a non-uniform velocity distribution. An expression for this ratio may be obtained by setting the penetration based on the average velocity equal to the corrected penetration obtained from a summation of the point values of penetration, and solving for the required correction factor, which will be a divisor for the migration velocity.

The correction factor "F" may be obtained from:

$$\exp\left(-\frac{k}{F}\cdot\frac{1}{u_a}\right) = \frac{1}{Nu_a}\sum_{i=1}^{N} u_i \exp(-k/u_i) = p \ . \qquad (50)$$

Therefore,

$$F = -\frac{k}{u_a(\ln p)} \ . \qquad (51)$$

Whether the quantity F correlates reasonably well with statistical measures of velocity non-uniformity is yet to be established. A limited number of traverse calculations seem to indicate a correlation between the factor F and the normalized standard deviation of the velocity traverse. Figure 12 shows F as a function of the ideal efficiency for several values of gas velocity standard deviation. These curves were obtained by computer evaluation of equation 51, and the data on which the calculations are based were obtained from Preszler and Lajos.[25] The standard deviations have

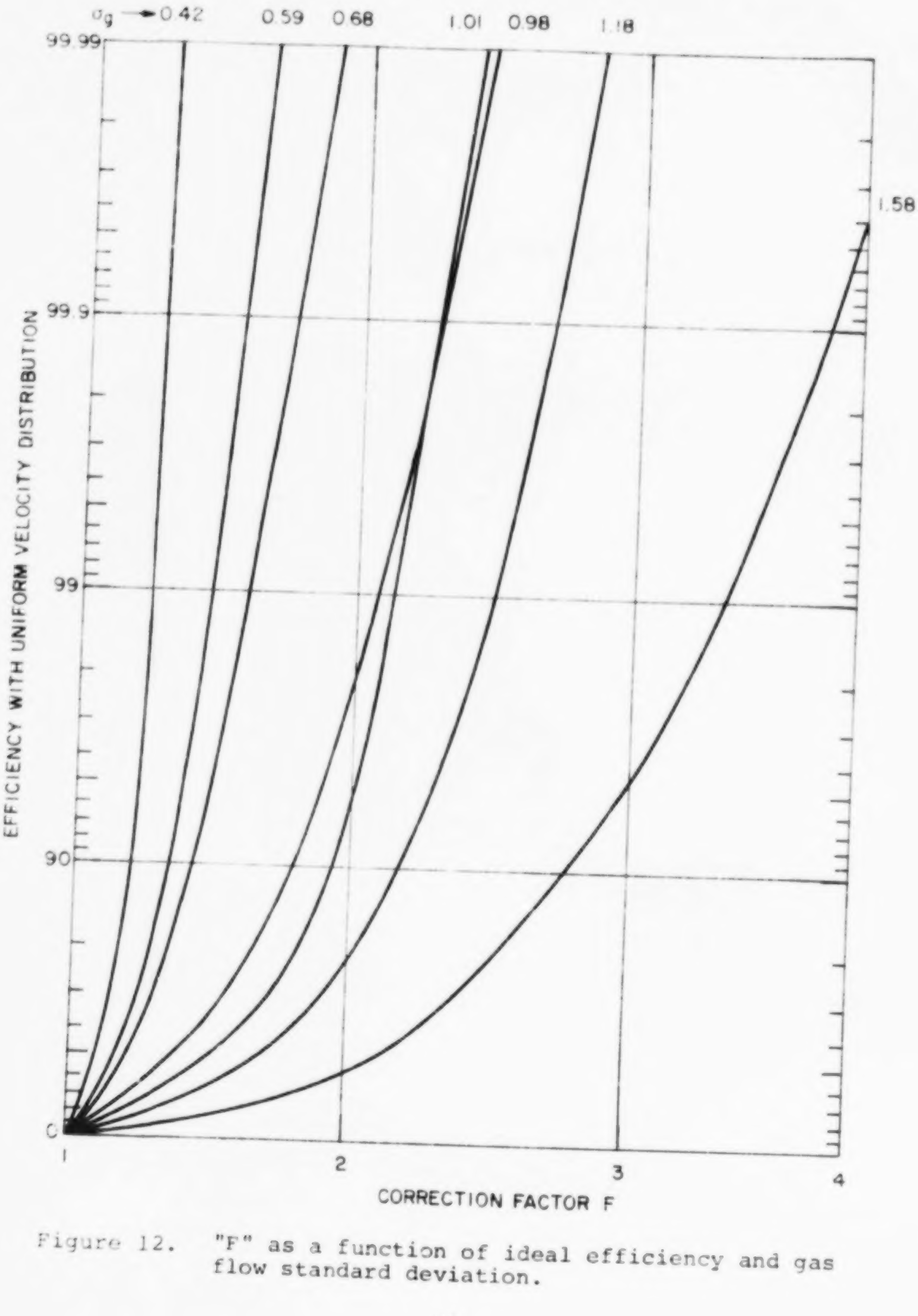

Figure 12. "F" as a function of ideal efficiency and gas flow standard deviation.

been normalized to represent a fraction of the mean. The overlapping of the curves for standard deviations of 1.01 and 0.98 indicates that the standard deviation alone does not completely determine the relationship between F and collection efficiency.

The data in Figure 12 were used to obtain the following empirical relationship between F, the normalized standard deviation of the gas velocity distribution, and the ideal collection predicted for the particle size under consideration:

$$F = 1 + 0.766\ \eta\sigma_g^{1.786} + 0.0755\ \sigma_g \ln\left(\frac{1}{1-\eta}\right) \quad , \tag{52}$$

where

$$\sigma_g = \frac{\sqrt{\frac{1}{N}\sum_{i=1}^{N}(u_a-u_i)^2}}{u_a} \quad . \tag{53}$$

This relationship is based on a pilot plant study, and should be regarded as an estimating technique only. If it is desirable to simulate the performance of a particular precipitator, the preferred procedure would be to obtain the relationship between F, η and σ_g for the conditions to be simulated from a velocity traverse at the entrance to the unit.

Equation 52 is included in the computer program following the theoretical calculations. The program evaluates F from the ideal collection predicted for each particle size and the value of σ_g chosen for the input data. The quantity F is used in combination with an empirical representation of reentrainment and sneakage as described in the following section.

Effect of Gas By-Passage

Gas sneakage occurs when gas by-passes the electrified areas of an electrostatic precipitator by flowing through the hoppers or through the high voltage insulation space. Sneakage is reduced by frequent baffles which force the gas to return to the main gas passages between the collection plates. If there were no baffles, the percent sneakage would establish the minimum possible penetration because it would be the percent volume having zero collection efficiency. With baffles, the sneakage re-mixes with part of the main flow and then re-by-passes in the next unbaffled area. The limiting penetration due to sneakage will therefore depend on the amount of sneakage gas per section, the degree of re-mixing, and the number of sections.

If we make the simplifying assumption that perfect mixing occurs following each baffled section, an expression for the effect of gas sneakage may be derived as follows:

Let S = fractional amount of gas sneakage per section
η = collection fraction of a given size particle obtained with no sneakage for total collection area
η_j = collection fraction per section of a given particle size = $1 - (1 - \eta)^{1/N_s}$
N_s = number of baffled sections
p_j = penetration from section j.

Then the penetration from section one is given by:

$$p_1 = S + (1 - \eta_j)(1 - S) \quad , \tag{54}$$

and from section 2

$$\begin{aligned} p_2 &= Sp_1 + (1 - \eta_j)(1 - S)p_1 \\ &= p_1[S + (1 - \eta_j)(1 - S)] \\ &= [S + (1 - \eta_j)(1 - S)]^2 \quad , \end{aligned} \tag{55}$$

and from section N_s (the last section),

$$P_{N_s} = [S + (1 - \eta_j)(1 - S)]^{N_s}$$
$$= [S + (1 - S)(1 - \eta)^{1/N_s}]^{N_s} \quad . \qquad (56)$$

Figure 13 shows a plot of the degradation of efficiency from 99.9% design efficiency versus percent sneakage with number of baffled sections as a parameter. For high efficiencies, the number of baffled sections should be at least four and the amount of sneakage should be held to a low percentage. With a high percentage of sneakage, even a large number of baffled sections fails to help significantly. As the next section will indicate, this graph can also be applied to reentrainment.

We can define a by-pass or sneakage factor, B, analogous to the gas flow quality factor, in the form of a divisor for the migration velocity in the exponential argument of the Deutsch equation:

$$B = \frac{\ln (1 - \eta)}{N_s \ln [S + (1-S)(1-\eta)^{1/N_s}]} \quad . \qquad (57)$$

Figure 14 shows a plot of the factor versus sneakage for a family of ideal efficiency curves for five baffled sections. Similar curves can easily be constructed for different numbers of sections.

The foregoing estimation of the effects of sneakage is a simplification in that the sneakage gas passing the baffles will not necessarily mix perfectly with the main gas flow, and the flow pattern of the gas in the by-passage zone will not be uniform and constant. The formula is derived to help in designing and analyzing precipitators by establishing the order of magnitude of the problem. Considerable experimental data will be required to confirm the theory and establish numerical values of actual sneakage rates.

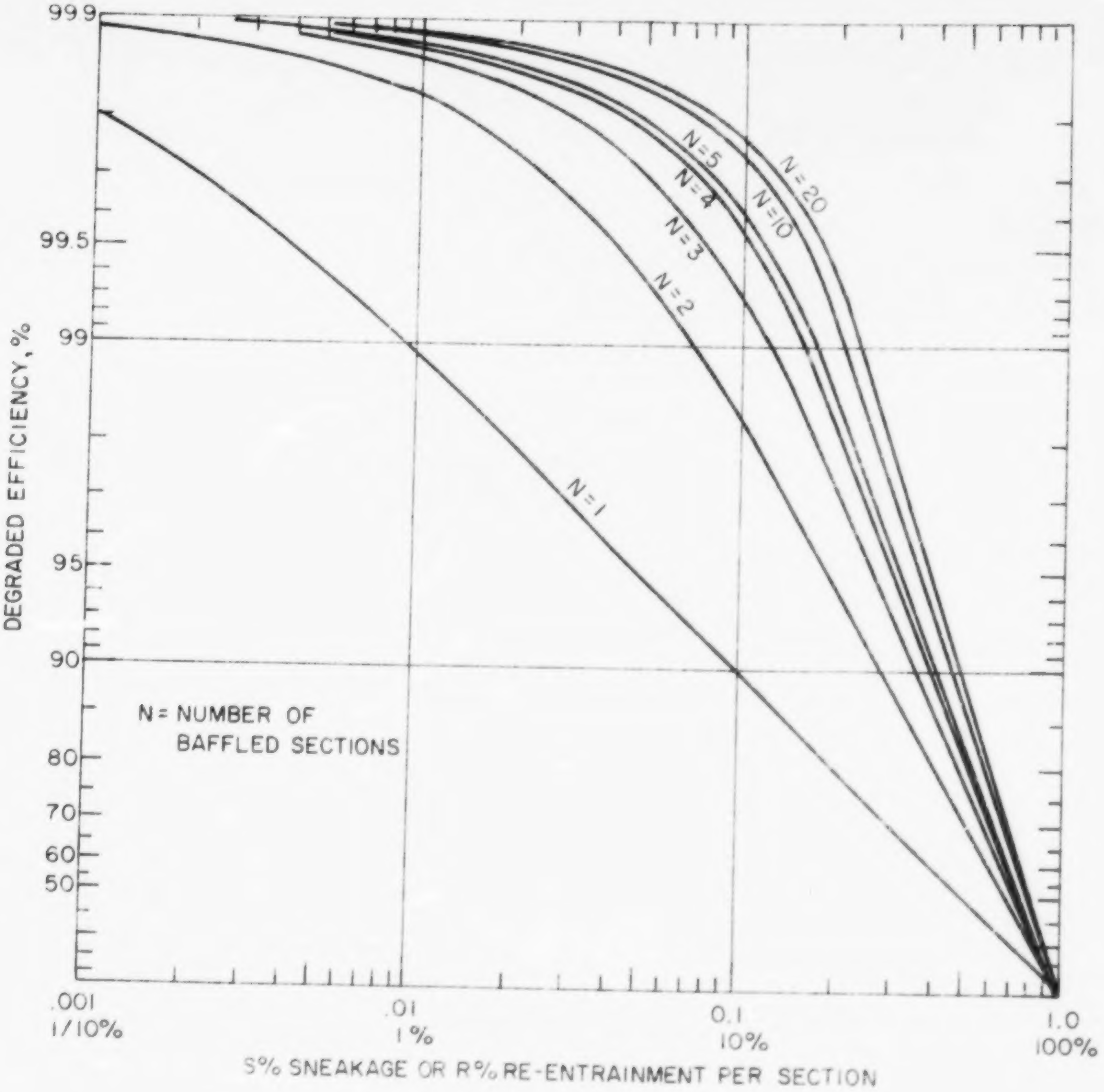

Figure 13. Degradation from 99.9% efficiency with sneakage.

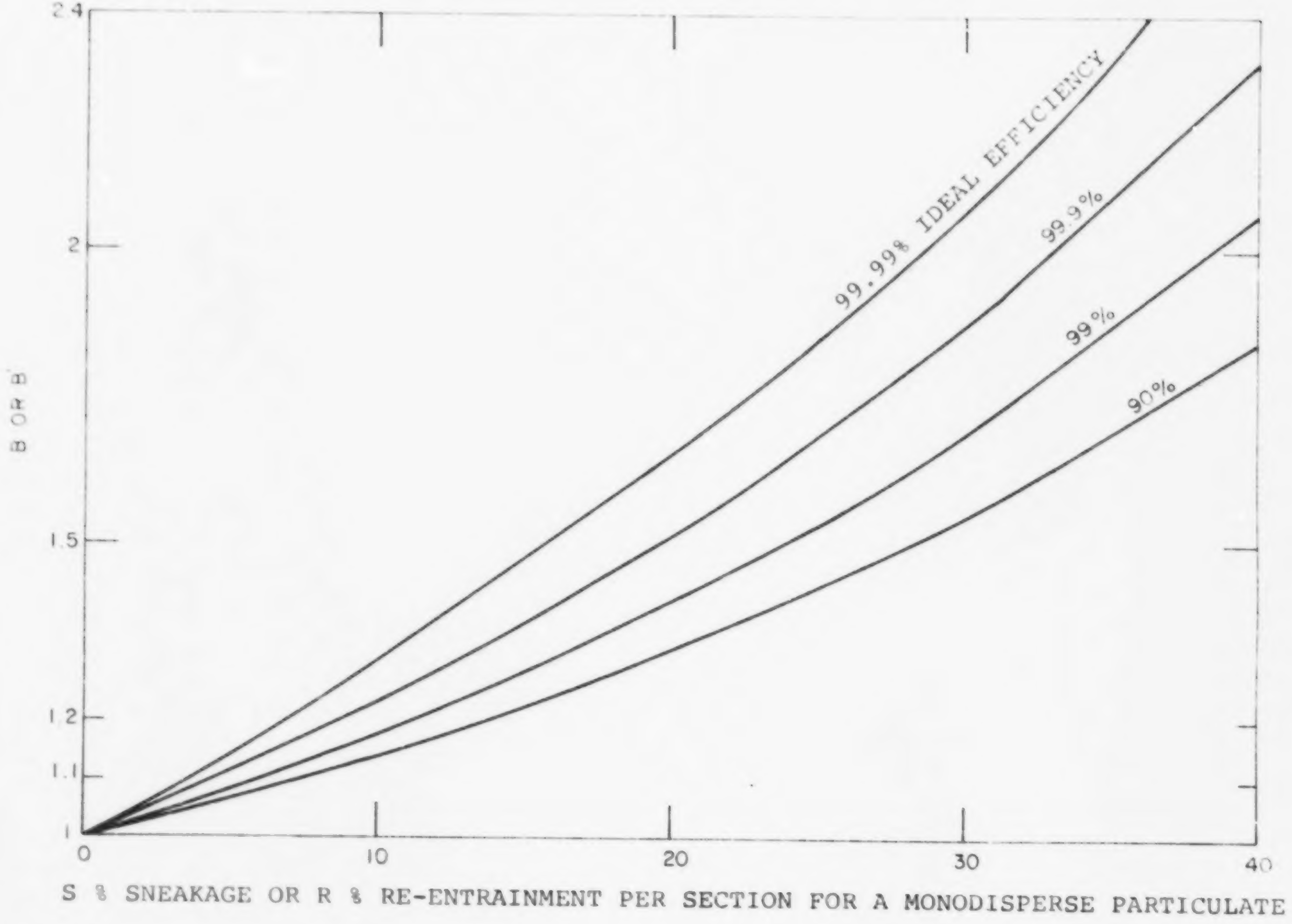

Figure 14. Correction factor for gas sneakage when Ns=5.

Effect of Rapping Reentrainment

Rapping reentrainment is defined as the amount of material that is recaptured by the gas stream after being knocked from the collection plates by rapping or vibration. With perfect rapping, the sheet of collected material would not reentrain, but would migrate down the collection plate in a stick-slip mode, sticking by the electrical holding forces and slipping when released by the rapping forces. However, the rapping forces are necessarily large to overcome adhesion forces, and much of the material is released into the gas stream as sheets, agglomerates, and individual particles. Most of the material is recharged and recollected at a later stage in the precipitator.

We will make the simplifying assumptions that (1) the fraction of material reentrained does not vary with particle size or position, (2) the reentrained material is perfectly mixed in the gas stream following rapping.

Let R = fraction of mass of a given particle size that is reentrained
η = collection fraction of a given particle size obtained with no reentrainment for total collection area
η_j = collection fraction per section of a given particle size = $1 - (1-\eta)^{1/N_R}$
N_R = number of stages over which the reentrainment is assumed to occur
p_j = penetration from section j.

Then the penetration from section 1 is given by

$$p_1 = R\eta_j + 1-\eta_j \quad , \tag{58}$$

and from section 2,

$$\begin{aligned} p_2 &= R\eta_j p_1 + (1 - \eta_j)p_1 \\ &= p_1\,[R\eta_j + (1 - \eta_j)] \\ &= [R\eta_j + (1 - \eta_j)]^2 \quad , \end{aligned} \tag{59}$$

and from the last section,

$$\begin{aligned} p_{N_R} &= [R\eta_j + (1 - \eta_j)]^{N_R} \\ &= [R(1 - (1 - \eta)^{1/N_R}) + (1 - \eta)^{1/N_R}]^{N_R} \\ &= [R - R(1 - \eta)^{1/N_R} + (1 - \eta)^{1/N_R}]^{N_R} \\ &= [R + (1 - \eta)^{1/N_R}\,(1 - R)]^{N_R} \quad . \end{aligned} \tag{60}$$

This is analogous to the formula for sneakage, so the effect of reentrainment can be expected to be similar to the effect of sneakage, provided that a constant fraction of the material is always reentrained. It is doubtful that such a condition exists, since precipitators frequently use different rapping programs on different sections, agglomeration occurs during collection, and different holding forces exist in different sections. However, until sufficient data on rapping losses PER SECTION as a function of particle size can be accumulated, the relationship may be used to estimate the effect of rapping reentrainment on precipitator performance.

Figure 15 shows the effect on resultant efficiency for a given size particle of various degrees of reentrainment for a four-section precipitator with the indicated values of no-reentrainment efficiency.

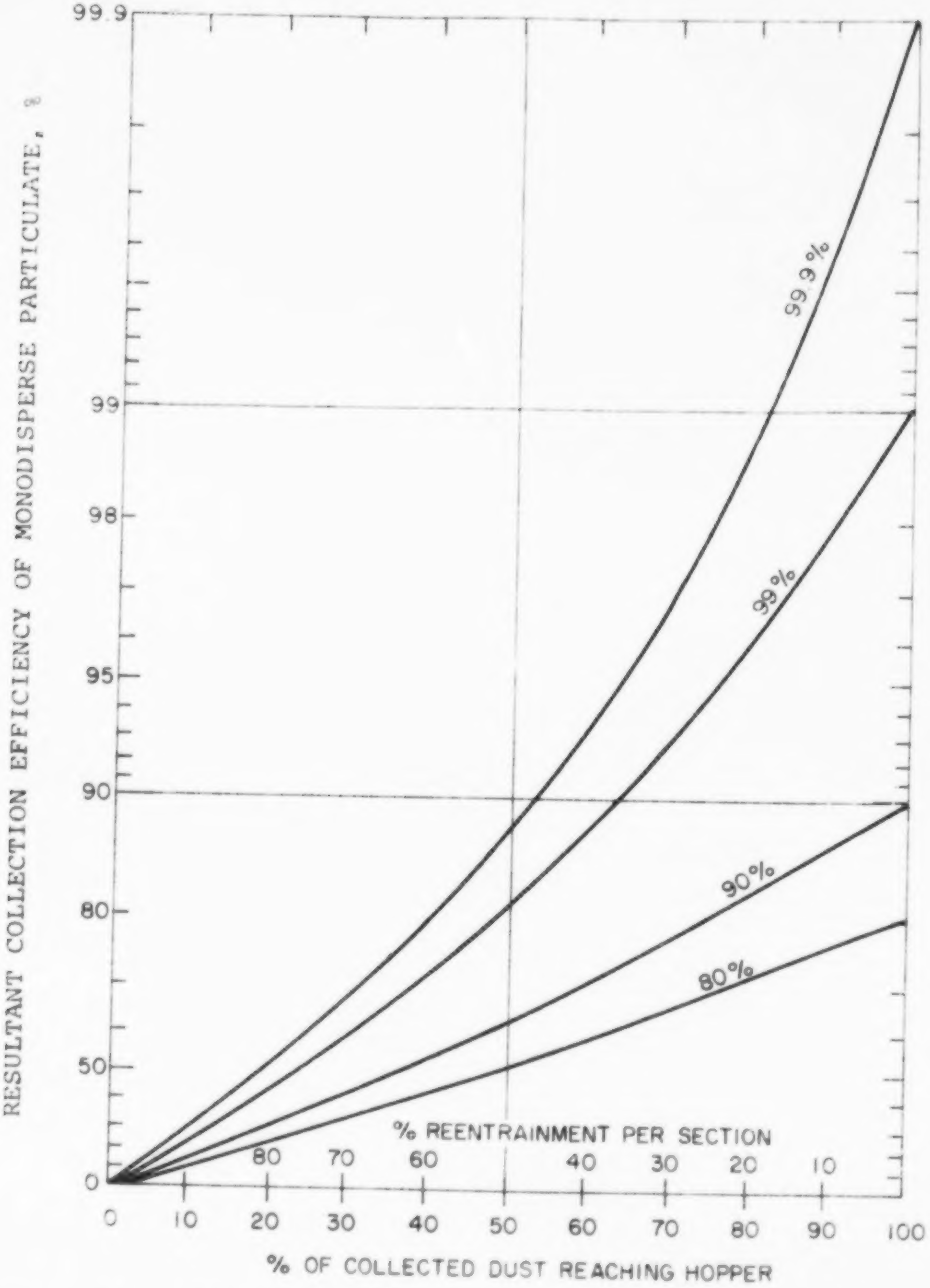

Figure 15. Effect of reentrainment on the efficiency of a four-section precipitator designed for a no reentrainment efficiency as indicated for a monodisperse particulate.

This analysis has considered only reentrainment due to rapping. Other forms of reentrainment are known to occur, however, such as: a) "saltation", losses which occur when large particles impact previously deposited smaller particles on the collection electrode, b) losses due to bouncing of particles following impaction on the collection surface, c) losses from erosion of the deposited dust layer caused by excessive gas velocity. These losses are expected to be relatively insignificant when compared with rapping losses, and the influence of such losses on the performance of a precipitator designed for high collection efficiencies is expected to be minor.

Since reentrainment and sneakage effects are estimated with identical mathematical expressions, a combined correction factor, B, is used in the computer model. From input values of the fraction of material assumed to be lost by reentrainment and sneakage, and the number of stages over which losses are assumed to occur, the program computes B from the ideal collection fraction for each particle size.

The correction factors B and F are used to calculate an "apparent" migration velocity for each particle size as follows:

$$w_e' = \frac{w_e}{F \cdot B} \quad . \tag{61}$$

The program contains an "IF" statement which truncates all collection fractions greater than 0.999999 at this value. This procedure holds the product of F and B constant at these high values of collection fraction for a given set of conditions.

From w_e', a reduced collection efficiency is obtained from the Deutsch equation. A reduced precipitation rate parameter is obtained from

$$w_p' = \frac{Q}{A_T} \ln \left(\frac{1}{1-\eta_T'}\right) , \qquad (62)$$

where η_T' is the overall mass collection fraction obtained from the individual reduced collection fractions.

SECTION III
INPUT DATA AND PROGRAM OUTPUT

INPUT DATA FORMAT

The input data required by the program consist of an estimate of the overall efficiency, the operating parameters and geometry of the electrostatic precipitator under consideration, pertinent characteristics of the gas and suspended particulate, and estimated values of parameters which account for non-ideal effects. Table 1 gives the input data required with the data card format. All input data are converted to MKS units prior to performing the calculations. The provisions for electrical sectionalization require that the length of each electrical section be rounded to the nearest integer number of feet. If there are sections in parallel, these must be combined by hand into overall sections across the [illegible] of the precipitator. Procedures for measuring or estimating the important input parameters are discussed below.

PARTICLE SIZE DISTRIBUTION

Since particle charge and electrical migration velocity are functions of particle diameter, collection efficiency under a given set of electrical conditions is also a function of particle size. The overall mass collection efficiency is therefore influenced by the size distribution of the particulate entering the precipitator. In-situ measurements of particle size distributions in the range of interest for coal-fired power plants are conducted primarily by inertial sizing devices known as cascade impactors. The impactors can be inserted directly into the duct or flue, thus eliminating any condensation and sample loss problems which occur when external sampling is used.

TABLE 1

INPUT DATA AND DATA CARD FORMAT

Card Set	Variable	Units	Format
1	Number of different particle sizes (maximum of 20)	-	I2
	Number of submicron particle sizes (maximum of 8)	-	I2
	Overall Card Format		(I2,8X,I2)
2	Particle diameters	microns	10F8.0
3	Percentages of size distribution for all particle diameters	percent	10F8.0
4	Identification information	-	40A2
5	Gas volume flow rate	ft^3/min	10F8.0
	Dust load	gr/ft^3	10F8.0
	Precipitator length	ft	10F8.0
	Gas velocity	ft/sec	10F8.0
	Estimated efficiency	%	10F8.0
	Dust density	kg/m^3	10F8.0
	Dust resistivity-multiplier of 10^x	ohm-cm	10F8.0
	Value of x	-	10F8.0
	Gas temperature	°F	10F8.0
	Pressure	atm	10F8.0
6	Fraction of sneakage and/or reentrainment	none	10F8.2
	Normalized standard deviation of gas velocity distribution	none	10F8.2
	Number of stages for sneakage and/or reentrainment	none	10F8.2
7	Number of steps for Runge-Kutta integration for charge subroutine 0	none	I2
	Number of points used in numerical integration for charge subroutine 0	none	I2
	Charge subroutine selector, 0 or 1 (see text, Section II)	none	I2
	Dielectric constant	none	E11.4
	Ion mobility	m^2/volt-sec	E11.4
	Gas viscosity	kg/(m-sec)	E11.4
	Mean thermal speed of ions	cm/sec	E11.4
	Overall Card Format		(3(I2),4(E11.4))
8	Number of electrical sections in direction of gas flow	none	I2
9	Lengths of electrical sections	ft	40(I2)

TABLE I

(Continued)

Card Set	Variable	Units	Format
10	Area of first electrical section	ft^2	E11.4
	Applied voltage of first section	volts	E11.4
	Current for first section	amps	E11.4
	Wire length for first section	ft	E11.4
	Corona wire radius for first section	in.	E11.4
	Wire to plate spacing for first section	in.	E11.4
	No. of wires per linear section for first section	none	E11.4
	1/2 wire to wire spacing for first section	in.	E11.4

Repeat for each electrical section

Overall Format (7(1PE11.4))

Table 2 shows some characteristics of several commercially available cascade impactors.[26] Measurements have been conducted by Southern Research Institute with a modified Brink impactor at the inlet of several precipitators collecting ash from coal-fired boilers. Results from two such measurements are presented in Figures 16 and 17.

Although the principle of operation of inertial impactors is relatively simple, accurate results are obtained only with careful attention to the technique employed in the use of the devices. A detailed discussion of operating procedures is available elsewhere.[27] The size distribution data are entered into the program in the form of a histogram. Data card sets 1, 2, and 3 in Table 1 are employed to transmit the particle size information.

MEASUREMENT OF RESISTIVITY

Measurement of dust resistivity is influenced by a number of factors which cause the values as measured by the various methods to differ by as much as two decades. Since the useful current density in a precipitator can be strongly influenced by resistivity, it is apparent that resistivity must be known precisely if it is to be used as a basis for precipitator performance or sizing.

The relationship between dust resistivity and current density as given in the following section is based on resistivity values as determined with a point-plane probe. The following is a brief discussion of factors involved in measurement of resistivity for the purpose of defining the problem. A more complete discussion is presented in a report entitled "Techniques for Measuring Fly Ash Resistivity."[28]

Table 2. SIZE FRACTIONATING POINTS OF SOME COMMERCIAL CASCADE IMPACTORS FOR UNIT DENSITY SPHERES

Stage	Modified Brink	Andersen Mark III	U. of W. (Pilat)	ERC Tag
	0.85 LPM	14 LPM	14 LPM	14 LPM
Cyc	18.0 μm			
0	11.0			11.1 μm
1	6.29	14.0 μm	39.0 μm	7.7
2	3.74	8.71	15.0	5.5
3	2.59	5.92	6.5	4.0
4	1.41	4.00	3.1	2.8
5	0.93	2.58	1.65	2.0
6	0.56	1.29	0.80	1.3
7		0.80	0.49	0.9
8		0.51		0.6

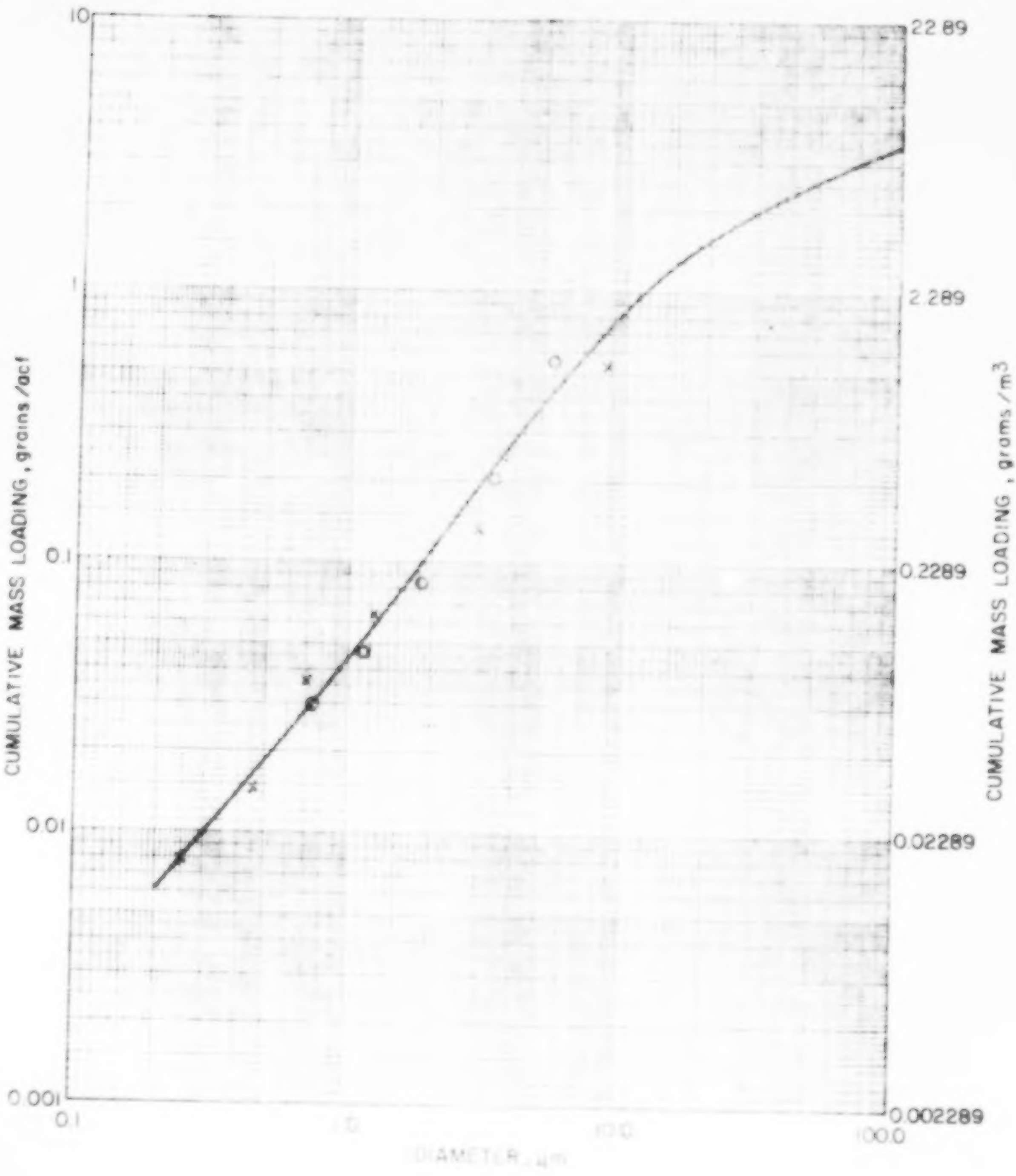

Figure 16. Inlet size distribution obtained from modified Brink impactor from power station burning an Eastern coal.

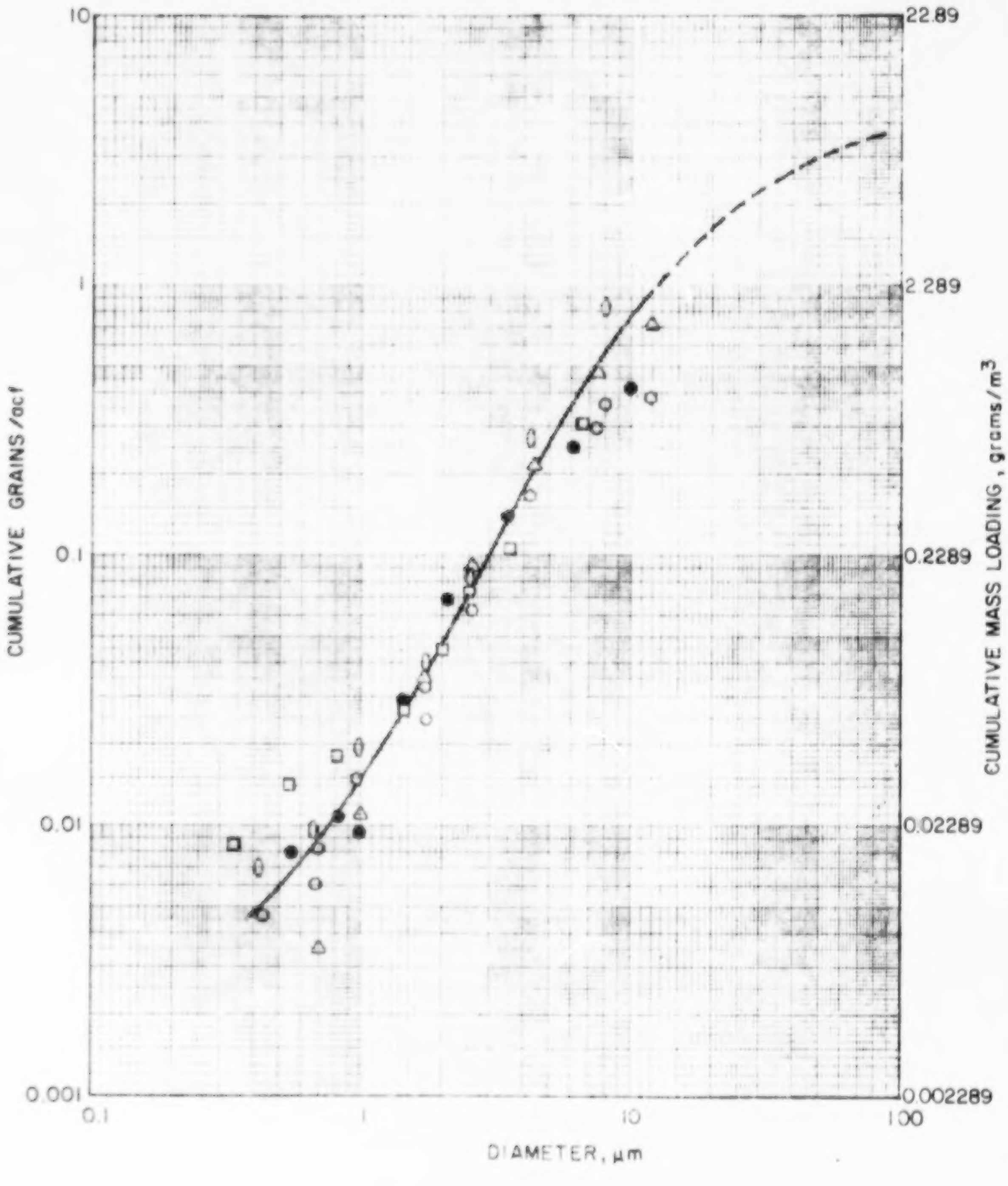

Figure 17. Size data from Brink impactor measurements at inlet of precipitator collecting a low sulfur Western coal.

Electrical resistivity of a dust layer is measured by determining the current flow through a defined volume of dust when a given voltage is impressed across the dust layer. The ratio of the voltage to current is the resistance of the dust, and resistivity is calculated from the geometry of the measurement cell.

Procedures for measurement of electrical resistivity are classified as laboratory methods if the dust is extracted from the duct and the measurement is made in an environment other than the flue gas, and in-situ if measurement is made either in the duct or in the gaseous atmosphere of the duct. Laboratory measurements generally agree with those taken in-situ at temperatures of about 200°C and higher. Above 200°C, resistivity of fly ash is determined primarily by ash composition and is largely independent of flue gas composition.

Bickelhaupt[29] has developed an expression to predict volume resistivity for fly ashes produced from the efficient burning of coals as a function of ash chemistry, temperature, and porosity for the high temperature region at one level of field strength. At lower temperature, resistivity is influenced by flue gas composition and laboratory measurements do not, as a rule, correlate with in-situ values. Research is continuing in an effort to predict low temperature resistivity values from ash and flue gas composition.

Among the factors which cause different results to be obtained from different measuring techniques are the particle size distribution of the collected sample, the method of depositing the sample, and the magnitude of the electric field at which the measurement is made. Although no existing method is considered to be an ideal procedure for in-situ resistivity determinations, the point-to-plane probe is recommended because of the following advantages:

- The particulate collection mechanism is the same as that in an electrostatic precipitator.
- The dust-gas and dust-electrode interfaces are the same as those in an electrostatic precipitator.
- The measured electric fields and current densities are comparable to those in an electrostatic precipitator.
- Flue gas conditions are preserved.
- Values obtained for the resistivity are in general consistent with the electrical behavior observed in the precipitator.

It should be noted, however, that resistivity data obtained with this technique usually exhibit considerable scatter. The scatter may be caused in part by the variations of the properties of the small collected sample due to composition changes. A precipitator tends to average short-term compositional variations because considerable time is required to collect a dust layer. Resistivity measurements should thus be averaged over a long period of time to be statistically valid.

Resistivity values are entered into the program in data card number five in Table 1. The program uses the resistivity value and the input current density to calculate the electric field in the deposited dust layer. With respect to the use of the computer program, however, the most important usage of the dust-resistivity value is the determination of allowable current density, which is discussed in the following section.

ALLOWABLE CURRENT DENSITY

Corona current influences the electric field and particle charging rate, and hence is one of the most significant input parameters in determining precipitator performance. Current and voltage relationships in a precipitator are governed by electrode geometry and by the mobility of the charge carriers. Limitations on current therefore limit the precipitator operating voltage and hence the electric field. The current also influences the field due to the space charge resulting from the presence of ions or charged particulate in the interelectrode space.

Electrical conditions in a precipitator are limited by either breakdown of the gas in the interelectrode space or by breakdown in the collected dust layer. For any given geometry, an increase in voltage is accompanied by an increase in electric field. When the field exceeds that required to initiate a spark and to propagate it across the interelectrode space, the electrical operating conditions will be limited by these sparking conditions. Breakdown of the collected dust layer can occur as a spark or as a back corona depending upon the resistivity and thickness of the dust layer. In a single stage precipitator, the corona current must pass through the dust layer to the grounded or collecting electrode. The voltage drop across the dust layer is

$$V_d = j\rho t \, , \tag{63}$$

where

j = current density, amps/cm^2

ρ = dust resistivity, ohm-cm

t = dust layer thickness, cm.

The electric field in the dust layer (E_d) is the product of the current density (j) and the resistivity (ρ).

The electric field in the dust layer can be increased to the point that the gases in the interstitial space break down electrically. This breakdown results from the acceleration of free electrons to ionization velocity to produce an avalanche condition similar to that at the corona electrode. When this breakdown occurs, the voltage drop across the dust layer is added to that between the corona electrode and dust surface. If this voltage is sufficiently high, a spark will occur. The rate of sparking for a given precipitator geometry will determine the operating electrical conditions in such a circumstance. If the electrical resistivity of the dust is very high and if the dust layer is sufficiently thin, the voltage drop across the dust layer can occur at a condition which would not cause breakdown of the gases in the interelectrode space. Under these conditions, the dust layer will be continuously broken down electrically and will discharge positive ions into the interelectrode space. The effect of these positive ions is to reduce the effective density of negative ions for charging and reduce the electric field associated with the space charge. Both the magnitude and rate of charging are affected by such a back corona condition. Effective precipitator current is therefore limited to that corresponding to the electrical breakdown conditions whether the breakdown occurs as sparkover or back corona.

The maximum permissible current density as a function of ash resistivity based on dust breakdown strengths of 10 and 20 kV/cm are shown in Figure 18. Line 3 on this figure is based on field observations, and is discussed later. Average current densities in practical precipitators are less than those predicted on the basis of electrical breakdown because of non-uniform current densities resulting from electrode geometry and because the plate area or length of corona wire powered by a single TR set is large. Consequently, theoretical current

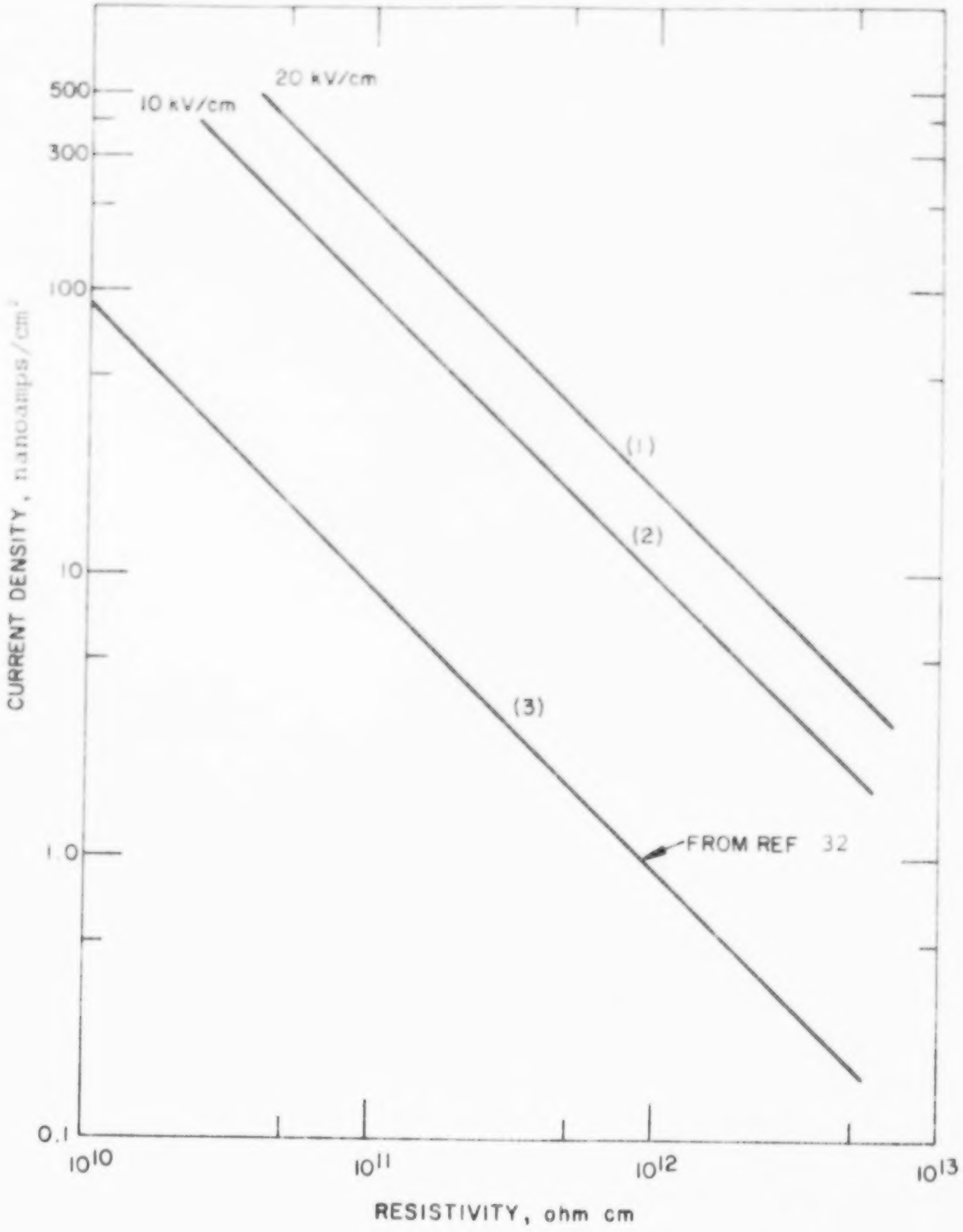

Figure 18. Current density as a function of resistivity.

density-resistivity relationships must be modified to accomodate these conditions. At present there is no theoretical basis for making the required adjustments.

Field experience shows that current density for cold side precipitators is limited to around 50 to 70 nA/cm^2 ($1x10^{-9}$ A = 1 nA) due to electrical breakdown of the gases in the interelectrode region. Consequently, this constitutes a current limit under conditions where breakdown of the dust layer does not occur.

Practically, current can be increased in a precipitator somewhat beyond that corresponding to the onset of back corona since current density in a wire-plate geometry is fairly non-uniform. If there is severe non-uniformity, breakdown can occur at localized points corresponding to areas of highest current density and it is possible for beneficial effects to be achieved by increasing the current density above that corresponding to the onset of back corona. However, for reasons stated, the improved performance would be marginal and for practical purposes, current density should be considered as being limited to that at which breakdown of the dust layer occurs.

Breakdown of the dust layer has been studied extensively by Penney and Craig,[10] Pottinger,[11] and others and can be influenced by many factors. The presence of conducting particles can cause localized areas of high electric field and hence breakdown may occur at lower than average electric fields. The size distribution of the dust also influences breakdown strength by changing the volume of interstices. It has also been found that breakdown strength varies with dust resistivity, the higher breakdown strength being associated with the higher resistivity.

All of these conditions contribute to the difficulty of determining allowable current densities on a purely theoretical basis. However, if allowance is made for current non-uniformity due to electrode geometry, variations in spacing due to erection and manufacturing tolerance, etc., some estimates can be made that agree to a fair approximation with observed conditions. Curve 3 of Figure 18 was obtained from the literature,[32] and is based on the observation that critical current densities in full-scale precipitators can be reduced from the theoretical dust breakdown values by a factor of about 10. The use of this curve should give a conservative estimate of the allowable current density as a function of resistivity.

DETERMINATION OF VOLTAGE-CURRENT CHARACTERISTICS

The voltage-current relationships for an electrostatic precipitator are governed by the mechanical design of the collector system, the size and concentration of dust particles in the gas stream, the presence of a dust layer on the collection electrode, and the temperature and composition of the gas stream.

With respect to mechanical design characteristics, the corona electrode may consist of round wires, formed metallic strips, or specially formed members of barbed wire. Each of these structures provide different voltage versus current characteristics. Collection electrode spacing also influences the voltage-current characteristics. Typical plate spacing ranges from 22.86 cm to 30.48 cm (9 to 12 inches). Corona current starts at a lower voltage for close spacing than for wide spacing. The increased space charge associated with the wide spacing causes a further decrease in current for a given applied voltage.

As has been discussed previously, the particulate matter suspended in the effluent gas stream influences the electrical conditions. Large quantities of fine particles will acquire an electrical charge with a resultant decrease in current at a given voltage. As the charged particulate is collected, this relatively immobile space charge is removed with an increase in current for a given applied voltage. This current suppression with dust load is shown in Figure 19 for a precipitator operating on a power station boiler utilizing coal with a sulfur content of about two and one half percent.

The voltage drop across the dust layer results in an increase in the applied voltage required to achieve a given current density as shown in Figure 20. The condition illustrated is for a DC voltage-current curve with a one centimeter thick dust layer with a resistivity of 1×10^{11} ohm-centimeter on a typical second field volt-ampere curve.

The actual electrical conditions that are active for electrical collection exclude the voltage drop in the dust layer. Therefore, that portion represented by the shift in Figure 20 must be neglected in estimating performance. For estimating purposes, some average volt-ampere characteristics should be selected. In the inlet section, the voltage and consequently the electric field will be high while the outlet section with the very light dust load will operate at a somewhat reduced voltage. Therefore, the proper choice for a representative voltage-current characteristic will lie somewhere in between. A reasonable approximation to the average electrical conditions in the precipitator is given in Figure 19 by the curves labeled "typical".

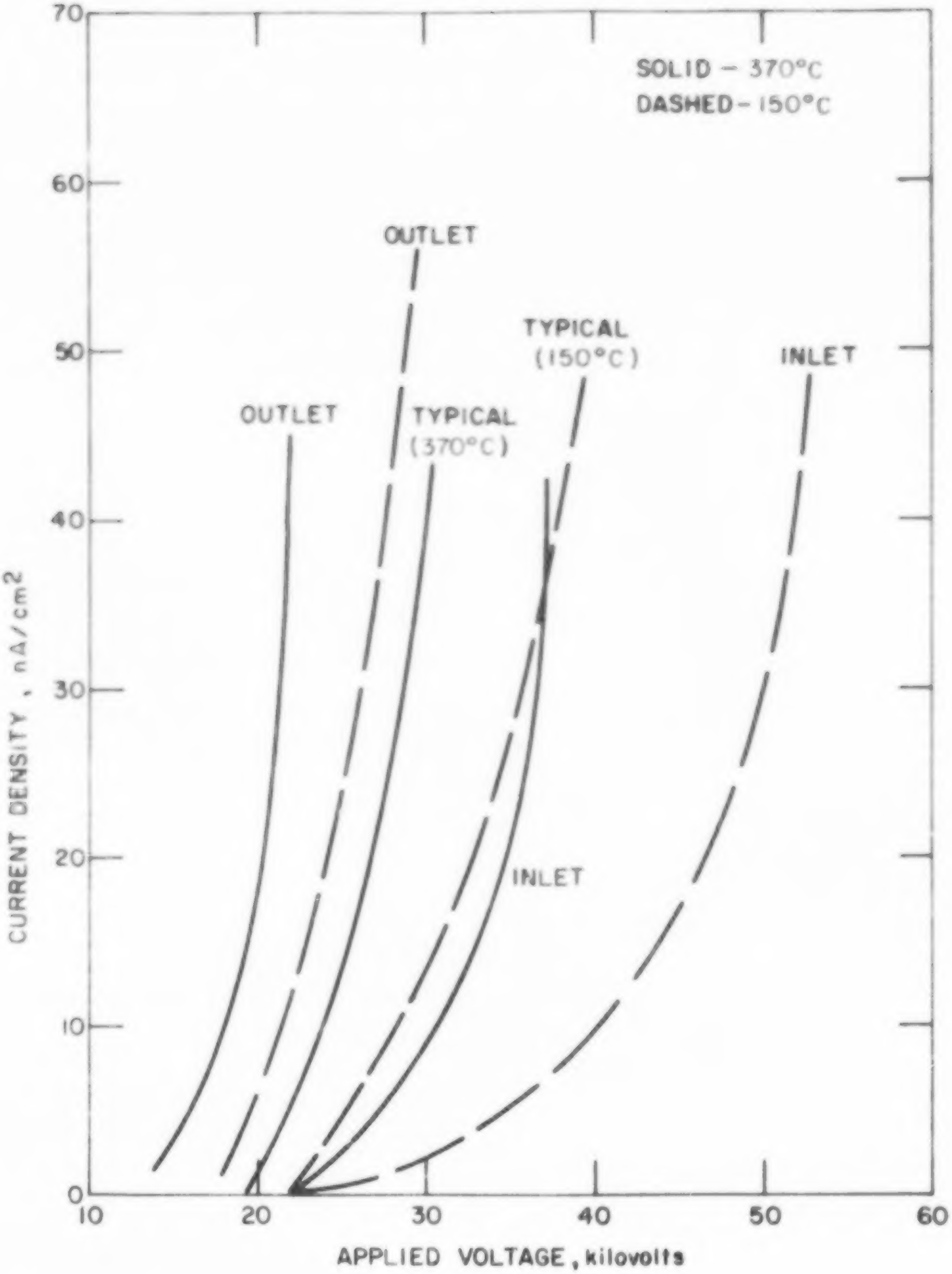

Figure 19. Comparison between the voltage vs current characteristics for cold side and hot side precipitators. Corona wire radius = .277 cm (.109"), plate spacing = 22.86 cm (9").

As has been discussed previously, the particulate matter suspended in the effluent gas stream influences the electrical conditions. Large quantities of fine particles will acquire an electrical charge with a resultant decrease in current at a given voltage. As the charged particulate is collected, this relatively immobile space charge is removed with an increase in current for a given applied voltage. This current suppression with dust load is shown in Figure 19 for a precipitator operating on a power station boiler utilizing coal with a sulfur content of about two and one half percent.

The voltage drop across the dust layer results in an increase in the applied voltage required to achieve a given current density as shown in Figure 20. The condition illustrated is for a DC voltage-current curve with a one centimeter thick dust layer with a resistivity of 1×10^{11} ohm-centimeter on a typical second field volt-ampere curve.

The actual electrical conditions that are active for electrical collection exclude the voltage drop in the dust layer. Therefore, that portion represented by the shift in Figure 20 must be neglected in estimating performance. For estimating purposes, some average volt-ampere characteristics should be selected. In the inlet section, the voltage and consequently the electric field will be high while the outlet section with the very light dust load will operate at a somewhat reduced voltage. Therefore, the proper choice for a representative voltage-current characteristic will lie somewhere in between. A reasonable approximation to the average electrical conditions in the precipitator is given in Figure 19 by the curves labeled "typical".

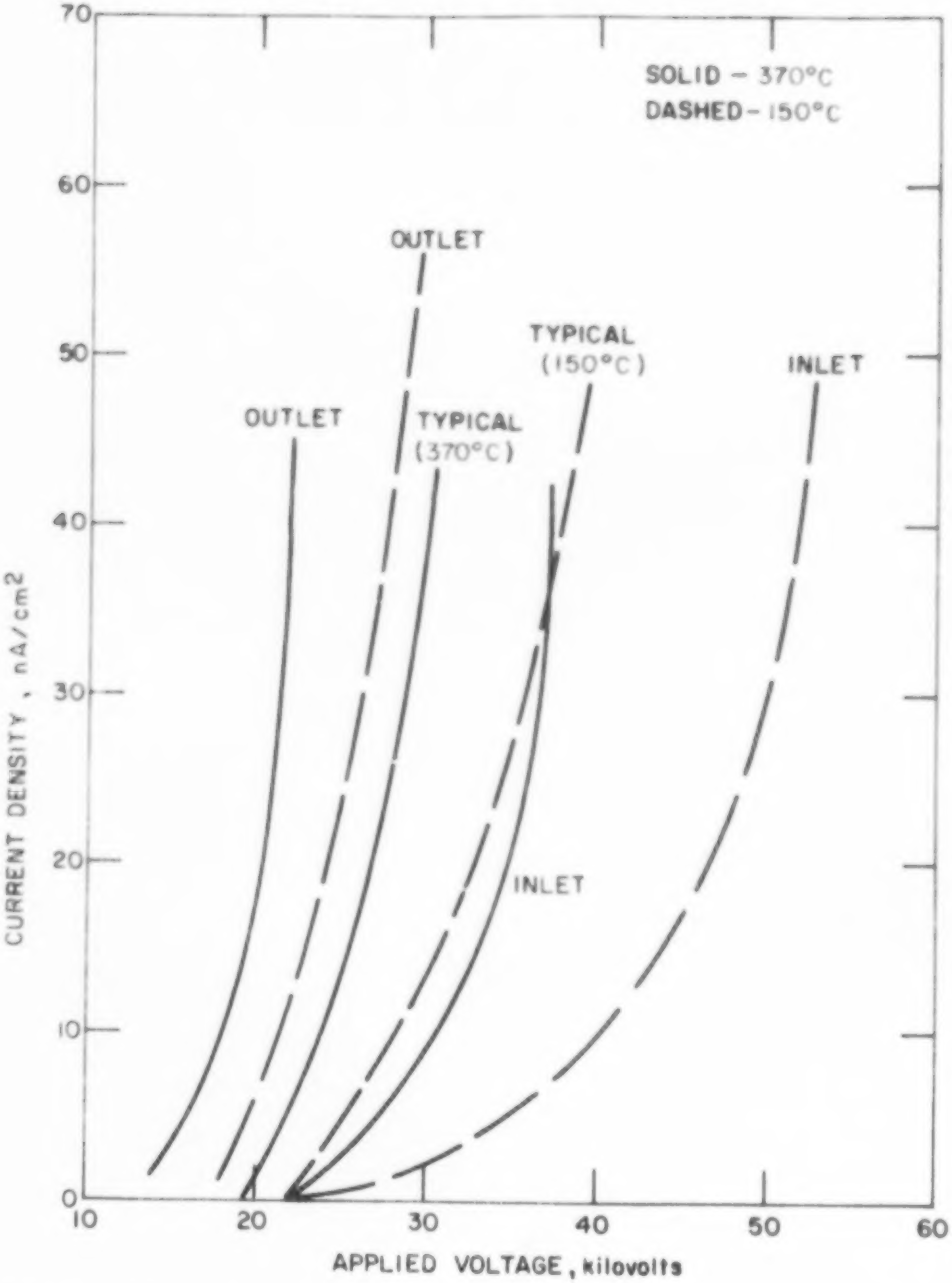

Figure 19. Comparison between the voltage vs current characteristics for cold side and hot side precipitators. Corona wire radius = .277 cm (.109"), plate spacing = 22.86 cm (9").

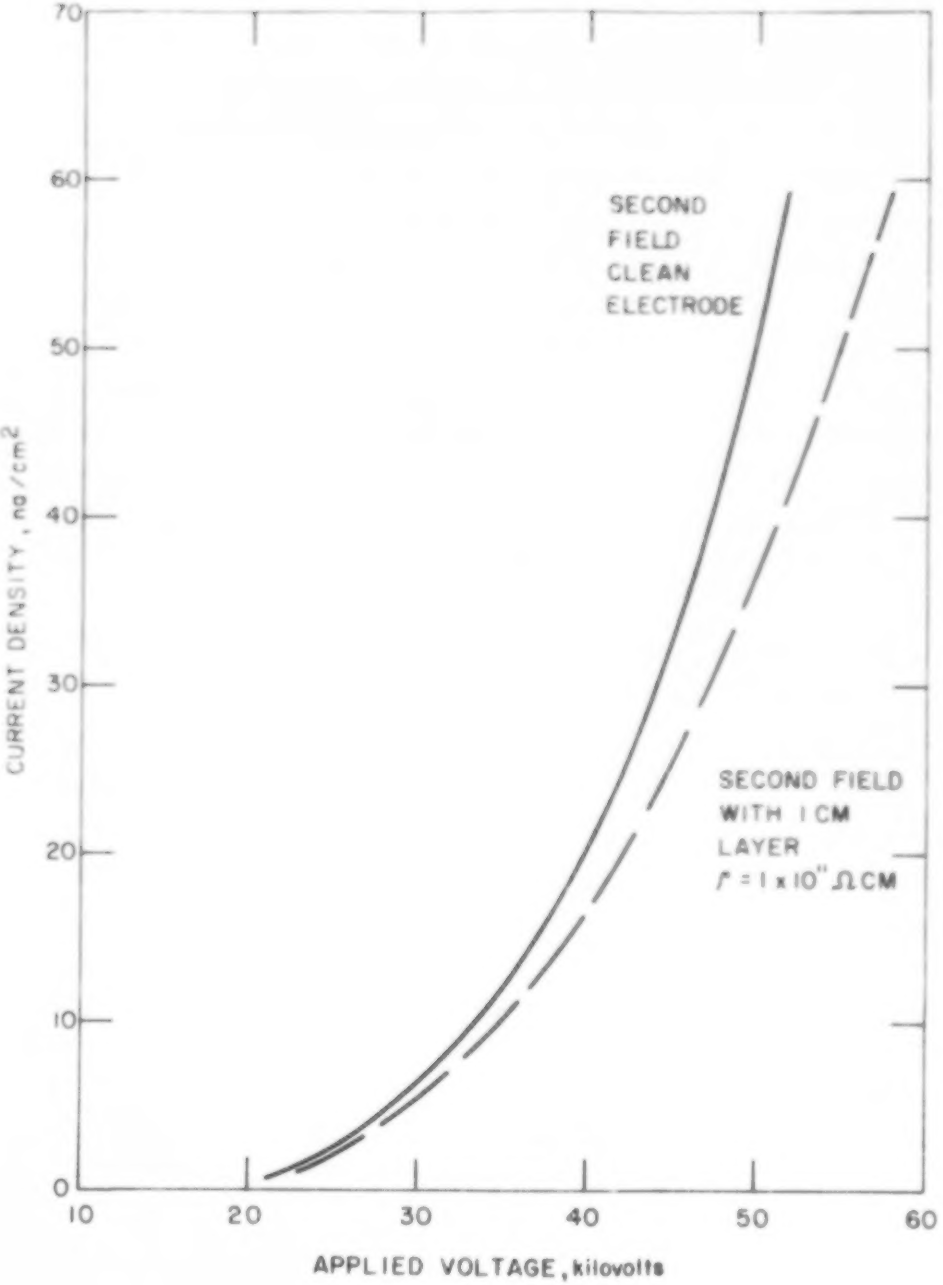

Figure 20. Voltage vs current characteristic for second field clean electrode and 1 cm layer of $1x10^{11}$ ohm-cm dust.

The voltage-current characteristics are different for precipitators operating prior to the air preheater from those operated subsequent to it for two reasons: the gas temperature is on the order of 270°C for the former and 150°C for the latter, and because of the increased gas volume at the higher temperature, the dust loading is less for the hot side unit. The increased temperature leads to an increase in current at each applied voltage because of the reduced gas density, as well as electrical sparkover occurring at a lower voltage. The decreased dust loading at the high temperature causes a reduction in the space charge that suppresses the current. Figure 19 illustrates the difference in the V-I characteristics of precipitators in the two temperature regions.

Voltage and current data are entered in the program in data card set 10 (Table 1).

ELECTRICAL SECTIONALIZATION

Sectionalization of a precipitator can be expressed in terms of the number of transformer rectifier (TR) sets used per unit of gas flow, or the plate area served by a TR set.

In terms of performance, a large number of TR sets for a given gas flow or plate area, will permit each section to operate at a higher voltage and current and hence at higher collection efficiency. From a maintenance standpoint, large power supplies with the large attendent plate area contribute to excessive electrical failure for the discharge electrodes and greater precipitator outage time. Another consequence of poor sectionalization is that outage of one section disables a larger portion of the precipitator.

Performance requirements can be met by several combinations of precipitator size and degree of sectionalization. Based on only performance considerations, the choice might be determined by economic trade off. However, reliability and maintenance considerations should be overriding factors that dictate the degree of sectionalization.

White[13] has shown that theoretically expected reductions in operating voltage occur as identical wire pipe sections are connected to the same power supply due to the variation in voltage with spark rate. For a given overall spark rate, each pipe would operate at a lower effective spark rate and lower voltage as the number of units is increased.

In full scale precipitators an additional factor influencing precipitator electrical conditions is variation in mechanical and erection details resulting in electrode misalignment and sharp edges or points that cause high localized electric fields. With large plate areas, variations are likely to occur in localized areas resulting in voltage limitations for an entire section. A high degree of sectionalization tends to minimize the effect of these mechanical and constructional variations.

The trend in precipitator design has been toward larger TR sets and larger electrical sections. Some TR sets of up to 4 amps secondary current have been installed on larger fly ash precipitators. Such sets can supply up to 37,180 m^2 (400,000 ft^2) of plate area. Earlier precipitator TR sets were designed to supply 1858 to 3716 m^2 (20-40,000 ft^2) of plate area. During sparkover, the energy that can be dissipated is determined both by the energy stored in the precipitator capacitance, and the energy that the power supply can provide. The energy stored in the precipitator-distributed capacitance continues to supply the spark even though the power supply voltage is removed. In the case of large power supplies and large plate areas, the energy dissipated can cause rapid failure of the discharge electrodes and severe maintenance problems.

From a design standpoint, precipitators should be engineered according to one of two philosophies. If sparking is to be permitted, a reasonably high degree of sectionalization should be provided. If large power supplies are to be used, spark rates should be maintained at very low levels (around 1 per minute) in order to minimize electrical erosion of the electrode material. In the latter case, a lower operating voltage and current would result and increased plate area must be provided.

The computer program is capable of representing electrical sectionalization in the direction of gas flow. If there are multiple TR sets across the width of a precipitator longitudinal section, these sets must be combined manually to give an average voltage and current for the section.

PROGRAM OUTPUT

Figure 21 gives a typical example of the output from the program using data from a laboratory-scale precipitator. The following information is given.

(1) Identification of the data set.
(2) Input data which pertain to the entire precipitator.
(3) Input data and derived quantities which pertain to a particular electrical section.
(4) Results obtained for each incremental length which indicate the status of the calculations. These quantities are:

    - (a) the ratio of total space charge to ionic space charge,
    - (b) the average electric field between wire and plate, volt/m,
    - (c) the electric field adjacent to the collecting electrode, volt/m,
    - (d) the average free ion density, no./m^3,
    - (e) the current density, nanoamperes/cm^2,
    - (f) the mass median diameter of the particulate collected in the length increment, m,
    - (g) the mass of dust collected in the length increment, kg/m^3, and
    - (h) the increment number.

(5) Inlet particle size distribution.

(6) Calculated collection efficiency, the Cunningham correction factor, the effective migration velocity (cm/sec), the reduced effective migration velocity, and the reduced collection efficiency for each particle size.

(7) Estimated and computed values of the overall mass efficiency.

(8) The mass median diameter of the uncollected dust, m (from the theoretical calculations).

(9) The precipitation rate parameter, cm/sec.

(10) Input values of normalized gas velocity standard deviation, the fraction of dust assumed lost per stage from reentrainment and/or sneakage, and the number of stages over which the losses are assumed to occur.

(11) The reduced overall efficiency obtained from the use of the empirical corrections.

(12) The reduced precipitation rate parameters obtained from the reduced overall efficiency, cm/sec.

(13) The ratio of the charge accumulated to the modified saturation charge (Section II), based on conditions in the last increment, for the submicron particles as a function of increment number.

(14) The charge accumulated (in coul) on submicron particles as a function of increment number.

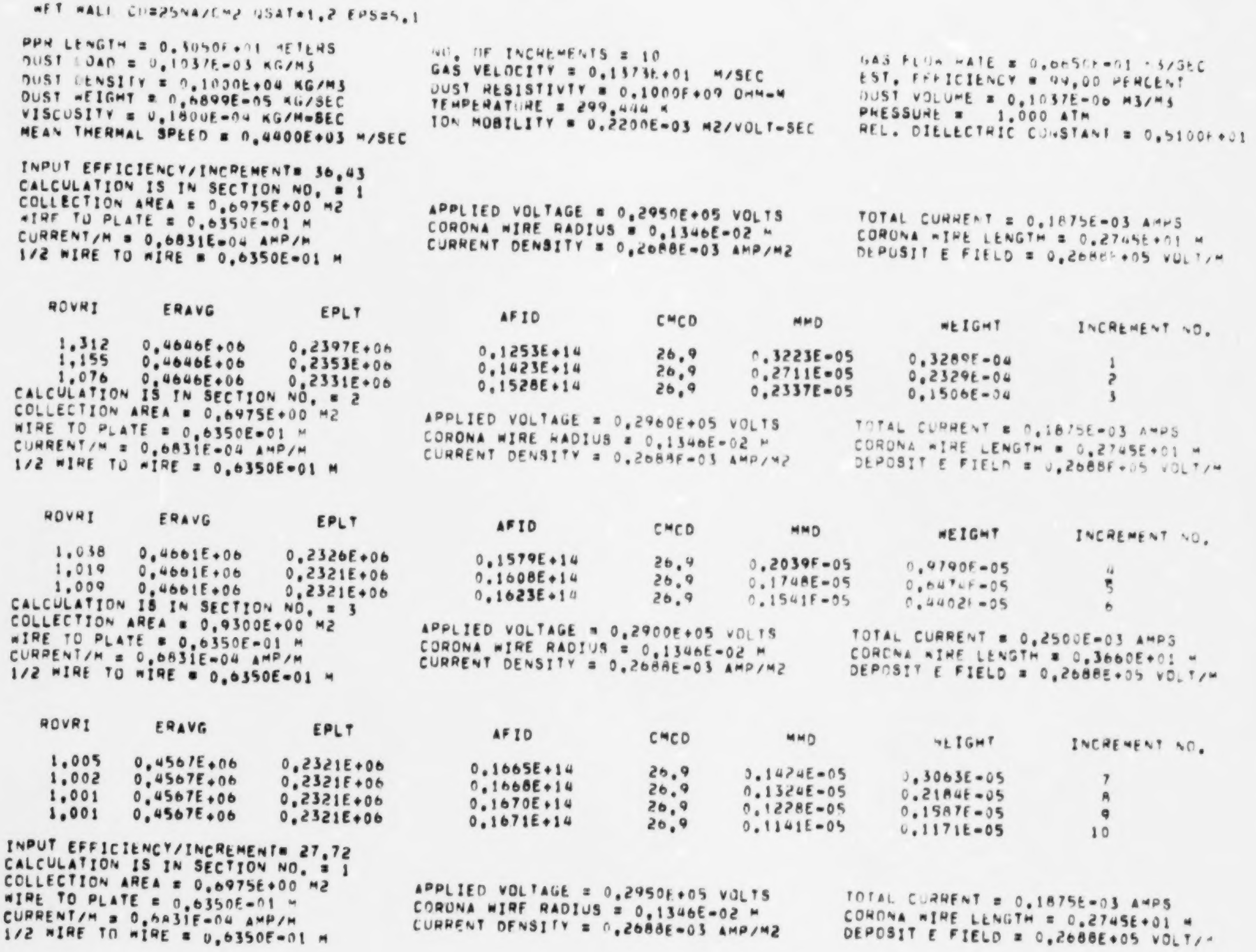

```
WET WALL CD=25NA/CM2 USAT=1,2 EPS=5,1

PPR LENGTH = 0,3050E+01 METERS              NO, OF INCREMENTS = 10                          GAS FLOW RATE = 0,6650E-01 M3/SEC
DUST LOAD = 0,1037E-03 KG/M3                GAS VELOCITY = 0,1573E+01  M/SEC                EST, EFFICIENCY = 99,00 PERCENT
DUST DENSITY = 0,1000E+04 KG/M3             DUST RESISTIVTY = 0,1000E+09 OHM-M              DUST VOLUME = 0,1037E-06 M3/M3
DUST WEIGHT = 0,6899E-05 KG/SEC             TEMPERATURE = 299,444 K                         PRESSURE =   1,000 ATM
VISCOSITY = 0,1800E-04 KG/M-SEC             ION MOBILITY = 0,2200E-03 M2/VOLT-SEC           REL. DIELECTRIC CONSTANT = 0,5100E+01
MEAN THERMAL SPEED = 0,4400E+03 M/SEC

INPUT EFFICIENCY/INCREMENT= 36,43
CALCULATION IS IN SECTION NO, = 1
COLLECTION AREA = 0,6975E+00 M2             APPLIED VOLTAGE = 0,2950E+05 VOLTS              TOTAL CURRENT = 0,1875E-03 AMPS
WIRE TO PLATE = 0,6350E-01 M                CORONA WIRE RADIUS = 0,1346E-02 M               CORONA WIRE LENGTH = 0,2745E+01 M
CURRENT/M = 0,6831E-04 AMP/M                CURRENT DENSITY = 0,2688E-03 AMP/M2             DEPOSIT E FIELD = 0,2688E+05 VOLT/M
1/2 WIRE TO WIRE = 0,6350E-01 M

   ROVRI      ERAVG         EPLT               AFID          CMCD        MMD           WEIGHT        INCREMENT NO.

   1,312   0,4646E+06    0,2397E+06         0,1253E+14      26,9    0,3223E-05     0,3289E-04          1
   1,155   0,4646E+06    0,2353E+06         0,1423E+14      26,9    0,2711E-05     0,2329E-04          2
   1,076   0,4646E+06    0,2331E+06         0,1528E+14      26,9    0,2337E-05     0,1506E-04          3
CALCULATION IS IN SECTION NO, = 2
COLLECTION AREA = 0,6975E+00 M2             APPLIED VOLTAGE = 0,2960E+05 VOLTS              TOTAL CURRENT = 0,1875E-03 AMPS
WIRE TO PLATE = 0,6350E-01 M                CORONA WIRE RADIUS = 0,1346E-02 M               CORONA WIRE LENGTH = 0,2745E+01 M
CURRENT/M = 0,6831E-04 AMP/M                CURRENT DENSITY = 0,2688E-03 AMP/M2             DEPOSIT E FIELD = 0,2688E+05 VOLT/M
1/2 WIRE TO WIRE = 0,6350E-01 M

   ROVRI      ERAVG         EPLT               AFID          CMCD        MMD           WEIGHT        INCREMENT NO.

   1,038   0,4661E+06    0,2326E+06         0,1579E+14      26,9    0,2039E-05     0,9790E-05          4
   1,019   0,4661E+06    0,2321E+06         0,1608E+14      26,9    0,1748E-05     0,6474E-05          5
   1,009   0,4661E+06    0,2321E+06         0,1623E+14      26,9    0,1541E-05     0,4402E-05          6
CALCULATION IS IN SECTION NO, = 3
COLLECTION AREA = 0,9300E+00 M2             APPLIED VOLTAGE = 0,2900E+05 VOLTS              TOTAL CURRENT = 0,2500E-03 AMPS
WIRE TO PLATE = 0,6350E-01 M                CORONA WIRE RADIUS = 0,1346E-02 M               CORONA WIRE LENGTH = 0,3660E+01 M
CURRENT/M = 0,6831E-04 AMP/M                CURRENT DENSITY = 0,2688E-03 AMP/M2             DEPOSIT E FIELD = 0,2688E+05 VOLT/M
1/2 WIRE TO WIRE = 0,6350E-01 M

   ROVRI      ERAVG         EPLT               AFID          CMCD        MMD           WEIGHT        INCREMENT NO.

   1,005   0,4567E+06    0,2321E+06         0,1665E+14      26,9    0,1424E-05     0,3063E-05          7
   1,002   0,4567E+06    0,2321E+06         0,1668E+14      26,9    0,1324E-05     0,2184E-05          8
   1,001   0,4567E+06    0,2321E+06         0,1670E+14      26,9    0,1228E-05     0,1587E-05          9
   1,001   0,4567E+06    0,2321E+06         0,1671E+14      26,9    0,1141E-05     0,1171E-05         10
INPUT EFFICIENCY/INCREMENT= 27,72
CALCULATION IS IN SECTION NO, = 1
COLLECTION AREA = 0,6975E+00 M2             APPLIED VOLTAGE = 0,2950E+05 VOLTS              TOTAL CURRENT = 0,1875E-03 AMPS
WIRE TO PLATE = 0,6350E-01 M                CORONA WIRF RADIUS = 0,1346E-02 M               CORONA WIRE LENGTH = 0,2745E+01 M
CURRENT/M = 0,6831E-04 AMP/M                CURRENT DENSITY = 0,2688E-03 AMP/M2             DEPOSIT E FIELD = 0,2688E+05 VOLT/M
1/2 WIRE TO WIRE = 0,6350E-01 M
```

Figure 21. Typical Output Information from Computer Model.

Reproduced from
best available copy.

```
    ROVRI      ERAVG         EPLT              AFID          CMCD       MMD           WEIGHT       INCREMENT NO.

    1.238   0.4646E+06   0.2376E+06        0.1328E+14       26.9    0.3221E-05    0.3107E-04          1
    1.134   0.4646E+06   0.2347E+06        0.1450E+14       26.9    0.2706E-05    0.2329E-04          2
    1.074   0.4646E+06   0.2331E+06        0.1530E+14       26.9    0.2334E-05    0.1503E-04          3
CALCULATION IS IN SECTION NO. = 2
COLLECTION AREA = 0.6975E+00 M2              APPLIED VOLTAGE = 0.2960E+05 VOLTS       TOTAL CURRENT = 0.1875E-03 AMPS
WIRE TO PLATE = 0.6350E-01 M                 CORONA WIRE RADIUS = 0.1346E-02 M        CORONA WIRE LENGTH = 0.2745E+01 M
CURRENT/M = 0.6831E-04 AMP/M                 CURRENT DENSITY = 0.2688E-03 AMP/M2      DEPOSIT E FIELD = 0.2688E+05 VOLT/M
1/2 WIRE TO WIRE = 0.6350E-01 M

    ROVRI      ERAVG         EPLT              AFID          CMCD       MMD           WEIGHT       INCREMENT NO.

    1.042   0.4661E+06   0.2328E+06        0.1573E+14       26.9    0.2035E-05    0.9756E-05          4
    1.024   0.4661E+06   0.2322E+06        0.1601E+14       26.9    0.1744E-05    0.6445E-05          5
    1.013   0.4661E+06   0.2320E+06        0.1617E+14       26.9    0.1540E-05    0.4375E-05          6
CALCULATION IS IN SECTION NO. = 3
COLLECTION AREA = 0.9300E+00 M2              APPLIED VOLTAGE = 0.2900E+05 VOLTS       TOTAL CURRENT = 0.2500E-03 AMPS
WIRE TO PLATE = 0.6350E-01 M                 CORONA WIRE RADIUS = 0.1346E-02 M        CORONA WIRE LENGTH = 0.3660E+01 M
CURRENT/M = 0.6831E-04 AMP/M                 CURRENT DENSITY = 0.2688E-03 AMP/M2      DEPOSIT E FIELD = 0.2688E+05 VOLT/M
1/2 WIRE TO WIRE = 0.6350E-01 M

    ROVRI      ERAVG         EPLT              AFID          CMCD       MMD           WEIGHT       INCREMENT NO.

    1.008   0.4567E+06   0.2320E+06        0.1660E+14       26.9    0.1423E-05    0.3046E-05          7
    1.004   0.4567E+06   0.2320E+06        0.1665E+14       26.9    0.1323E-05    0.2172E-05          8
    1.003   0.4567E+06   0.2320E+06        0.1668E+14       26.9    0.1227E-05    0.1578E-05          9
    1.001   0.4567E+06   0.2320E+06        0.1670E+14       26.9    0.1140E-05    0.1165E-05         10
PARTICLE SIZE RANGE STATISTICS

   DIAMETER-METERS     PERCENT OF TOTAL     EFFICIENCY       CCF         W          W*          EFF*
    0.2500000E-06          0.280000         71.860634      1.5942      3.627      3.291       68.3485
    0.3500000E-06          0.550000         73.541920      1.4170      3.803      3.448       70.0421
    0.4500000E-06          1.000000         76.458817      1.3222      4.137      3.745       73.0016
    0.5500000E-06          1.400000         79.401150      1.2629      4.519      4.084       76.0180
    0.7000000E-06          3.700000         83.314363      1.2063      5.122      4.616       80.0890
    0.9000000E-06          4.500000         87.473246      1.1604      5.942      5.335       84.5126
    0.1100000E-05          4.500000         90.606186      1.1312      6.765      6.050       87.9377
    0.1300000E-05          5.300000         92.953348      1.1110      7.587      6.757       90.5799
    0.1600000E-05         10.700000         95.415375      1.0902      8.017      7.801       93.4596
    0.2000000E-05          9.000000         97.412830      1.0722     10.454      9.162       95.9367
    0.2600000E-05         16.000000         98.905010      1.0555     12.913     11.143       97.9669
    0.3500000E-05         13.000000         99.702742      1.0412     16.643     13.975       99.2445
    0.5000000E-05         30.069999         99.967566      1.0289     22.979     18.218       99.8286

   EFFICIENCY - STATED = 96.31     COMPUTED = 96.33     CONVERGENCE OBTAINED
   MMD OF EFFLUENT= 0.8670E-06
   PRECIPITATION RATE PARAMETER =  9.452

    SIGMA=   0.0000  WITH   0.0800SNEAKAGE OVER   4.0000  STAGES
CORR. EFF. =  95.1246
CORRECTED PRECIPITATION RATE PARAMETER =    8.64
```

Figure 21 (continued).

```
CHARGING RATES FOR SUB-MICRON PARTICLES FROM SUBROUTINE CHARGN

INCREMENT NO.      Q/QSATE FOR INDICATED PARTICLE SIZES
   0.2500E-06   0.3500E-06   0.4500E-06   0.5500E-06   0.7000E-06   0.9000E-06
 1  0.7880        0.8013       0.8090       0.8125       0.8134       0.8106
 2  0.9128        0.9358       0.9507       0.9585       0.9615       0.9574
 3  0.9702        1.0046       1.0276       1.0393       1.0438       1.0383
 4  1.0078        1.0515       1.0791       1.0919       1.0954       1.0876
 5  1.0344        1.0871       1.1171       1.1298       1.1316       1.1213
 6  1.0562        1.1158       1.1471       1.1591       1.1593       1.1467
 7  1.0744        1.1384       1.1698       1.1808       1.1791       1.1644
 8  1.0906        1.1579       1.1892       1.1993       1.1960       1.1793
 9  1.1052        1.1750       1.2061       1.2153       1.2105       1.1922
10  1.1184        1.1903       1.2211       1.2294       1.2234       1.2035


CHARGE ACCUMULATED ON SUBMICRON PARTICLES EACH INCREMENT

INCREMENT        CHARGE FOR INDICATED PARTICLE SIZES
       0.2500E-06    0.3500E-06    0.4500E-06    0.5500E-06    0.7000E-06    0.9000E-06
  1   0.32145E-17   0.51457E-17   0.76030E-17   0.10577E-16   0.15992E-16   0.24967E-16
  2   0.37237E-17   0.60093E-17   0.89353E-17   0.12478E-16   0.18905E-16   0.29490E-16
  3   0.39577E-17   0.64514E-17   0.96577E-17   0.13530E-16   0.20523E-16   0.31980E-16
  4   0.41112E-17   0.67525E-17   0.10142E-16   0.14215E-16   0.21538E-16   0.33500E-16
  5   0.42197E-17   0.69808E-17   0.10499E-16   0.14707E-16   0.22250E-16   0.34539E-16
  6   0.43085E-17   0.71656E-17   0.10781E-16   0.15089E-16   0.22794E-16   0.35321E-16
  7   0.43826E-17   0.73106E-17   0.10994E-16   0.15372E-16   0.23164E-16   0.35864E-16
  8   0.44487E-17   0.74359E-17   0.11177E-16   0.15612E-16   0.23515E-16   0.36324E-16
  9   0.45082E-17   0.75459E-17   0.11335E-16   0.15821E-16   0.23802E-16   0.36721E-16
 10   0.45623E-17   0.76439E-17   0.11476E-16   0.16005E-16   0.24054E-16   0.37070E-16
STOP  011111
$END
```

Figure 21 (continued).

SECTION IV
RESULTS

COAL-FIRED POWER BOILERS

This section presents results obtained from the computer model using input data representative of conditions encountered for coal-fired power boilers. Table 3 describes the source of the more important input parameters. These input data will serve to illustrate the trends predicted by the model and will also provide an indication of the approximate plate area requirements which may be expected for various control efficiencies as a function of conditions. Coal-fired power boilers were chosen to illustrate the use of the model because this is the most extensive application area for electrostatic precipitators and the only one in which appropriate data are available.

Implicit in the use of the current density-resistivity relationship of Figure 18, curve 3, is the assumption that the electric field in the deposited dust layer is sufficiently low to prevent the occurrence of back corona or excessive sparking. The selection of dielectric constant values of 6.0 and 100 for the low and high current densities, respectively, may be justified on the basis of resistivity. For a resistivity of 2×10^{11} ohm-cm, curve 3 of Figure 18 indicates a current density of 5×10^{-9} amps/cm^2 may be used. Particles with such a resistivity would behave as a dielectric, and a dielectric constant of 6 may be used to approximate the dielectric behavior of fly ash under high resistivity conditions.[34] For the current density values of 20 and 40×10^{-9} amps/cm^2, resistivity values from Figure 18 are 5×10^{10} ohm-cm and 2.5×10^{10} ohm-cm, respectively. White[35] indicates that particles with resistivity in this range may be considered

Table 3. Input Data for Figures 22 through 28.

Data Element	Data
Particle size distribution	Histogram from Figure 16
Current-voltage	Typical 150°C curve, Figure 19
Current density-resistivity relationship	Curve 3 of Figure 18
Dust loading	9.16 grams/m^3
Dust density	2.27 grams/cm^3
Dielectric constant	6.0 for current density of 5x10^{-9} amps/cm^2 100 for current density of 20 and 40x10^{-9} amps/cm^2
Gas ion mobility	2.2 cm^2/(volt-sec) at 150°C 3.35 cm^2/(volt-sec) at 370°C
Precipitator dimensions	Length 11 m Plate to plate spacing 22.8 cm Plate area 28930 m^2 Inlet cross sectional area 301 m^2 Corona wire radius .135 cm Corona wire spacing in direction of gas flow 20 cm
Gas viscosity	2.2x10^{-5} kg/(m-sec) 2.8x10^{-5} at 370°C
Charge subroutine selection	CHARGN (SRI model)

as conductors for purposes of calculating particle charge values. The use of a dielectric constant value of 100 is equivalent to assuming that the particle is behaving as a conductor.

There is considerable uncertainty in the value of gas ion mobility which should be used in the program. The value reported in the literature[36] for oxygen ions in air at room temperature is about 2.2 $cm^2/(volt\text{-}sec)$. If temperature were the only variable influencing the gas ion mobility, the value of 2.2 $cm^2/(volt\text{-}sec)$ would be increased in going from 20°C to 150°C by the ratio of the absolute temperatures. However, the presence of fine particulate and small amounts of highly electronegative gases with low mobilities in flue gases would be expected to lower the overall effective ion mobility by a significant amount. Since there is no rigorous procedure for calculating effective mobility under these conditions, the value to be used in the program was estimated by using the room temperature value for oxygen. The program estimates the effects of particulate on the effective mobility as described in Section II. For the calculations at 370°C, the mobility value of 2.2 $cm^2/(volt\text{-}sec)$ was increased by the ratio of the absolute temperature change from 150°C in order to indicate the trend caused by the temperature change. The selection of an appropriate value for ion mobility is important because of the influence the value has on the calculated electric field at the plate and the value of particle charge.

Figure 22 gives the effective, i.e., length averaged migration velocities obtained by the program for the indicated current densities and temperatures. These results do not include the correction factors discussed previously.

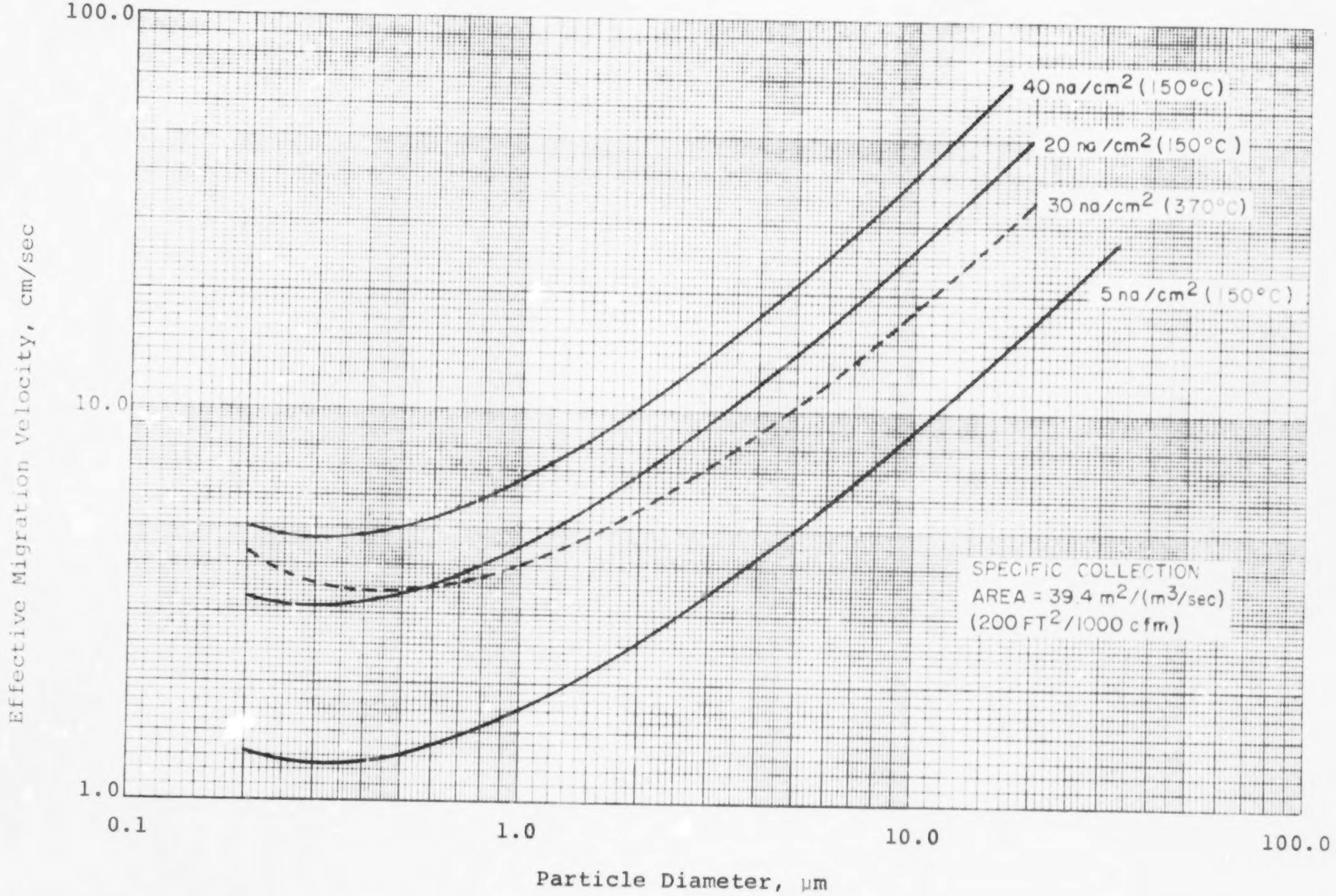

Figure 22. Effective Migration Velocity as a Function of Current Density and Particle Size.

The specific collection area (SCA) influences the effective migration velocities through the residence time which is available for particle charging. With larger SCA's, more residence time is allowed, and the w_e values will increase. This variation is most significant for the lower values of current density (10 nanoamps/cm^2 or less). Since low current densities generally require SCA's higher than 39.4 m^2/(m^3/sec) in order to meet design efficiency levels, the values indicated on Figure 22 for 5 nanoamps/cm^2 will be conservative from the standpoint of particle charging dynamics.

Note that high temperature operation results in a significant decrease in w_e values for comparable current densities. This is a consequence of the differing voltage-current characteristics, and the changes in physical properties of the gas with increasing temperature. The practical implication of this trend is that for comparable values of resistivity, current density, and size distribution, higher SCA's will be required for a given collection efficiency. However, if the dust resistivity severely limits the allowable current density, the relative potential advantage for high temperature operation is indicated by a comparison of the high temperature w_e curve with the low temperature curve at a current density of 5 nA/cm^2.

Figure 23 gives a comparison of effective migration velocity values obtained from the computer program with those obtained from inertially-determined fractional efficiency measurements on a coal-fired power boiler. The computed w_e values are somewhat higher than those given in Figure 22 because of the change in SCA. The value of 55.7 m^2/(m^3/sec) from Figure 23 represents conditions during the test period. In addition to the theoretical predictions, Figure 23 shows the effect of correcting for a gas velocity standard deviation (σ_g) of 0.25 using the empirical relationship given in Section II. The

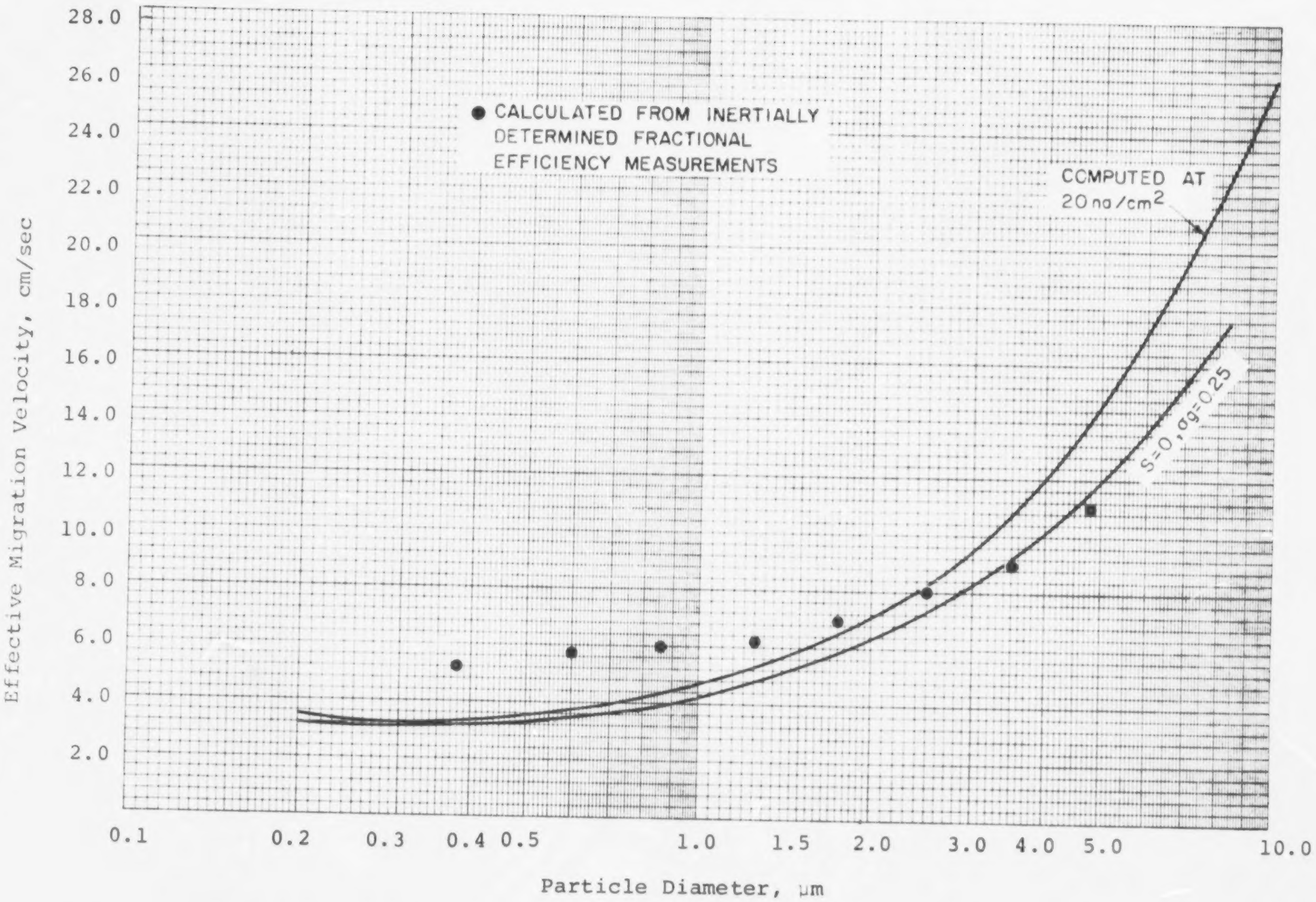

Figure 23. Effective Migration Velocities for a Full-Scale Precipitator on a Coal-Fired Boiler (SCA = 55.7 $m^2/(m^3/sec)$.

indication that S=0 means that no corrections for reentrainment or sneakage losses were made. A comparison of the w_e values in Figure 23 indicates that the theoretical predictions are low for the particle diameters below 2.0 μm diameter and high for larger particles. Possible causes for this are (1) the under-prediction of fine particle collection due to particle concentration gradients and (2) under-prediction of large particle penetration due to reentrained agglomerates. Due to limitations in the measurement technique, no data are available for particle diameters larger than 5.0 μm. Figure 24 shows the fractional efficiency data from which the w_e values of Figure 23 were calculated.

Figures 25 through 28 present results obtained from the program in terms of overall mass efficiency as a function of SCA for current densities of 5, 20, and 40 nanoamps/cm^2 at 150°C, and for a current density of 30 nanoamps/cm^2 at 370°C. Also given are test results obtained under conditions approximating the electrical conditions represented by the given values of current density. A comparison of the limited amount of applicable test data with the computed results indicates that the theoretically-predicted overall mass efficiencies are higher than those obtained from the field measurements. The measurements were taken with sampling techniques which insured that essentially all of the particulate mass larger than 0.3 μm diameter was captured by the sampling device. The use of the empirical correction factors discussed in Section II reduces the computed values of overall mass collection efficiency to the range of values obtained from the field measurements.

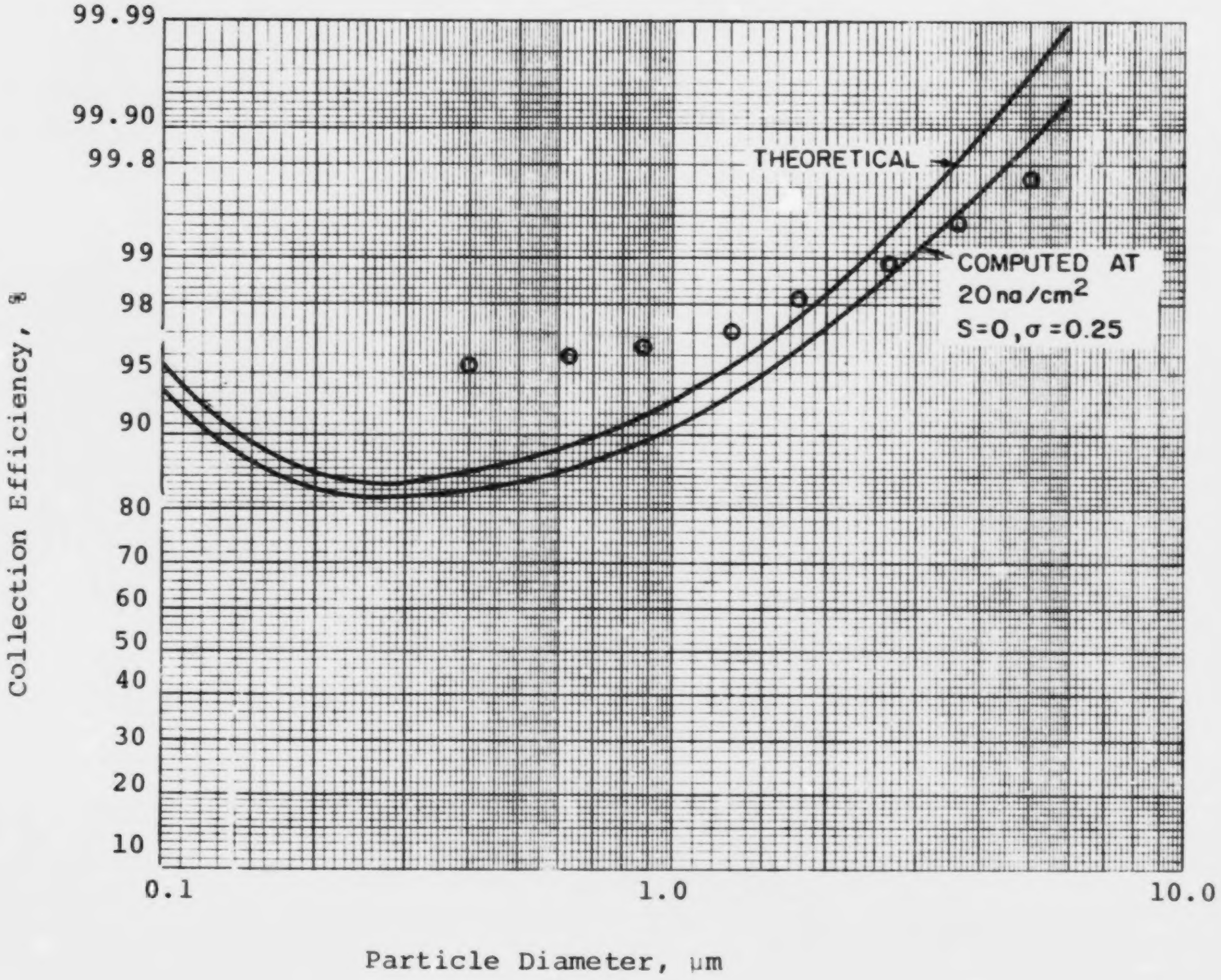

Figure 24. Fractional Collection Efficiencies for a Full-Scale Precipitator on a Coal-Fired Power Boiler.

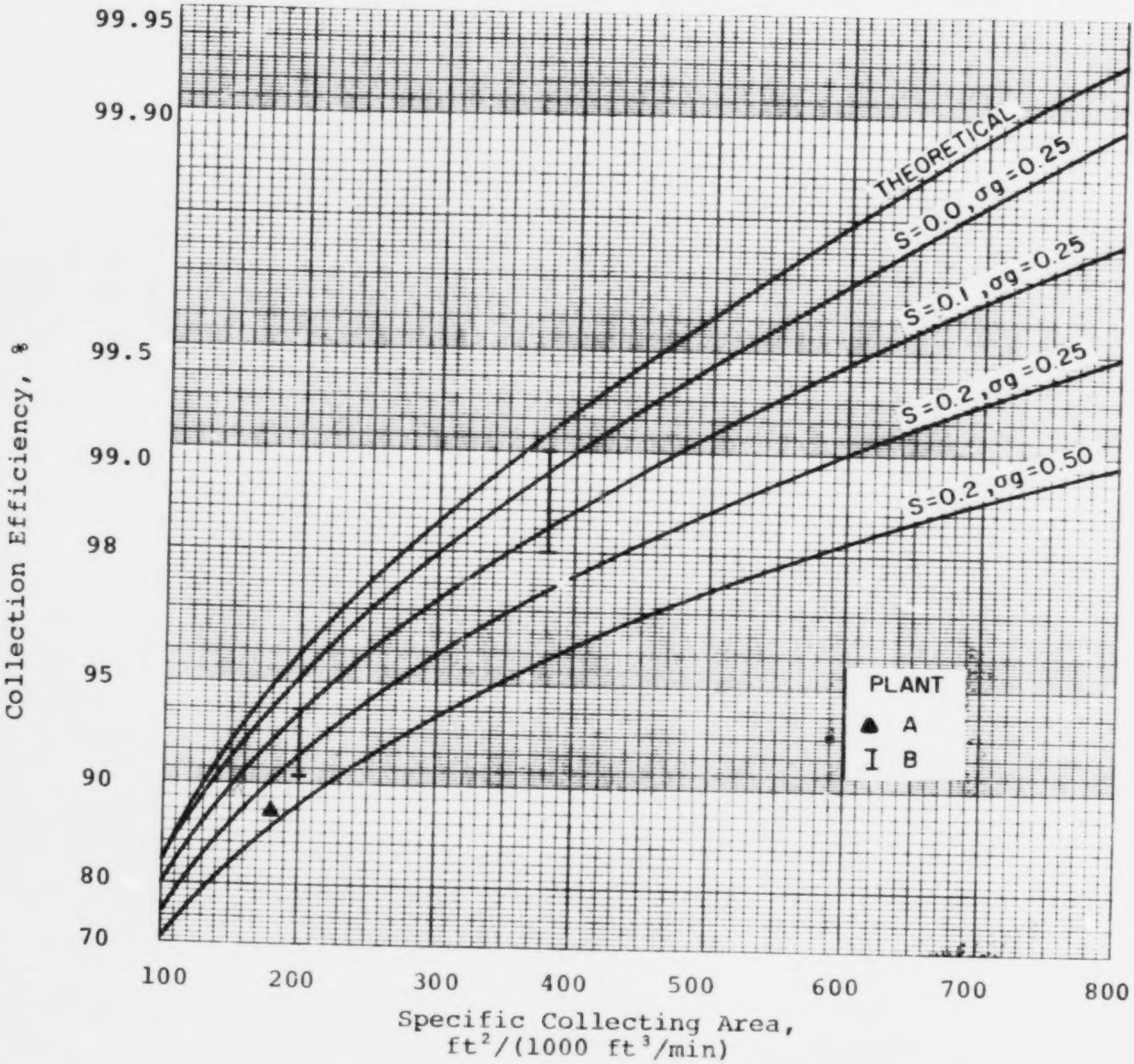

Figure 25. Computed Performance Curves at 5 nA/cm².

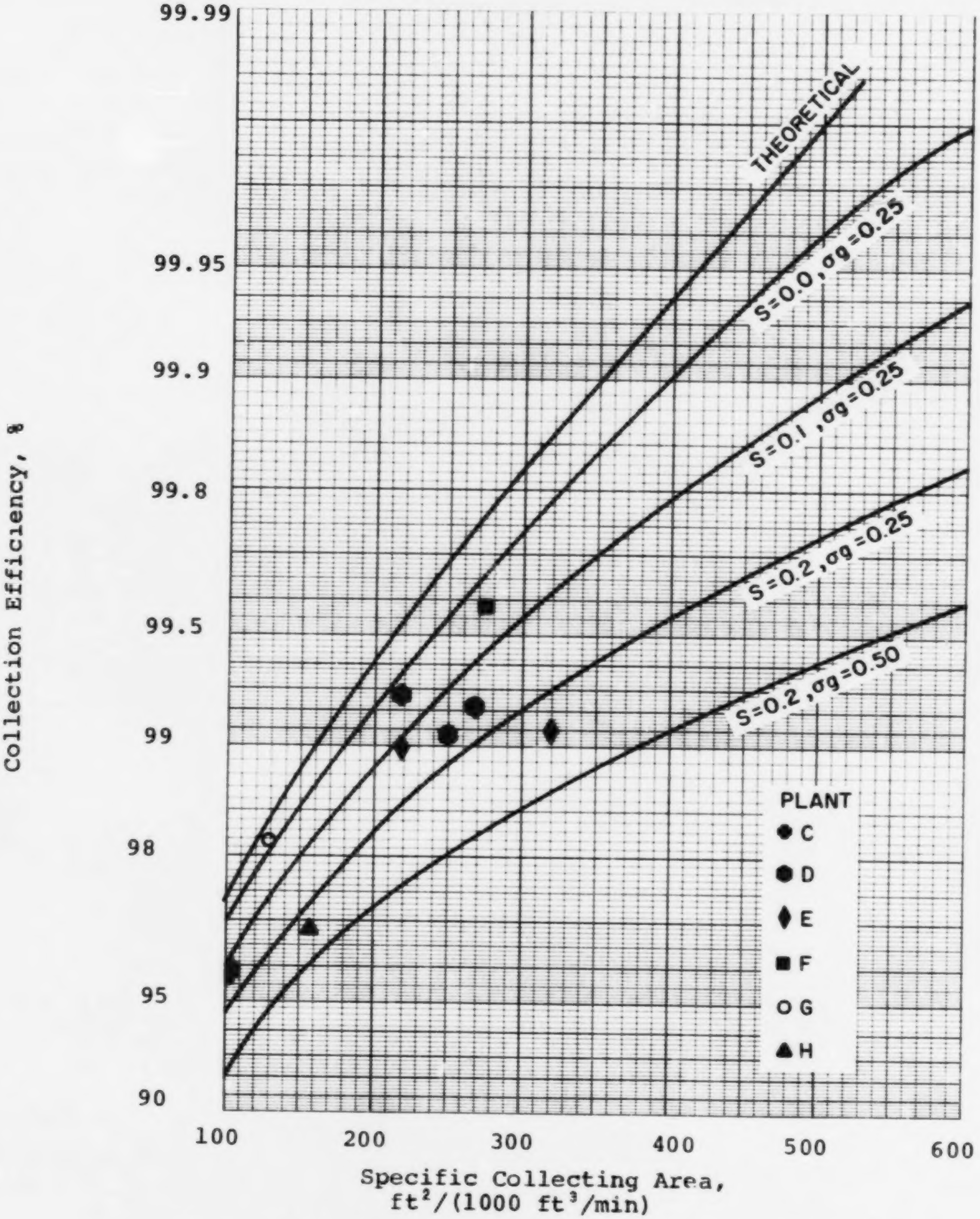

Figure 26. Computed Performance Curves at 20 nA/cm^2.

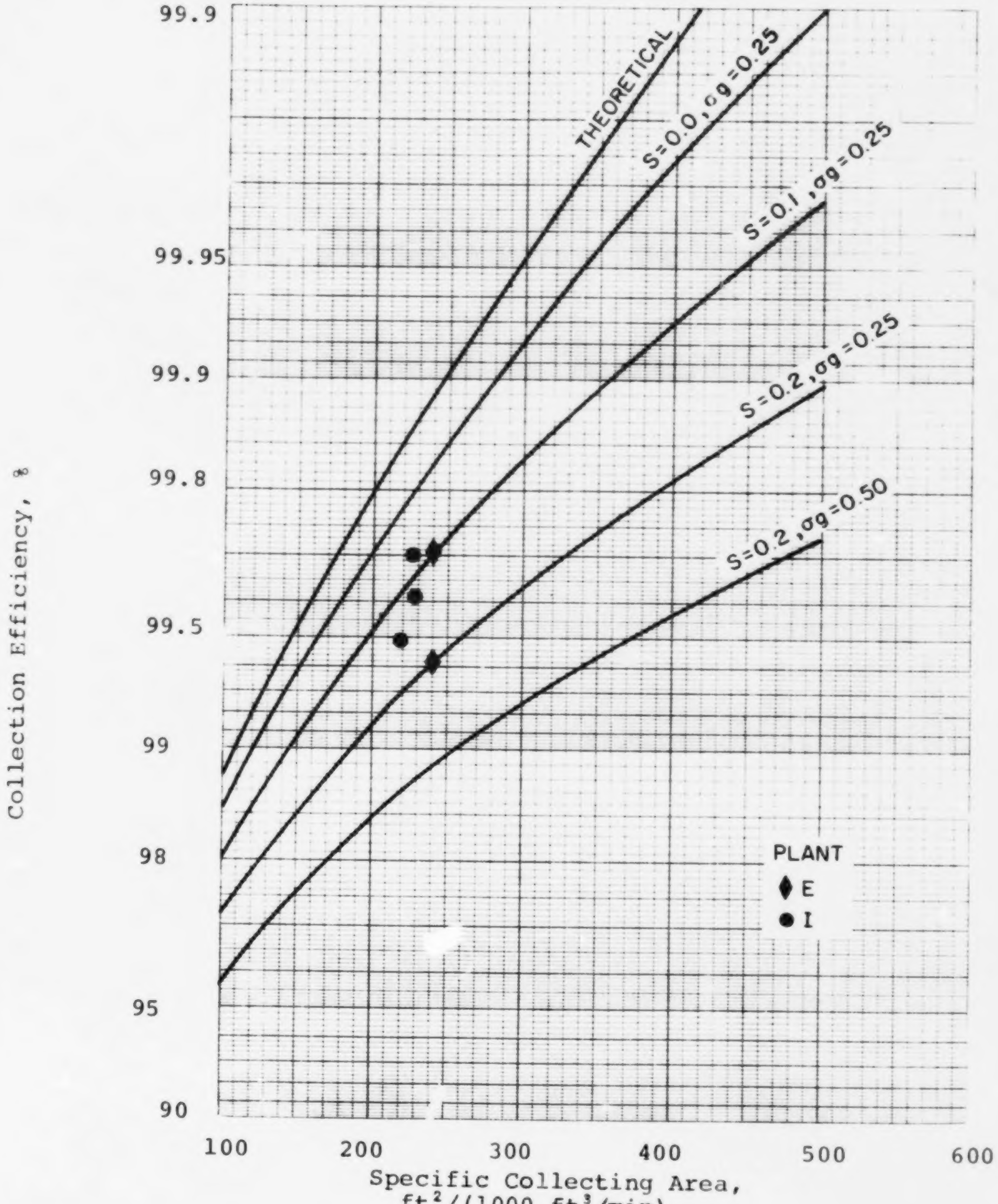

Figure 27. Computed performance curves at 40 nA/cm^2.

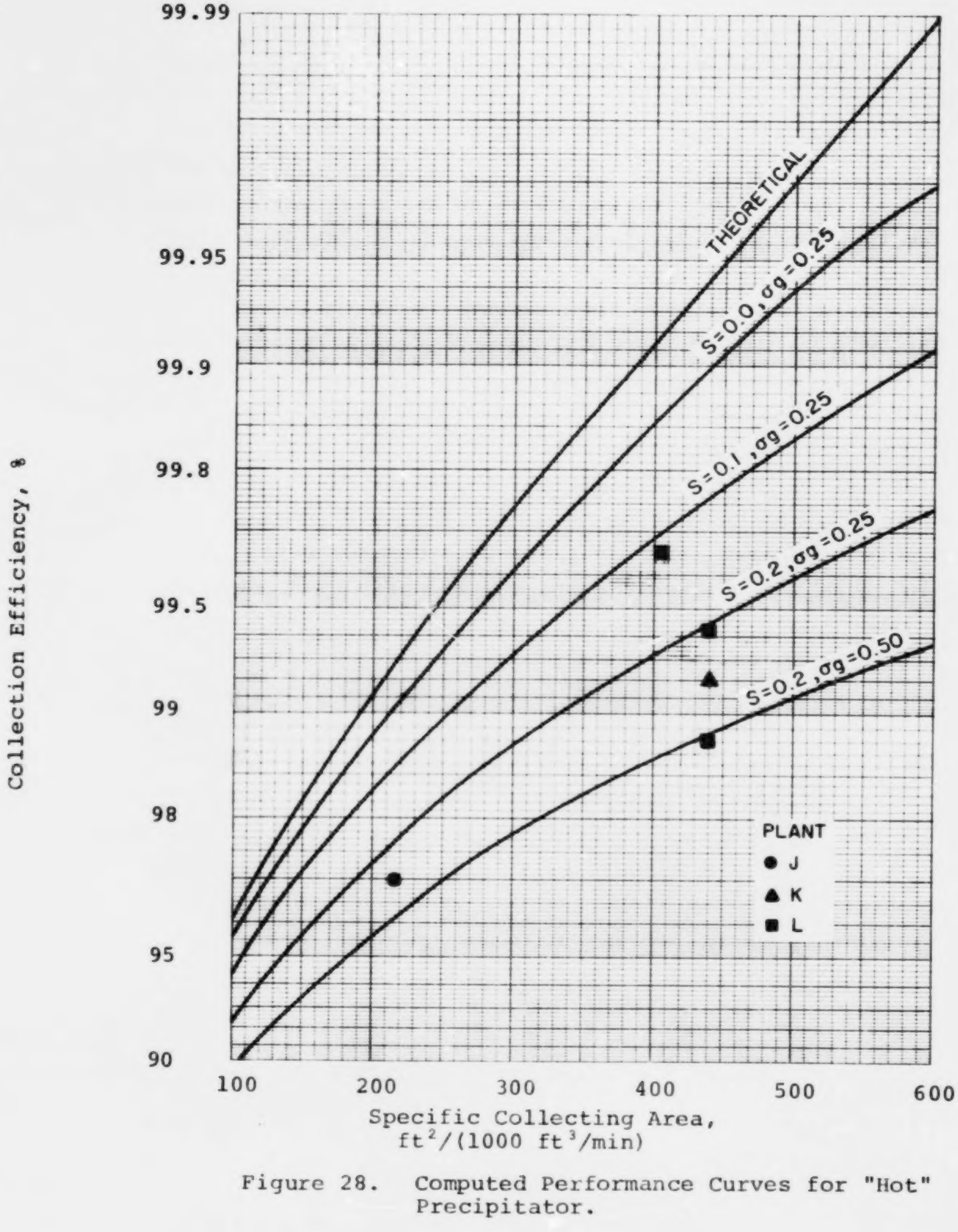

Figure 28. Computed Performance Curves for "Hot" Precipitator.

Reentrainment and sneakage effects were combined by assuming that the indicated fractional losses per stage occurred over four effective stages. Note that high efficiency (greater than 99.5%) precipitators operating on the low temperature side of the air heater fall reasonably close to the computed line obtained with $\sigma_g = 0.25$ and $S=0.1$. A gas velocity distribution with a standard deviation of 0.25 is generally considered to be a good distribution for a full-scale unit. The computed results show that a poor distribution ($\sigma_g = 0.5$) seriously degrades performance. The detrimental effects of sneakage and reentrainment are also indicated in the decrease of computed performance resulting from variations in the parameter S. A more definitive comparison of computed with measured performance than currently available data permit is expected to result from future test programs on full scale precipitators in which the gas velocity distributions will be determined and efforts will be made to quantify losses caused by reentrainment and sneakage.

It should be noted that these calculations do not directly indicate the increasing reentrainment that would occur with high gas velocities. In general, gas velocities greater than about 1.5 m/sec (5 ft/sec) will be accompanied by excessive reentrainment. Therefore, variations in SCA for a given precipitator installation which are achieved by gas flow variation may require different correction factors for reentrainment at each value of SCA.

EFFECT OF VARIATIONS IN SIZE DISTRIBUTION

Since the particle size distribution has a major effect on the results obtained from the computer model, it is of interest to examine the program output for differing size distributions with other conditions held constant.

Particle size distributions are characterized by two or more parameters. One parameter is a measure of the mean particle diameter, and the other parameter or parameters are measures of the polydispersity of the size distribution. As is shown below, both the mean particle diameter and the distribution polydispersity affect the overall efficiency-SCA relationship. Thus, the common practice of specifying a mean particle diameter is not adequate for sizing an ESP.

Log normal particle size distributions with mass median diameters of 25, 10, 5, and 2 μm were used as input data to the computer model. The geometric standard deviation of the distribution was held constant at 2.8. Other important input data were: a current density of 20 nanoamps/cm^2, an applied voltage of 33 kV, $\sigma_g = 0.25$, and $S = 0.1$ over 4 stages. The results from these computer simulations are given in Figure 29. As would be expected, the computed performance is a strong function of the mass median diameter of the distributions.

Figure 30 presents results obtained from the program using a log normal particle size distribution with a mass median diameter of 10.0 μm and geometric standard deviations of 1.0 (a monodisperse distribution), 2.0 and 5.0. Other input data were identical to those used in generating the curves for Figure 29. Figure 30 shows that predicted performance decreases with increasing values of particle size standard deviations. This decrease results from the influence of the increasing proportions of fine particulate which are present with the

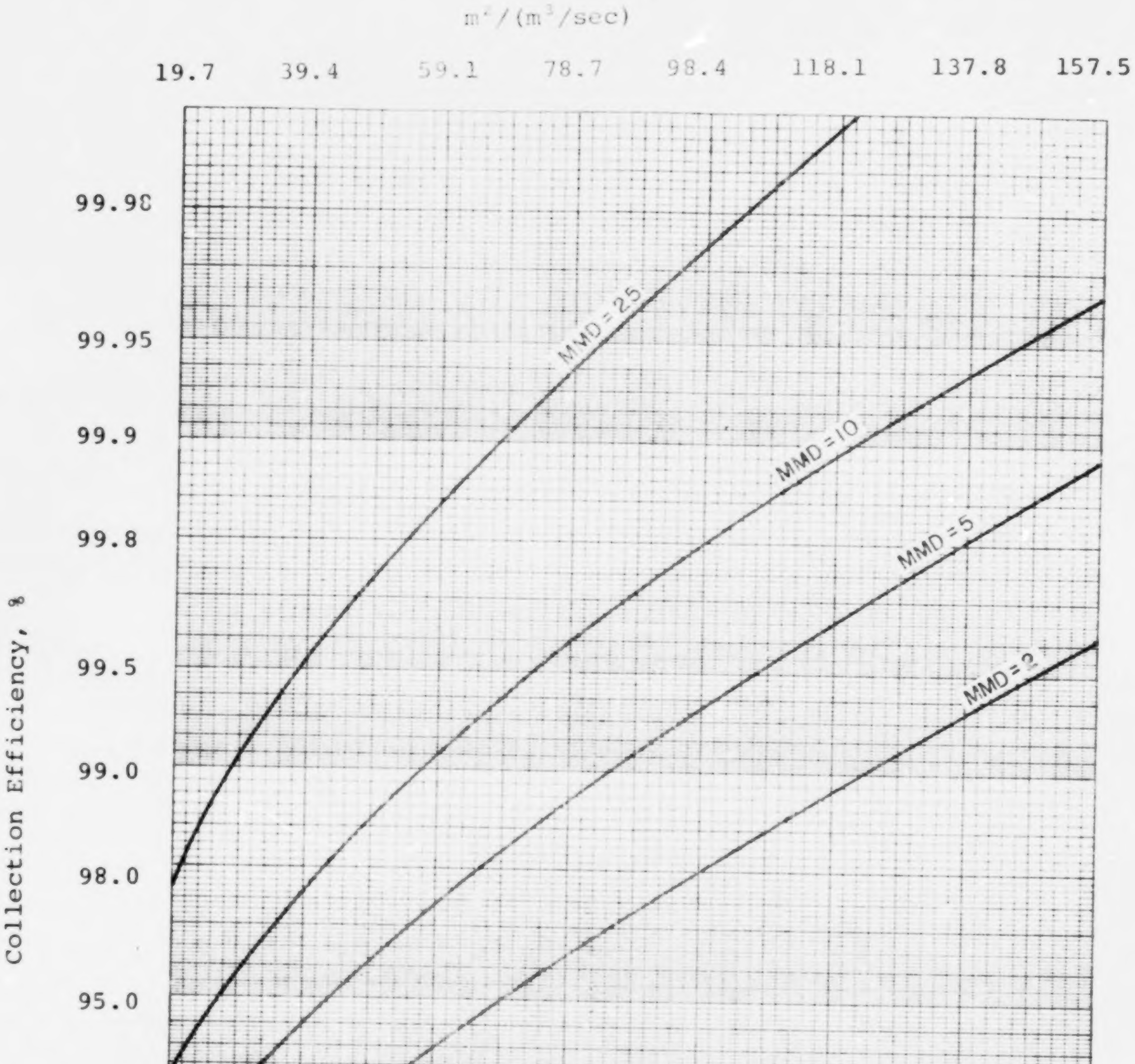

Figure 29. Effect of Mass Median Diameter on Computed Performance ($\sigma_p = 2.8$).

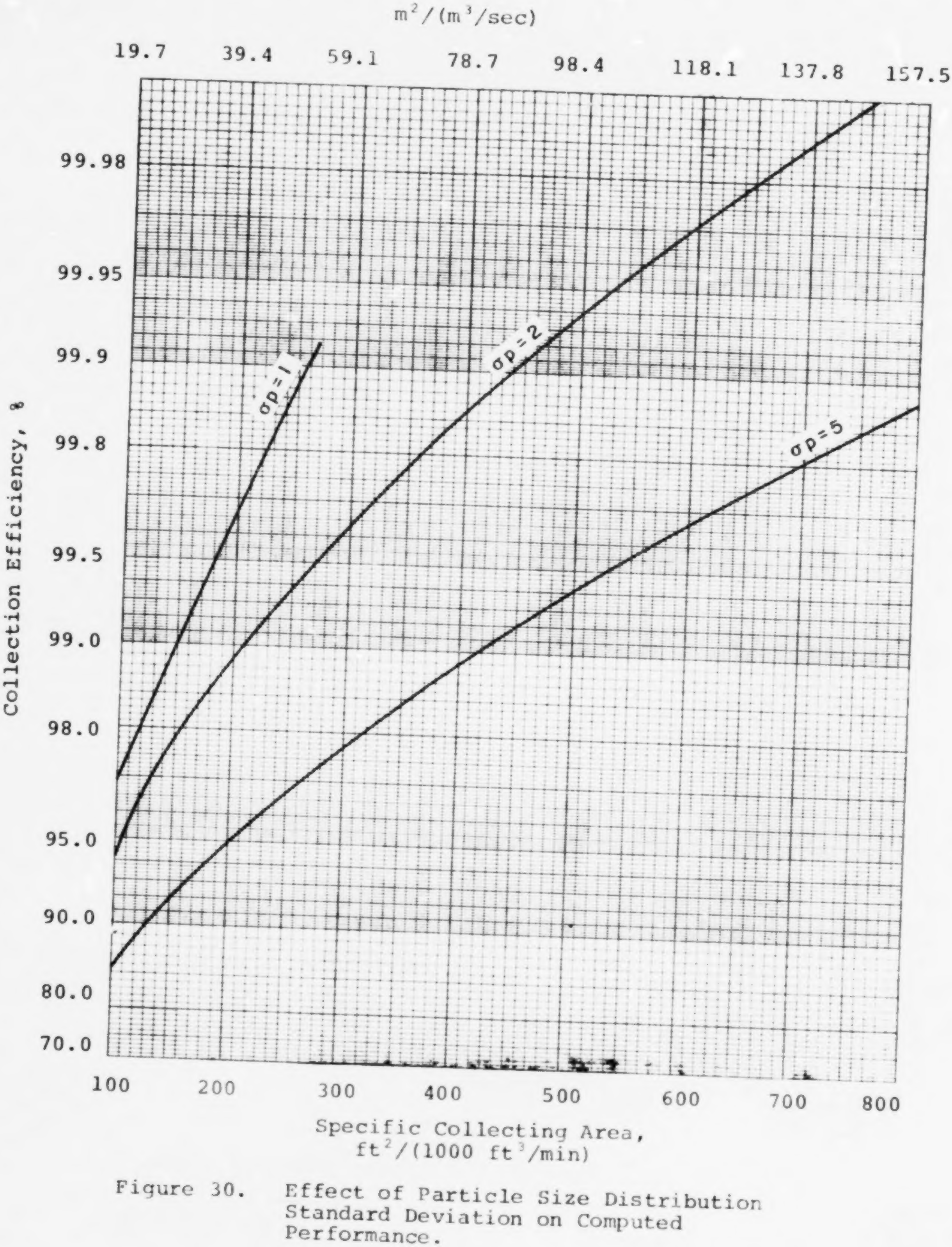

Figure 30. Effect of Particle Size Distribution Standard Deviation on Computed Performance.

larger values of standard deviation. Note that the use of a monodisperse distribution with a diameter of 10.0 μm gives results vastly different from those obtained with realistic values of standard deviation.

SECTION V
COLLECTION OF HIGH RESISTIVITY DUST

The degradation of precipitator performance resulting from the presence of a layer of high resistivity dust on the collection electrode has been well documented in the literature and will not be repeated here. When such a dust is to be collected by electrostatic precipitation, there are two basic design philosophies available: a) alter the resistivity of the dust by introducing chemical conditioning agents or by changing the operating temperature, or b) enlarge the collection area so that the design collection efficiency can be obtained under the electrical constraints imposed by the high resistivity dust. As the preceding sections have indicated, the required collection area increases as dust resistivity increases above values in the 10^{10} ohm-cm range. The uncertainty in the required collection area also increases because the sensitivity of precipitator performance to resistivity changes is greater in the high resistivity region. Therefore, a direct economic comparison of the options is often misleading because of the uncertainty associated with option b) and the economic consequences that may result from undersizing the precipitator. It is advisable, therefore, to consider methods for lowering resistivity into the 10^{10} ohm-cm range rather than attempt to design for adverse electrical operating conditions. In the following paragraphs, a brief description of the methods for lowering resistivity will be given.

CHANGE IN OPERATING TEMPERATURE

The shape of the resistivity-temperature relationship for most fly ash from coal-fired boilers suggests that acceptable resistivities may be obtained by operating the precipitator either below about 110°C or above 345°C. Low temperature operation has been successfully used to solve a high resistivity problem,[37] but this method has not found widespread acceptance. The principal disadvantages of this approach are that resistivity in the low temperature range is quite sensitive to changes in fuel composition, and extensive in-situ resistivity-temperature data are required to give a firm basis for design. A more detailed[38] discussion of the low temperature approach is given elsewhere.

For the coal-fired power boiler application, high temperature operation of the precipitator ahead of the air preheater is becoming the most commonly used solution to the high resistivity problem. The principal advantages of this approach are that, at temperatures in the 315 to 370°C range, resistivities above 10^{11} ohm-cm are rarely, if ever, encountered, and the sensitivity of precipitator operation to fuel composition is reduced. However, Bickelhaupt[39] has shown that in the high temperature range considerable differences in resistivity occur due to differences in the chemical composition of the ashes. Therefore, resistivity measurements in the design temperature range are desirable prior to selecting a collection area in order to determine whether the dust resistivity will impose any constraints on the electrical operating conditions. The principal disadvantages of high temperature operation are the increased gas volume which must be treated and the lowered operating voltages which result from the decreased gas density.

USE OF CHEMICAL CONDITIONING AGENTS

Compounds which have been injected in the flue gas ahead of the precipitator with the objective of lowering ash resistivity include sulfuric acid vapor, sulfur trioxide, ammonia, ammonium sulfate, sulfamic acid, and ammonium bisulfate. Of these compounds, the most commonly used are sulfuric acid vapor and sulfur trioxide. It has been established that proper injection of these compounds can effectively "condition" fly ash by lowering resistivity to an acceptable range.[40] The principal disadvantages are the possibility of introducing a sulfuric acid aerosol into the atmosphere, and the difficulties of maintaining a chemical processing plant to properly inject the corrosive and toxic compounds. However, the use of conditioning agents can be economically attractive when compared with the cost of the other methods of lowering dust resistivity. Detailed discussions of the use of conditioning agents are given by Dismukes.[41,42]

An additional conditioning agent is currently under investigation. Bickelhaupt[29] has shown that the resistivity of the fly ash is related to the alkali metal content, principally sodium, of the ash. Preliminary tests show that the addition of trace quantities of sodium oxide to the coal feed also results in a reduction of the resistivity. However, the limited experience with this material precludes a definitive analysis of the long-term effect on the behavior of a precipitator.

In general, the use of conditioning agents has not been widely accepted. The primary usage has been for overcoming high resistivity problems in existing precipitators.

SECTION VI
ESTIMATION OF PROGRAM OUTPUT

It is recognized that the general usefulness of the computer model would be enhanced by presenting the results in a form which would not require access to a computer. In principle, it is feasible to prepare tables or plots of effective migration velocities for a range of particle sizes, precipitator operating conditions, and electrode geometries. With this information, and assumed values of the parameters which estimate the effect of non-ideal conditions, the computed overall mass efficiency for a given specific collecting area may be obtained by integrating over the size distribution of the particulate to be collected. However, since the procedures used for estimating the effects of reentrainment, gas sneakage, and gas velocity distribution have not been evaluated by comparison with field data specifically relating to these factors, the state of development of the model is such that the preparation of generalized nomographs is not justified at this time. Therefore, this section presents a procedure which will enable the reader to estimate the program output for electrical conditions and an electrode geometry which pertain primarily to the largest application area for electrostatic precipitators - the collection of fly ash from coal-fired power boilers. If the actual conditions in the precipitator to be simulated differ from those on which the following estimation procedure is based, the computer program should be utilized to generate the appropriate relationships between collection efficiency and specific collection area.

The estimation procedure involves the solution of the equation:

$$\eta_0 = 1 - \int_{a_1}^{a_2} [\exp - (w_e'A/Q)] \, f(a)da \quad , \qquad (64)$$

where η_0 is the overall mass collection fraction, w_e' is the apparent migration velocity of particles of radius a corrected for reentrainment, sneakage, and gas velocity distribution, A/Q is the specific collecting area, f(a) is the fraction of the particles between a and a + da, and a_1 and a_2 are the lower and upper limits on the size distribution. Since w_e' is a function of both a and the ideal collection fraction, numerical techniques are required to evaluate equation 64 even if the functional form of f(a) is known.

Since the particle size distribution is changing as a function of length within the computer model, it is more convenient to represent the size distribution in the program as a histogram. Equation 64 then becomes

$$\eta_0 = 1 - \sum_{i=1}^{N} [\exp(-w_e' A/Q)] Z_i \qquad (65)$$

where Z_i is the fraction of the particles in the ith radius interval. The following is an outline of the procedure to be followed in estimating the program output, and Table 5 gives an example of the manual calculation using a histogram representation of the size distribution.

If equation 65 is to be used:

(1) Construct a histogram representation of the particle size distribution to be collected. The distribution should be obtained from in-situ techniques. The size distribution histogram illustrated in Table 5 was obtained from Figure 16.

(2) Determine the resistivity of the dust to be collected at the operating temperature from direct measurements at the source or from measurements at the same temperature on a similar source.

(3) Estimate the allowable current density from curve 3 of Figure 18. If the allowable current density is less than 5.0 nanoamps/cm^2 (i.e., a resistivity above 2x10^{11} ohm-cm) it is recommended that consideration be given to the procedures for lowering dust resistivity to an acceptable range. Estimating precipitator plate area requirements for dust resistivities in the 10^{11}-10^{12} ohm-cm range is difficult because relatively small variations in resistivity can significantly alter performance through sparking or back corona.

(4) Determine the effective migration velocities from Table 4, which is a tabulation of the data plotted in Figure 22. For the illustration in Table 5, a current density of 20 nanoamps/cm^2 is used.

(5) Select values of gas velocity standard deviation and reentrainment/sneakage. For the illustration in Table 5, $\sigma g = 0.25$, $S = 0.1$, $N = 4$.

(6) Estimate the specific collection area required for the desired overall mass efficiency from Figures 25 through 28. For the example in Table 5, an SCA value of 39.4 m^2/(m^3/sec) is obtained from Figure 26 for a reduced efficiency of 98.9.

(7) Calculate the collection efficiency for each particle size from the relationship:

$$E = 100\ \eta = 100\ (1.0 - \exp\ (-A_p\ w_e/Q)),$$

where E = collection efficiency of each particle size

η = collection fraction of each particle size

Table 4. THEORETICAL EFFECTIVE MIGRATION VELOCITIES AS A FUNCTION OF CURRENT DENSITY, TEMPERATURE, AND PARTICLE DIAMETER

	Effective Migration Velocity, cm/sec			
Temperature, °C	150	150	150	370
Current Density, nA/cm^2	5	20	40	30
Particle Diameter, µm				
0.2	1.335	3.312	5.023	4.195
0.3	1.249	3.136	4.758	3.550
0.55	1.377	3.500	5.307	3.478
0.85	1.620	4.167	6.313	3.839
1.25	1.957	5.109	7.739	4.448
1.75	2.375	6.297	9.542	5.251
2.50	2.987	8.080	12.250	6.468
3.50	3.784	10.469	15.874	8.085
4.50	4.569	12.885	19.532	9.697
6.00	5.739	16.572	25.100	12.117
8.50	7.699	22.868	34.357	16.186
12.50	10.903	33.582	49.610	22.831
20.00	17.070	53.298	78.785	34.726
27.50	23.316	73.065	108.005	47.414

TABLE 5. EXAMPLE OF MANUAL CALCULATION OF OVERALL COLLECTION EFFICIENCY

Size Distribution Histogram Diameter µm	Size Distribution Histogram % of total	w_e m/sec	Theoretical Collection Efficiency %	F	B	w_e' m/sec	Reduced Collection Efficiency %
0.15	0.077	0.0380	77.596	1.078	1.134	0.0311	70.561
0.20	0.0729	0.0312	72.813	1.071	1.131	0.0273	65.855
0.30	0.1875	0.0314	70.861	1.069	1.130	0.0260	63.972
0.55	0.3625	0.0350	74.752	1.074	1.132	0.0288	67.747
0.85	0.375	0.0417	80.575	1.083	1.137	0.0338	73.574
1.25	0.725	0.0511	86.587	1.094	1.144	0.0408	79.925
1.75	0.950	0.0630	91.592	1.106	1.153	0.0494	85.656
2.5	2.25	0.0808	95.830	1.122	1.168	0.0616	91.146
3.5	2.50	0.105	98.370	1.141	1.191	0.0770	95.158
4.5	2.50	0.129	99.370	1.160	1.218	0.0912	97.230
6.0	4.75	0.166	99.852	1.187	1.267	0.110	98.685
8.5	6.75	0.229	99.987	1.234	1.373	0.135	99.500
12.5	9.75	0.336	99.9998	1.312	1.631	0.157	99.793
20.0	13.75	0.533	99.9999	1.326	1.683	0.239	99.992
27.5 and larger	55.0	0.730	99.9999	1.326	1.683	0.328	99.9997
			E_0 = 99.41				E_0' = 98.88

Conditions:

SCA = 39.37 $m^2/(m^3/sec)$, or 200 $ft^2/(1000\ ft^3/min)$

Current Density = 20×10^{-9} $amps/cm^2$

$\sigma_g = 0.25$

S = 0.1

A_p/Q = specific collecting area, [39.4 $m^2/m^3/sec$) for the illustrated example]

w_e = effective migration velocity of the particle size under consideration.

Truncate all collection fractions greater than 0.999999 at this value.

(8) If the theoretical value of overall collection efficiency is desired, it may be obtained from:

$$E_0 = \sum_{i=1}^{n} Z_i \eta_i ,$$

where E_0 = overall mass efficiency, %

n = number of particle sizes

Z_i = % of mass represented by particle size i

η_i = collection fraction of particle size i.

This is an optional step.

(9) Calculate the corrected migration velocities, w_e', for each particle size as follows:

a) Evaluate "F", the empirical correction factor for gas velocity standard deviation from

$$F = 1.0 + 0.766\ \eta\sigma_g^{1.786} + 0.0755\ \sigma_g \ln\left(\frac{1}{1-\eta}\right).$$

For the example, $\sigma_g = 0.25$.

b) Evaluate B from

$$B = \frac{\ln (1-\eta)}{N_s \ln [S + (1-S)(1-\eta)^{1/N_s}]} \quad . ,$$

For the example, $S = 0.1$ and $N_s = 4.0$.

c) Calculate w_e' from

$$w_e' = \frac{w_e}{F \bullet B} \quad .$$

(10) Calculate a reduced collection efficiency for each particle size from

$$E' = 100\eta' = 100\ (1.0 - \exp\ (-A_p w_e'/Q)),$$

(11) Obtain the reduced overall efficiency from

$$E_0' = \sum_{i=1}^{n} \quad (Z_i\ \eta'_i)$$

where E_0' = reduced overall mass efficiency

η'_i = reduced collection fraction of particle size i.

The variation in theoretical and reduced overall collection efficiency with variation in specific collection area may be obtained by repeating the above procedure from steps 6 through 11. Note that the overall efficiencies computed in Table 4 agree with the computed values shown in Figure 26. For higher values of SCA, the manual estimating procedure will produce somewhat lower overall efficiencies than would the computer program, since the effect of increased particle charging time is not accounted for with the manual calculations.

SECTION VII
ACKNOWLEDGEMENTS

The subroutine for calculating electric fields in wire plate geometry was written and evaluated by Dr. Wallace B. Smith, Head of the Physics Section. Procedures for representing non-ideal effects were developed by Mr. Norman L. Francis, Research Engineer. The assistance of Dr. Leslie Sparks, EPA Project Officer, is also gratefully acknowledged.

SECTION VIII
REFERENCES

1. Oglesby, Sabert, Jr. and Grady B. Nichols. A Manual of Electrostatic Precipitator Technology, Vol. I (August 1970). Southern Research Institute, Birmingham, Alabama.

2. Leutert, G. and B. Böhlen. The Spatial Trend of Electric Field Strength and Space Charge Density in Plate Type Electrostatic Precipitators. Staub. 32(7), July 1972.

3. Cooperman, P. A Theory for Space Charge Limited Currents with Application to Electrostatic Precipitators. Trans. AIEE, Vol. 79. March 1960.

4. Penney, G. W. and R. E. Matick. A Probe Method for Measuring Potential in DC Corona. AIEE Preprint. 1957.

5. Tassicker, O. J. Aspects of Forces on Charged Particles in Electrostatic Precipitators. Ph.D. Dissertation. Dept. of Elec. Eng., Wallongong Univ. College, Univ. of S. Wales. July 1972.

6. Peek, F. W. Dielectric Phenomena in High Voltage Engineering, 3rd Edition. New York, McGraw-Hill, 1929.

7. White, H. J. Particle Charging in Electrostatic Precipitation. AIEE., 1186-1191, May 1951.

8. Hewitt, G. H. The Charging of Small Particles for Electrostatic Precipitation. AIEE. 76:300-306, July 1957.

9. Fuchs, N., I. Petrjanoff, and B. Rotzeig. On the Rate of Charging of Droplets by an Ionic Current. Trans. Faraday Society, 1131-1138, February 1936.

10. Liu, Benjamin Y. H., Kenneth T. Whitby, and Henry H. S. Yu. Diffusion Charging of Aerosol Particles at Low Pressures. J. Appl. Phys. 38(4):1592-1597, March 1967.

11. Mirzabekyan, G. Z. Aerosol Charging in a Corona-Discharge Field. Strong Electric Fields in Technological Processes (Ion Technology). V. I. Popkov, Ed. Energy Publishing House, Moscow, 20-38, 1969.

12. Murphy, A. T., F. T. Adler, and G. W. Penney. A Theoretical Analysis of the Effects of an Electric Field on Charging of Fine Particles. AIEE Trans., 318-326, September 1959.

13. Stratton, J. A. Electromagnetic Theory. McGraw Hill Book Co., Inc., New York, p. 205, 1941.

14. White, H. J. Industrial Electrostatic Precipitation. Addison-Wesley Publishing Co., Inc., Reading, Mass. 1963. p. 138.

15. Liu, B. Y. H. and Hsu-Chi Yeh. On the Theory of Charging of Aerosol Particles in an Electric Field. J. Appl. Phys., 39(3):1396-1402, February 1968.

16. Pauthenier, M. M. and M. Moreau-Hanot. Charging of Spherical Particles in an Ionizing Field. Journal de Physique et Le Radium (Paris)., 3(7):590-613, 1932.

17. Hildebrand, F. B. Introduction to Numerical Analysis. McGraw-Hill, 1956.

18. White, op.cit., p. 157.

19. Fuchs, N. A. The Mechanics of Aerosols. New York, The Macmillan Co., 1964. Chap. 2.

20. Deutsch, W. Ann. der Physik. 68:335 (1922).

21. White, op.cit., p. 165.

22. White, op.cit., p. 185.

23. Nichols, G. B. and J. P. Gooch. An Electrostatic Precipitator Performance Model. Southern Research Institute, Birmingham, Alabama. Contract CPA 70-166. The Environmental Protection Agency, Research Triangle Park, N. C., July 1972.

24. White, op.cit., p. 238-293.

25. Preszler, L. and T. Lajos. Uniformity of the Velocity Distribution Upon Entry into an Electrostatic Precipitator of a Flowing Gas. Staub. 32(11):1-7, November 1972.

26. Smith. W. B., K. M. Cushing, and J. D. McCain. Particulate Sizing Techniques for Control Device Evaluation. Southern Research Institute, Birmingham. Alabama. Contract 68-02-0273. The Environmental Protection Agency, Research Triangle Park, N. C. July 12, 1974, p. 10.

27. Ibid. Appendix A.

28. Nichols, G. B. Techniques for Measuring Fly Ash Resistivity. Final Report to Environmental Protection Agency. Contract No. 68-02-1303. Southern Research Institute, August 5, 1974.

29. Bickelhaupt, Roy E. Volume Resistivity-Fly Ash Composition Relationship. Environ. Science and Technology. 9(4), April 1975.

30. Penney, G. W. and S. Craig. Pulsed Discharges Preceding Sparkover at Low Voltage Gradients. AIEE Winter General Meeting. New York. January 29-February 3, 1961.

31. Pottinger. J. F. The Collection of Difficult Material by Electrostatic Precipitation. Australian Chem. Process Eng. 20(2):17-23, February 1967.

32. Hall, Herbert J. Trends in Electrical Precipitation of Electrostatic Precipitators. Proceedings of the Electrostatic Precipitator Symposium. Birmingham, Alabama. Paper I-C. February 23-25, 1971.

33. White, op.cit., p. 219-230.

34. Tassicker, O. J. The Temperature and Frequency Dependence of the Dielectric Constant of Power Station Fly Ash. Staub-Reinhalt. Luft. 31(8), August 1971.

35. White, op.cit., p. 146.

36. White, op.cit., p. 135.

37. Berube, D. T. Low Gas Temperature Solution to High Resistivity Ash Problem. Proceedings of the Electrostatic Precipitator Symposium, Paper II-E, Birmingham, Alabama, February 23-25, 1971.

38. Nichols, G. B. and J. P. Gooch, op.cit., p. 103.

39. Bickelhaupt, Roy E., op.cit.

40. Dismukes, Edward B. A Study of Resistivity and Conditioning of Fly Ash. Final Report to Environmental Protection Agency, Contract No. CPA 70-149. Southern Research Institute. February 1972.

41. Dismukes, op.cit.

42. Dismukes, Edward B. Conditioning of Fly Ash with Sulfur Trioxide and Ammonia. Report to Tennessee Valley Authority and Environmental Protection Agency (EPA Contract No. 68-02-1303). Southern Research Institute. January 1975.

SECTION IX
APPENDICES

APPENDIX 1

Listing of FORTRAN Variables

```
C                   LIST OF VARIABLES AND UNITS FOR THE MAIN PROGRAM OF THE
C                   ELECTROSTATIC PRECIPITATOR PERFORMANCE MODEL
C   PI              VALUE OF THE CONSTANT PI
C   E               ELEMENTARY CHARGE UNIT (COULOMBS)
C   U               ION MOBILITY (METER **2/VOLT-SECOND)
C   BC              BOLTZMANN'S CONSTANT (JOULES/DEGREES KELVIN)
C   EPS             RELATIVE DIELECTRIC CONSTANT
C   EPSO            PERMITTIVITY OF FREE SPACE (COULOMB **2/NEWTON-METER **2)
C   VIS             GAS VISCOSITY (KILOGRAM/METER-SECOND)
C   NS              NUMBER OF DIFFERENT PARTICLE SIZES IN THE PARTICLE SIZE
C                   DISTRIBUTION
C   JLY             NUMBER OF PARTICLE SIZES LESS THAN 1,0 MICRON IN DIAMETER
C   DIAM(J)         DIAMETERS OF THE DIFFERENT PARTICLE SIZES (MICRONS--METERS)
C   RAD(J)          RADII OF THE DIFFERENT PARTICLE SIZES (METERS)
C   PCNT(J)         PERCENTAGE OF PARTICLES PER CUBIC METER OF GAS OF EACH SIZE
C                   EXPRESSED AS A DECIMAL
C   ITL             NAME OF PLANT - IDENTIFICATION
C   LK              INDICATOR WHICH PRINTS THE INPUT DATA IF EQUAL TO 0 AND DOES
C                   NOT PRINT IF EQUAL TO 1
C   A               COLLECTION PLATE AREA (FEET**2---METERS **2)
C   VG              GAS FLOW RATE (FEET**3SECOND---METERS**3/SECOND)
C   VO              APPLIED VOLTAGE (VOLTS)
C   TC              TOTAL CURRENT (AMPERES)
C   DL              DUST LOAD (GRAINS/FEET**3---KILOGRAMS/METER**3)
C   WL              TOTAL LENGTH OF CORONA WIRE (FEET---METERS)
C   AC              CORONA WIRE RADIUS (INCHES---METERS)
C   B               WIRE TO PLATE SPACING (INCHES---METERS)
C   PL              LENGTH OF PRECIPITATOR (FEET---METERS)
C   VGAS            GAS VELOCITY (FEET/SECOND---METERS/SECOND)
C   ETAO            DESIGN EFFICIENCY - STATED EFFICIENCY
C   DD              DUST DENSITY (KILOGRAM/METER**3)
C   RHO             DUST RESISTIVITY (OHM-METER)
C   X               POWER OF 10 OF THE VALUE OF THE RESISTIVITY
C   TEMP            TEMPERATURE (DEGREES FARENHEIT---DEGREES RANKINE)
C   P               PRESSURE (ATMOSPHERES)
C   SY              1/2 WIRE TO WIRE SPACING (INCHES---METERS)
C   SNUCK           PERCENTAGE OF SNEAKAGE AND REENTRAINMENT IN EACH SECTION
C                   EXPRESSED AS A DECIMAL
C   ZIGGY           STANDARD DEVIATION OF THE VELOCITY DISTRIBUTION
C   ZNUMS           NUMBER OF STAGES OVER WHICH SNEAKAGE AND REENTRAINMENT OCCUR
C   NN              NUMBER OF POINTS SPECIFIED FOR USE IN THE RUNGE-KUTTA SCHEME
C                   FOR SOLVING THE DIFFERENTIAL EQUATION DESCRIBING THE SRI
C                   CHARGING THEORY
C   NUMINC          NUMBER OF POINTS SPECIFIED FOR USE IN THE SIMPSON'S RULE
C                   INTEGRATION OVER THETA IN REGION II OF THE SRI CHARGING THEORY
C   NCALC           DIRECTS THE PROGRAM TO USE THE SRI CHARGING THEORY WHEN IT IS
C                   EQUAL TO 0 AND TO OBTAIN A CHARGING RATE BY ADDING THE FIELD
C                   CHARGING RATE AND THE DIFFUSIONAL CHARGING RATE WHEN IT IS
C                   EQUAL TO 1
C   VAVG            ROOT MEAN SQUARE VELOCITY OF THE IONS (CENTIMETERS/SECOND)
C   VAVC            ROOT MEAN SQUARE VELOCITY OF THE IONS (METERS/SECOND)
C   NUMSEC          NUMBER OF LINEAR ELECTRICAL SECTIONS IN THE PRECIPITATOR
C   LSECT(I)        LENGTHS OF THE DIFFERENT LINEAR SECTIONS EXPRESSED TO THE
C                   NEAREST FOOT (FEET)
C   AS(I)           COLLECTION PLATE AREAS IN THE DIFFERENT LINEAR SECTIONS
C                   (FEET**2---METERS**2)
C   VOS(I)          APPLIED VOLTAGES IN THE DIFFERENT LINEAR SECTIONS (VOLTS)
C   TCS(I)          CURRENT IN THE DIFFERENT LINEAR SECTIONS (AMPERES)
C   WLS(I)          WIRE LENGTH IN THE DIFFERENT LINEAR SECTIONS (FEET TO METERS)
C   ACS(I)          CORONA WIRE RADII IN THE DIFFERENT LINEAR SECTIONS
```

```
C                   (INCHES TO METERS)
C   WS(I)           WIRE TO PLATE SPACING IN THE DIFFERENT LINEAR SECTIONS
C                   (INCHES TO METERS)
C   NWS(I)          NUMBER OF CORONA WIRES IN THE DIFFERENT LINEAR SECTIONS
C   SYS(I)          1/2 THE WIRE TO WIRE SPACING IN THE DIFFERENT LINEAR SECTIONS
C                   (INCHES TO METERS)
C   NF              NUMBER OF INCREMENTS INTO WHICH THE PRECIPITATOR IS DIVIDED
C   DV              DUST VOLUME (METER**3(DIRT)/METER**3 (GAS))
C   SX              WIRE TO PLATE SPACING (METERS)
C   VERGE           INITIAL ESTIMATE OF THE SPACE CHARGE DENSITY AT THE CORONA WIRE
C                   TO START THE CALCULATION OF THE ELECTRIC FIELD AT THE PLATE
C                   (COULOMBS/METER**3)
C   VOL(J)          TOTAL VOLUME FOR EACH PARTICLE SIZE PER CUBIC METER OF GAS
C                   (METER**3/METER**3(GAS))
C   W               WEIGHT OF DUST PER SECOND PASSING INTO THE PRECIPITATOR
C                   (KILOGRAMS/SECOND)
C   CD              CURRENT DENSITY AT THE PLATE (AMPERES/METER**2)
C   ET              ELECTRIC FIELD IN DEPOSIT (VOLTS/METER)
C   CL              CURRENT PER METER OF CORONA WIRE (AMPERES/METER)
C   TDK             TEMPERATURE (DEGREES KELVIN)
C   ZMFP            MEAN FREE PATH (METERS)
C   NPRINT          INDICATOR WHICH DESIGNATES WHEN TO PRINT CERTAIN RESULTS
C   X               EXPONENT IN THE DEUTSCH EQUATION FOR THE STATED EFFICIENCY
C   DXS(J)          TOTAL NUMBER OF PARTICLES REMOVED PER CUBIC METER OF GAS IN
C                   EACH SIZE RANGE (NUMBER/METER**3)
C   XNO(J)          NUMBER OF PARTICLES PER CUBIC METER OF GAS IN EACH SIZE RANGE
C                   AT THE START OF EACH INCREMENT (NUMBER/METER**3)
C   ONO(J)          INITIAL NUMBER OF PARTICLES PER CUBIC METER OF GAS IN EACH SIZE
C                   RANGE (NUMBER/METER**3)
C   ETAPF           EFFICIENCY PER 0.3 METER INCREMENT
C   SW              TOTAL AMOUNT OF MATERIAL REMOVED (KILOGRAMS)
C   DW(I)           AMOUNT OF MATERIAL REMOVED PER INCREMENT ON A TOTAL WEIGHT
C                   BASIS (KILOGRAMS)
C   ZWT             TOTAL WEIGHT OF DUST PER CUBIC METER OF GAS REMOVED UP TO A
C                   GIVEN INCREMENT (KILOGRAMS/METER**3)
C   ROVRI           RATIO OF TOTAL SPACE CHARGE DENSITY TO IONIC SPACE CHARGE
C                   DENSITY IN THE I-TH INCREMENT
C   ERAVG           AVERAGE CHARGING FIELD (VOLTS/METER)
C   KK              DO LOOP INDEX USED IN THE RUNGE-KUTTA SCHEME FOR SOLVING THE
C                   DIFFERENTIAL EQUATION DESCRIBING THE SRI CHARGING THEORY
C                   (KK=1)
C   ECHARG          ELEMENTARY CHARGE UNIT (STATCOULOMBS)
C   BOLTZ           BOLTZMANN'S CONSTANT (ERGS/DEGREES KELVIN)
C
C                   CONSTANT FACTORS USED IN THE SRI CHARGING THEORY
C   RATIO
C   G
C   VC
C   FACTRC
C   COEFFC
C   TINC            TIME INTERVAL FOR THE GAS TO TRAVEL ONE FOOT (SECONDS)
C   INDEX           INDICATOR WHICH KEEPS TRACK OF HOW MANY FEET THE CALCULATION IS
C                   INTO A GIVEN SECTION
C   NSECT           INDICATOR WHICH KEEPS TRACK OF WHICH SECTION THE CALCULATION IS
C                   IN
C   NCOOP           INDICATOR WHICH TELLS THE PROGRAM TO MAKE CERTAIN CALCULATIONS
C                   AT THE START OF EACH SECTION
C   NWIRE           NUMBER OF WIRES
C   EZERO           AVERAGE CHARGING FIELD (STAT-VOLTS/CENTIMETER)
C
```

```
C                       FACTORS USED IN THE SRI CHARGING THEORY
C   W
C   WR
C   WG
C   FID                 FREE ION DENSITY (NUMBER/METER**3)
C   SUM                 ION DENSITY REQUIRED TO CHARGE ALL PARTICLES TO SATURATION
C                       IN A GIVEN INCREMENT (NUMBER/METER**3)
C   TMFP                CORRECTION FACTOR ADDED TO PARTICLE RADIUS FOR CALCULATION OF
C                       SATURATION CHARGE (METERS)
C   QSAT(J)             NUMBER OF CHARGES FOR SATURATION FOR A PARTICULAR PARTICLE
C                       SIZE
C   AFID                AVERAGE FREE ION DENSITY (NUMBER/METER**3)
C   AVGFID              AVERAGE FREE ION DENSITY (NUMBER/CENTIMETER**3)
C   TIMEI               TIME AT THE START OF A GIVEN INCREMENTAL LENGTH (SECONDS)
C   TIMEF               TIME AT THE END OF A GIVEN INCREMENTAL LENGTH (SECONDS)
C   H                   INCREMENT SIZE TAKEN IN THE RUNGE-KUTTA SCHEME (SECONDS)
C   RSIZE               RADIUS OF A GIVEN PARTICLE SIZE (CENTIMETERS)
C   SCHARG              NUMBER OF CHARGES AT SATURATION FOR A GIVEN PARTICLE SIZE
C
C                       FACTORS USED IN THE SRI CHARGING THEORY
C   DCONST
C   CONST
C   S
C   V
C   ECONST
C   FCONST
C   FACTRE
C   COEFF
C   XCD                 CURRENT DENSITY (NANO-AMPERES/METER**2)
C   UEC                 EFFECTIVE MOBILITY (METERS**2/VOLT-SECOND)
C   EPLT                ELECTRIC FIELD AT THE PLATE (VOLTS/METER)
C   SKIP                ELECTRIC FIELD AT THE PLATES IN THE PREVIOUS INCREMENT
C                       (VOLTS/METER)
C   SIGMA               DIFFERENCE BETWEEN THE RATIO OF THE TOTAL SPACE CHARGE
C                       DENSITY TO IONIC SPACE CHARGE DENSITY IN THE (I+1)-TH AND I-TH
C                       INCREMENTS
C   VCOOP(I,J)          ARRAY CONTAINING THE VALUES OF COOPERMAN'S POTENTIAL AT THE
C                       DIFFERENT POINTS IN THE GRID
C   CVERGE              CONVERGED VALUE OF THE SPACE CHARGE DENSITY AT THE WIRE IN
C                       CALCULATING THE ELECTRIC FIELD AT THE PLATE (COULOMBS/METER
C                       **3)
C   PROT                TOTAL CHARGE DENSITY DUE TO PARTICLES THAT REMAIN AFTER PASSING
C                       THROUGH A GIVEN INCREMENT (COULOMBS/METER**3)
C   WT                  TOTAL WEIGHT OF DUST PER CUBIC METER OF GAS REMOVED IN ALL
C                       PARTICLE SIZE RANGES IN A GIVEN INCREMENT (KILOGRAMS/METER**3)
C   CTIME               TOTAL TIME PARTICLES HAVE SPENT IN PRECIPITATOR AFTER THE
C                       I-TH INCREMENT (SECONDS)
C   NII                 DO LOOP INDEX FOR CHARGING SUBROUTINE ON WHICH THE DO LOOP
C                       OVERTIME INCREMENTS TERMINATES
C   NII1                DO LOOP INDEX FOR CHARGING SUBROUTINE ON WHICH THE DO LOOP
C                       OVERTIME INCREMENTS BEGINS
C   NII2                DO LOOP INDEX FOR CHARGING SUBROUTINE ON WHICH THE DO LOOP
C                       OVERTIME INCREMENTS TERMINATES
C   Q(J)                CHARGE ON EACH PARTICLE AFTER THE I-TH INCREMENT (COULOMBS)
C   XCD(I,J)            ARRAY WHICH CONTAINS THE CHARGE ON EACH PARTICLE SIZE AFTER
C                       EACH INCREMENT (COULOMBS)
C   EMV(J)              ARRAY CONTAINING THE EFFECTIVE MIGRATION VELOCITIES FOR THE
C                       DIFFERENT PARTICLE SIZES IN A GIVEN INCREMENT (METERS/SECOND)
C   X                   EXPONENT IN THE DEUTSCH EQUATION FOR THE CALCULATED EFFICIENCY
C   EFF                 CALCULATED EFFICIENCY FOR A GIVEN PARTICLE SIZE RANGE
```

```
C  DXNO            NUMBER OF PARTICLES PER CUBIC METER OF GAS REMOVED FOR A
C                  PARTICULAR SIZE RANGE (NUMBER/METER**3)
C  DXS(J)          TOTAL NUMBER OF PARTICLES PER CUBIC METER OF GAS REMOVED IN
C                  EACH SIZE RANGE AFTER I INCREMENTS (NUMBER/METER**3)
C  WS(J)           TOTAL WEIGHT OF DUST PER CUBIC METER OF GAS REMOVED IN EACH
C                  SIZE RANGE IN A GIVEN INCREMENT (KILOGRAMS/METER**3)
C  ZTW             PARTIAL SUM OF THE WEIGHT OF DUST REMOVED PER CUBIC METER OF
C                  GAS UP TO THE J-TH PARTICLE SIZE IN A GIVEN INCREMENT
C                  (KILOGRAMS/METER**3)
C  CZA             RATIO OF THE PARTIAL SUM OF THE WEIGHT OF DUST REMOVED PER
C                  CUBIC METER OF GAS UP TO THE J-TH PARTICLE SIZE IN A GIVEN
C                  INCREMENT TO THE TOTAL WEIGHT OF DUST REMOVED PER CUBIC METER
C                  OF GAS IN A GIVEN INCREMENT
C  CZB             RATIO OF THE PARTIAL SUM OF THE WEIGHT OF DUST REMOVED PER
C                  CUBIC METER OF GAS UP TO THE (J-1)-TH PARTICLE SIZE IN A GIVEN
C                  INCREMENT TO THE TOTAL WEIGHT OF DUST REMOVED PER CUBIC METER
C                  OF GAS IN A GIVEN INCREMENT
C  TL1             DIFFERENCE BETWEEN CZA AND CZB FOR USE IN INTERPOLATING TO
C                  FIND THE MASS MEDIAN DIAMETER OF THE COLLECTED DUST
C  TL2             DIFFERENCE BETWEEN 0.50 AND CZB FOR USE IN INTERPOLATING TO
C                  FIND THE MASS MEDIAN DIAMETER OF THE COLLECTED DUST
C  ZMD             INTERPOLATED MASS MEDIAN DIAMETER OF COLLECTED DUST (METERS)
C  ETC             EFFICIENCY FOR THE ENTIRE PRECIPITATOR LENGTH
C  DIFF            DIFFERENCE BETWEEN THE CALCULATED EFFICIENCY AND STATED
C                  EFFICIENCY
C  ATOTAL          TOTAL COLLECTION PLATE AREA FOR THE PRECIPITATOR
C                  (METERS ** 2)
C  SCOREF          TOTAL EFFICIENCY CORRECTED FOR GAS VELOCITY DISTRIBUTION, GAS
C                  SNEAKAGE, OR REENTRAINMENT
C  X               EFFICIENCY COMPUTED WITHOUT ACCOUNTING FOR GAS VELOCITY
C                  DISTRIBUTION, GAS SNEAKAGE, OR REENTRAINMENT
C  DIA             DIAMETER OF A PARTICULAR PARTICLE SIZE (METERS)
C  EFFSR           RATIO OF THE TOTAL NUMBER OF PARTICLES REMOVED PER CUBIC METER
C                  OF GAS IN A CERTAIN SIZE RANGE TO THE INITIAL NUMBER OF
C                  PARTICLES PER CUBIC METER OF GAS IN THAT SIZE RANGE =
C                  COLLECTION FRACTION WITH NO ACCOUNT FOR GAS VELOCITY
C                  DISTRIBUTION, GAS SNEAKAGE, OR REENTRAINMENT
C  XY              PERCENTAGE OF PARTICLES PER CUBIC METER OF GAS OF EACH SIZE
C                  EXPRESSED AS A PERCENT
C  XEP             COLLECTION FRACTION EFFSR EXPRESSED AS A PERCENT
C  F1              AIR QUALITY FACTOR TO ACCOUNT FOR GAS VELOCITY DISTRIBUTION
C  F2              FACTOR TO ACCOUNT FOR GAS SNEAKAGE AND REENTRAINMENT
C  ZNLFF           FACTOR TO ACCOUNT FOR GAS VELOCITY DISTRIBUTION, GAS SNEAKAGE,
C                  AND REENTRAINMENT
C  WY              EFFECTIVE MIGRATION VELOCITY OF A CERTAIN SIZE RANGE WITHOUT
C                  ACCOUNT FOR GAS VELOCITY DISTRIBUTION, GAS SNEAKAGE, OR
C                  REENTRAINMENT (METERS/SECOND)
C  WYP             EFFECTIVE MIGRATION VELOCITY OF A CERTAIN SIZE RANGE ACCOUNTING
C                  FOR GAS VELOCITY DISTRIBUTION, GAS SNEAKAGE, AND REENTRAINMENT
C                  (METERS/SECOND)
C  COREFF          COLLECTION EFFICIENCY FOR A CERTAIN SIZE RANGE ACCOUNTING FOR
C                  GAS VELOCITY DISTRIBUTION, GAS SNEAKAGE, AND REENTRAINMENT
C  SL              NUMBER OF EFFLUENT PARTICLES PER CUBIC METER OF GAS IN EACH
C                  SIZE RANGE (NUMBER/METER**3)
C  WSL             WEIGHT OF EFFLUENT PARTICLES PER CUBIC METER OF GAS IN EACH
C                  SIZE RANGE (KILOGRAMS/METER**3)
C  WTL             TOTAL WEIGHT OF EFFLUENT PARTICLES PER CUBIC METER OF GAS
C                  (KILOGRAMS/METER**3)
C  ZTW             PARTIAL SUM OF THE WEIGHT OF EFFLUENT DUST PER CUBIC METER
C                  OF GAS UP TO SOME J-TH PARTICLE SIZE (KILOGRAMS/METER**3)
```

```
C   CZA            RATIO OF THE PARTIAL SUM OF THE WEIGHT OF EFFLUENT DUST PER
C                  CUBIC METER OF GAS UP TO SOME J-TH PARTICLE SIZE TO THE
C                  TOTAL WEIGHT OF EFFLUENT DUST PER CUBIC METER OF GAS
C   CZB            RATIO OF THE PARTIAL SUM OF THE WEIGHT OF EFFLUENT DUST PER
C                  CUBIC METER OF GAS UP TO SOME (J-1)-THE PARTICLE SIZE TO THE
C                  TOTAL WEIGHT OF EFFLUENT DUST PER CUBIC METER OF GAS
C   TL1            DIFFERENCE BETWEEN CZA AND CZB FOR USE IN INTERPOLATING TO FIND
C                  THE MASS MEDIAN DIAMETER OF THE EFFLUENT DUST
C   TL2            DIFFERENCE BETWEEN 0.50 AND CZB FOR USE IN INTERPOLATING TO
C                  FIND THE MASS MEDIAN DIAMETER OF THE EFFLUENT DUST
C   ZMDL           INTERPOLATED MASS MEDIAN DIAMETER OF EFFLUENT DUST (METERS)
C   COREFW         PRECIPITATION RATE PARAMETER - CORRECTED EFFECTIVE MIGRATION
C                  VELOCITY (METERS/SECOND)
C   WZ             PRECIPITATION RATE PARAMETER - UNCORRECTED EFFECTIVE MIGRATION
C                  VELOCITY (METERS/SECOND)
C   YY(J)          ARRAY CONTAINING THE FRACTION OF SATURATION CHARGE OBTAINED
C                  IN A PARTICULAR SIZE RANGE AFTER A CERTAIN INCREMENT
```

```
C                       LIST OF VARIABLE NAMES AND UNITS FOR SUBROUTINE CMAN USED IN
C                       THE ELECTROSTATIC PRECIPITATOR PERFORMANCE MODEL
C   VO                  APPLIED VOLTAGE (NEGATIVE OF APPLIED VOLTAGE USED IN
C                       CALCULATIONS) (VOLTS)
C   NX                  NUMBER OF POINTS IN THE X-DIRECTION OF THE GRID
C   NY                  NUMBER OF POINTS IN THE Y-DIRECTION OF THE GRID
C   AX                  INCREMENT USED IN THE X-DIRECTION OF THE GRID
C   SX                  WIRE TO PLATE SPACING (METERS)
C   SY                  1/2 WIRE TO WIRE SPACING (METERS)
C   PI                  VALUE OF THE CONSTANT PI
C   AC                  CORONA WIRE RADIUS (METERS)
C   VCOOP(I,J)          ARRAY CONTAINING COOPERMAN'S VALUE FOR THE POTENTIAL AT
C                       DIFFERENT POINTS IN THE GRID (VOLTS)
C   X                   VALUE OF X USED IN COOPERMAN'S EXPRESSION V(X,Y) FOR THE
C                       POTENTIAL (METERS)
C   Y                   VALUE OF Y USED IN COOPERMAN'S EXPRESSION V(X,Y) FOR THE
C                       POTENTIAL (METERS)
C   M                   SERIES SUM IN COOPERMAN'S EXPRESSION IS TAKEN FROM M TO -M
C                       WHERE M= -1
C   E1                  ARGUMENTS FOR THE HYPERBOLIC COSINE FUNCTIONS IN THE NUMERATOR
C                       OF COOPERMAN'S EXPRESSION
C   F1                  ARGUMENTS FOR THE COSINE FUNCTIONS IN THE NUMERATOR OF
C                       COOPERMAN'S EXPRESSION
C   G1                  ARGUMENTS FOR THE HYPERBOLIC COSINE FUNCTIONS IN THE
C                       DENOMINATOR OF COOPERMAN'S EXPRESSION
C   H1                  ARGUMENTS FOR THE COSINE FUNCTIONS IN THE DENOMINATOR OF
C                       COOPERMAN'S EXPRESSION
C   E2                  HYPERBOLIC COSINE FUNCTIONS IN THE DENOMINATOR OF COOPERMAN'S
C                       EXPRESSION
C   F2                  COSINE FUNCTIONS IN THE NUMERATOR OF COOPERMAN'S EXPRESSION
C   G2                  HYPERBOLIC COSINE FUNCTIONS IN THE DENOMINATOR OF COOPERMAN'S
C                       EXPRESSION
C   H2                  COSINE FUNCTIONS IN THE DENOMINATOR OF COOPERMAN'S EXPRESSION
C   TT                  ARGUMENT FOR THE LOGARITHMIC FUNCTION IN THE NUMERATOR OF
C                       COOPERMAN'S EXPRESSION
C   TB                  ARGUMENT FOR THE LOGARITHMIC FUNCTION IN THE DENOMINATOR OF
C                       COOPERMAN'S EXPRESSION
C   F                   LOGARITHMIC FUNCTION IN THE NUMERATOR OF COOPERMAN'S EXPRESSION
C   G                   LOGARITHMIC FUNCTION IN THE DENOMINATOR OF COOPERMAN'S
C                       EXPRESSION
C   NUM                 SUM IN THE NUMERATOR OF COOPERMAN'S EXPRESSION
C   DENOM               SUM IN THE DENOMINATOR OF COOPERMAN'S EXPRESSION
```

```
C                     LIST OF VARIABLES AND UNITS FOR THE SUBROUTINE EFIELD USED
C                     IN THE ELECTROSTATIC PRECIPITATOR PERFORMANCE MODEL
C   UEQ               EFFECTIVE MOBILITY (METERS**2/VOLT-SECOND)
C   CD                CURRENT DENSITY AT THE PLATE (AMPERES/METER**2)
C   AC                CORONA WIRE RADIUS (METERS)
C   VO                APPLIED VOLTAGE (NEGATIVE OF APPLIED VOLTAGE USED IN
C                     CALCULATIONS) (VOLTS)
C   SX                WIRE TO PLATE SPACING (METERS)
C   SY                1/2 WIRE TO WIRE SPACING (METERS)
C   AEPLT             AVERAGE ELECTRIC FIELD AT THE PLATE (VOLTS/METER)
C   VCOOP(I,J)        ARRAY CONTAINING COOPERMAN'S VALUES FOR THE POTENTIAL AT THE
C                     DIFFERENT POINTS IN THE GRID (VOLTS)
C   VERGE             INITIAL ESTIMATE OF THE SPACE CHARGE DENSITY AT THE WIRE TO
C                     START THE CALCULATION OF THE ELECTRIC FIELD AT THE PLATE
C                     (COULOMBS/METER**3)
C   CVERGE            CONVERGED VALUE OF THE SPACE CHARGE DENSITY AT THE WIRE IN
C                     CALCULATING THE ELECTRIC FIELD AT THE PLATE (COULOMBS/METER**3)
C   QZERO             INITIAL ESTIMATE OF THE SPACE CHARGE DENSITY AT THE WIRE TO
C                     START EACH ITERATION IN THE CALCULATION OF THE ELECTRIC
C                     FIELD AT THE PLATES (COULOMBS/METER**3)
C   PI                VALUE OF THE CONSTANT PI
C   EPSO              PERMITTIVITY OF FREE SPACE (COULOMB**2/NEWTON-METER**2)
C   NX                NUMBER OF POINTS IN THE Y-DIRECTION OF THE GRID
C   MAXJ              UPPER LIMIT THAT THE CALCULATED CURRENT DENSITY CAN NOT EXCEED
C                     (AMPERES/METER**2)
C   MINJ              LOWER LIMIT THAT THE CALCULATED CURRENT DENSITY CAN NOT FALL
C                     BELOW (AMPERES/METER**2)
C   NX1               ONE LESS THAN THE TOTAL NUMBER OF POINTS IN THE X-DIRECTION
C                     OF THE GRID
C   NY1               ONE LESS THAN THE TOTAL NUMBER OF POINTS IN THE Y-DIRECTION
C                     OF THE GRID
C   Z                 INDICATOR WHICH COUNTS THE NUMBER OF TIMES THE CALCULATION
C                     ITERATES DUE TO LACK OF CONVERGENCE IN THE CURRENT DENSITY
C   V(I,J)            ARRAY CONTAINING THE VALUE OF THE POTENTIAL AT EACH POINT IN
C                     THE GRID DURING AN ITERATION AND INITIALLY CONTAINING
C                     COOPERMAN'S VALUES (VOLTS)
C   RHO(I,J)          ARRAY CONTAINING THE VALUE OF THE SPACE CHARGE DENSITY AT EACH
C                     POINT IN THE GRID DURING AN ITERATION (COULOMBS/METER**3)
C   EY(I,J)           ARRAY CONTAINING THE VALUE OF THE ELECTRIC FIELD PARALLEL TO
C                     THE PLATES AT EACH POINT IN THE GRID DURING AN ITERATION
C                     (VOLTS/METER)
C   EX(I,J)           ARRAY CONTAINING THE VALUE OF THE ELECTRIC FIELD PERPENDICULAR
C                     TO THE PLATES AT EACH POINT IN THE GRID DURING AN ITERATION
C                     (VOLTS/METER)
C   LL                INDICATOR WHICH COUNTS THE NUMBER OF TIMES THE CALCULATION
C                     ITERATES DUE TO LACK OF CONVERGENCE IN THE POTENTIAL AT EACH
C                     POINT IN THE GRID
C   OLDV(I,J)         ARRAY CONTAINING THE VALUE OF THE POTENTIAL AT EACH POINT
C                     IN THE GRID DURING THE PREVIOUS ITERATION (VOLTS)
C   OLDRO(I,J)        ARRAY CONTAINING THE VALUE OF SPACE CHARGE DENSITY AT EACH
C                     POINT IN THE GRID DURING THE PREVIOUS ITERATION (COULOMBS/
C                     METER**3)
C   CDNSTY(NX,J)      ARRAY CONTAINING THE VALUE OF THE CURRENT DENSITY AT EACH GRID
C   ACDNTY            AVERAGE CURRENT DENSITY AT THE PLATE (AMPERES/METER**2)
C                     POINT ON THE PLATES (AMPERES/METER**2)
C   EPLT              TOTAL ELECTRIC FIELD AT THE PLATE (VOLTS/METER)
```

```
      C                LIST OF VARIABLE NAMES AND UNITS FOR SUBROUTINE CHARGE USED
      C                IN THE ELECTROSTATIC PRECIPITATOR PERFORMANCE MODEL
      C   NII1         DO LOOP INDEX WHICH BEGINS A TIME PERIOD FOR CHARGING IN AN
      C                INCREMENT
      C   NII2         DO LOOP INDEX WHICH TERMINATES A TIME PERIOD FOR CHARGING IN AN
      C                INCREMENT
      C   AFID         AVERAGE FREE ION DENSITY (NUMBER/METER**3)
      C   QI           INITIAL CHARGE ON EACH PARTICLE AT THE BEGINNING OF AN
      C                INCREMENT (COULOMBS)
      C   J            INDEX REPRESENTING A CERTAIN PARTICLE SIZE
      C   VRMS         ROOT MEAN SQUARE VELOCITY OF THE IONS (METERS/SECOND)
      C   DELTT        DIFFERENTIAL TIME INTERVAL OVER WHICH CHARGING TAKES PLACE
      C                (SECONDS)
      C   DELTQ1       DIFFERENTIAL AMOUNT OF CHARGE ACQUIRED BY A CERTAIN PARTICLE
      C                SIZE DURING THE DIFFERENTIAL TIME INTERVAL DELTT DUE TO
      C                CLASSICAL FIELD CHARGING (COULOMBS)
      C   E            ELEMENTARY CHARGE UNIT (COULOMBS)
      C   U            ION MOBILITY (METERS**2/VOLT-SECOND)
      C   QSAT(J)      SATURATION CHARGE FOR A PARTICULAR PARTICLE SIZE (COULOMBS)
      C   EPSO         PERMITTIVITY OF FREE SPACE (COULOMB**2/NEWTON-METER**2)
      C   R            TEMPERATURE IN DEGREES RANKINE
      C   TEMP         TEMPERATURE IN DEGREES KELVIN
      C   RAD(J)       RADIUS OF A PARTICULAR PARTICLE SIZE
      C   PI           VALUE OF THE CONSTANT PI
      C   BC           VALUE OF BOLTZMANN'S CONSTANT (JOULES/DEGREE KELVIN)
      C   ARG          ARGUMENT OF THE EXPONENTIAL IN CLASSICAL DIFFUSION CHARGING
      C   DELTQ2       DIFFERENTIAL AMOUNT OF CHARGE ACQUIRED BY A CERTAIN PARTICLE
      C                SIZE DURING THE DIFFERENTIAL TIME INTERVAL DELTT DUE TO
      C                CLASSICAL DIFFUSION CHARGING (COULOMBS)
      C   DELTQ        TOTAL DIFFERENTIAL AMOUNT OF CHARGE ACQUIRED BY A CERTAIN
      C                PARTICLE SIZE DURING THE DIFFERENTIAL TIME INTERVAL DELTT
      C           LIST OF VARIABLES AND UNITS FOR THE SUBROUTINE CHARGN OF
      C           THE ELECTROSTATIC PRECIPITATOR PERFORMANCE MODEL
      C  ECHARG   ELEMENTARY CHARGE UNIT(STATCOULOMBS)
      C  SCHARG   NUMBER OF CHARGES AT SATURATION FOR A GIVEN PARTICLE SIZE
      C  NUMINC   NUMBER OF POINTS SPECIFIED FOR USE IN THE SIMPSON'S RULE
      C           INTEGRATION OVER THETA IN REGION II OF THE SRI CHARGING THEORY
      C  EZERO    AVERAGE CHARGING FIELD(STAT-VOLTS/CM)
      C  RSIZE    RADIUS OF A GIVEN PARTICLE SIZE
      C  AFID     AVERAGE FREE ION DENSITY(NUMBER/CENTIMETER**3)
      C  RATE     SUPPLIED STATEMENT FUNCTION WHICH CALCULATES THE CHARGING RATES
      C           AT THE DIFFERENT POINTS IN THE RUNGE-KUTTA SCHEME
      C  H        INCREMENT SIZE TAKEN IN THE RUNGE-KUTTA SCHEME(SECONDS)
      C  XI       TIME AT THE START OF EACH INCREMENT(SECOND)
      C  YI       NUMBER OF CHARGES ON A PARTICLE AT THE START OF EACH INCREMENT
      C  KK       DO LOOP INDEX USED IN THE RUNGE-KUTTA SCHEME FOR SOLVING THE
      C           DIFFERENTIAL EQUATION DESCRIBING THE SRI CHARGING THEORY(KK=1)
      C  NN       NUMBER OF POINTS SPECIFIED FOR USE IN THE RUNGE-KUTTA SCHEME
      C           SOLVING THE DIFFERENTIAL EQUATION DESCRIBING THE SRI CHARGING
      C           THEORY
      C  X        TIME AT THE END OF EACH INCREMENT(SECONDS)
      C  Y        NUMBER OF CHARGES ON A PARTICLE AT THE END OF EACH INCREMENT
      C
      C           FACTORS USED IN THE SRI CHARGING THEORY
      C  CONST
      C  V
      C  FCONST
      C  RH
      C  ECONST
      C  FACTOR
      C  COEFF
      C  H2       ONE-HALF THE INCREMENT SIZE CHOSEN FOR THE RUNGE-KUTTA
      C           SCHEME(SECONDS)
      C  T1       NUMBER OF CHARGES ACQUIRED AT A PARTICULAR POINT IN THE
      C           RUNGE-KUTTA SCHEME
      C  T2       NUMBER OF CHARGES ACQUIRED AT A PARTICULAR POINT IN THE
      C           RUNGE-KUTTA SCHEME
      C  T3       NUMBER OF CHARGES ACQUIRED AT A PARTICULAR POINT IN THE
      C           RUNGE-KUTTA SCHEME
      C  T4       NUMBER OF CHARGES ACQUIRED AT A PARTICULAR POINT IN THE
      C           RUNGE-KUTTA SCHEME
```

```
C                     LIST OF VARIABLES AND UNITS FOR THE STATEMENT FUNCTION RATE OF
C                     THE ELECTROSTATIC PRECIPITATOR PERFORMANCE MODEL
C   NTIME             INSTANTANEOUS CHARGING TIME(SECONDS)
C   NUMBER            INSTANTANEOUS NUMBER OF CHARGES ON A PARTICLE
C   NE                NEGATIVE OF THE INSTANTANEOUS CHARGE ON A PARTICLE
C                     (STATCOULOMBS)
C   ARCCOS            SUBROUTINE WHICH CALCULATES THE ARCCOSINE OF A NUMBER
C   THZERO
C   DELTAX            INCREMENT SIZE TAKEN FOR THE INTEGRATION OVER THE ANGLE THETA
C                     IN REGION II OF THE SRI CHARGING THEORY(RADIANS)
C   THETA             VALUES OF THE ANGLE THETA TAKEN FOR THE INTEGRATION OVER THETA
C                     IN REGION II OF THE SRI CHARGING THEORY(RADIANS)
C   SUMODD            SUM OF THE ODD TERMS CONTRIBUTING TO THE INTEGRAL IN THE
C                     SIMPSON'S RULE INTEGRATION SCHEME
C   RSTART            SOME RADIAL DISTANCE FROM WHICH A SEARCH IS INITIATED TO FIND
C                     THE RADIAL DISTANCE ALONG A GIVEN ANGLE AT WHICH THE TOTAL
C                     ELECTRIC FIELD IS ZERO FOR USE IN REGION II OF THE SRI
C                     CHARGING THEORY(CENTIMETERS)
C   TCONST            FACTOR APPEARING IN THE EQUATION GIVING THE CONDITION THAT THE
C                     TOTAL ELECTRIC FIELD BE ZERO FOR A PARTICULAR VALUE OF THETA
C   FCOS              FACTOR APPEARING IN THE EQUATION GIVING THE CONDITION THAT THE
C                     TOTAL ELECTRIC FIELD BE ZERO FOR A PARTICULAR VALUE OF THETA
C   ZERO              SUBROUTINE WHICH SEARCHES FOR THE RADIAL DISTANCE AT WHICH THE
C                     TOTAL ELECTRIC FIELD IS ZERO
C   RZERO             RADIAL DISTANCE AT WHICH THE TOTAL ELECTRIC FIELD IS ZERO
C                     FOR USE IN REGION II OF THE SRI CHARGING THEORY
C   ARG1              ARGUMENT OF THE EXPONENTIAL IN THE CHARGING RATE EXPRESSION
C                     FOR REGION II OF THE SRI CHARGING THEORY
C   YVAL              THE PART OF THE CHARGING RATE EXPRESSION IN REGION II WHICH
C                     DEPENDS ON THE ANGLE THETA, USED AS THE INTEGRAND IN THE
C                     INTEGRATION SCHEME
C   SUMEVN            SUM OF THE EVEN TERMS CONTRIBUTING TO THE INTEGRAL IN THE
C                     SIMPSON'S RULE INTEGRATION SCHEME
C   ARG2              ARGUMENT OF THE EXPONENTIAL IN THE CHARGING RATE EXPRESSION
C                     FOR THE ANGLE THZERO IN REGION II OF THE SRI CHARGING THEORY
C   ZVAL              THE PART OF THE CHARGING RATE EXPRESSION IN REGION II WHICH
C                     DEPENDS ON THE ANGLE THETA, EVALUATED AT THZERO
C   INTGRL            VALUE OF THE INTEGRAL APPEARING IN THE CHARGING RATE FOR
C                     REGION II
C   RATE1             CHARGING RATE FOR REGION II(NUMBER/SECOND)
C   ARG3              ARGUMENT OF THE EXPONENTIAL IN THE CHARGING RATE EXPRESSION
C                     FOR REGION III
C   RATE2             CHARGING RATE FOR REGION III (NUMBER/SECOND)
C   RATE3             CHARGING RATE FOR REGION I (NUMBER/SECOND)
C   RATE              TOTAL CHARGING RATE TO THE ENTIRE PARTICLE SURFACE
C                     (NUMBER/SECOND)
```

```
C                   LIST OF VARIABLES AND UNITS FOR THE SUBROUTINE ARCCOS OF
C                   THE ELECTROSTATIC PRECIPITATOR PERFORMANCE MODEL
C  RATIO            ARGUMENT OF THE ARCCOSINE FUNCTION
C  I                INDEX WHICH GIVES VALUES THAT GENERATE THE DIFFERENT
C                   COEFFICIENTS IN THE SERIES REPRESENTATION FOR THE ARCCOSINE
C                   FUNCTION
C                   FACTORS IN THE COEFFICIENTS OF THE DIFFERENT TERMS OF THE
C                   SERIES
C  U
C  V
C  W
C  TERM             A PARTICULAR TERM IN THE SERIES
C  SUM              SUM OF SUCCESSIVE TERMS IN THE SERIES
C  ACOS             VALUE OF THE ARCCOSINE FUNCTION
```

```
C                            LIST OF VARIABLES AND UNITS FOR THE SUBROUTINE ZERO OF THE
C                            ELECTROSTATIC PRECIPITATOR PERFORMANCE MODEL
C                            COEFFICIENTS OF A THIRD DEGREE POLYNOMIAL
C  A
C  B
C  C
C  D
C  Y                         I-TH POINT IN THE SEARCH FOR THE ZERO OF THE POLYNOMIAL
C  Z                         INCREMENT SIZE USED IN THE SEARCH FOR THE ZERO OF THE
C                            POLYNOMIAL
C  W                         (I+1)-TH POINT IN THE SEARCH FOR THE ZERO OF THE POLYNOMIAL
C  P1                        VALUE OF THE POLYNOMIAL AT THE I-TH POINT
C  P2                        VALUE OF THE POLYNOMIAL AT THE (I+1)-TH POINT
C  SUMA                      SUM OF THE ABSOLUTE VALUES OF THE POLYNOMIAL VALUES AT THE
C                            I-TH AND (I+1)-TH POINTS
C  ASUM                      ABSOLUTE VALUE OF THE SUM OF THE POLYNOMIAL VALUES AT THE
C                            I-TH AND (I+1)-TH POINTS
C  X                         INTERPOLATED APPROXIMATE VALUE FOR THE ZERO OF THE POLYNOMIAL
C  E                         VALUE OF THE CUBIC TERM IN THE POLYNOMIAL
C  F                         VALUE OF THE QUADRATIC TERM IN THE POLYNOMIAL
C  G                         VALUE OF THE LINEAR TERM IN THE POLYNOMIAL
C  H                         SUM OF THE VALUES OF THE QUADRATIC TERM AND THE CONSTANT
C                            TERM OF THE POLYNOMIAL
C  H1                        LOGARITHM TO THE BASE 10 OF H
C  H2                        VALUE OF H1 INCREASED BY 1
C  N                         H2 EXPRESSED AS AN INTEGER
C  P                         VALUE OF THE POLYNOMIAL SCALED BY 10 RAISED TO THE N POWER
```

APPENDIX 2

Program Listing

```
      DOUBLE PRECISION EFESR,DLOG
      REAL NZERO,INTGRL,NE,NUMBER,NTIME,NWIRE
      REAL NWS(20)
      DIMENSION DIAM(20),VOL(20),XNO(20),Q(20),ONO(20),DXS(20),PCNT(20),
     1WS(20),WSL(20),CCF(20),ITL(40),XMV(20),DW(40)
      DIMENSION XDC(40,20),YY(10),VCOOP(11,9)
      DIMENSION LSECT(20),AS(20),VOS(20),TCS(20),WLS(20),ACS(20),BS(20),
     1SYS(20)
      COMMON RAD(20),QSAT(20),U,E,EPSO,PI,ERAVG,BC,TEMP,EPS
      EXTERNAL RATE
C
C    CONSTANTS
C
      PI = 3.1415927
      E = 1.6E-19
      BC=1.38E-23
      EPSO = 8.85E-12
C
C
 4000 READ(2,5)NS,JLY
    5 FORMAT(I2,8X,I2)
      IF(NS-99)4500,9999,9999
 4500 READ(2,6)(DIAM(I),I=1,NS)
    6 FORMAT(10F8.0)
 8000 DO 3 I = 1,NS
      DIAM(I)=DIAM(I)*1.E-06
      RAD(I) = DIAM(I) / 2.
    3 CONTINUE
C
C
      WRITE(3,17)
   17 FORMAT('1')
C
      READ(2,4) (PCNT(I),I=1,NS)
C
      DO 7412 I = 1,NS
      PCNT(I) = PCNT(I) * 1.E-2
 7412 CONTINUE
C
 1000 READ(2,7) ITL
    7 FORMAT(40A2)
      LK=0
C
C          READ IN THOSE PARAMETERS WHICH ARE INDEPENDENT OF SECTION
C
      READ(2,4) VG,DL,PL,VGAS,ETAO,DD,RHO,X,TEMP,P
    4 FORMAT(10F8.0)
      READ(2,5004)SNUCK,ZIGGY,ZNUMB
 5004 FORMAT(10F8.2)
      READ(2,4864) NN,NUMINC,NCALC,EPS,U,VIS,VAVG
 4864 FORMAT(3(I2),4(E11.4))
C
C          READ IN THOSE PARAMETERS WHICH DEPEND ON SECTION
C
      READ(2,770) NUMSEC
  770 FORMAT(I2)
      READ(2,771) (LSECT(I),I=1,NUMSEC)
  771 FORMAT(40(I2))
      DO 1143 NSECT=1,NUMSEC
      READ(2,762) AS(NSECT),VOS(NSECT),TCS(NSECT),WLS(NSECT),ACS(NSECT),
     1BS(NSECT),NWS(NSECT),SYS(NSECT)
 762  FORMAT(7(1PE11,4))
 1143 CONTINUE
C
      PL = PL * 0,305
      NF = PL / ,3 + ,5
C
C         CONVERSION
C
      VG = VG * 4,73E-4
      DL = DL * 2,29E-03
      RHO = RHO * 10,**(X-2,)
      DV = DL / DD
      VGAS=VGAS*,305
      VAVG=VAVG/100,
      VERGE=-,2E-4
C
      WRITE(3,3010) ITL
 3010 FORMAT('0',40A2/)
C
C
C
      DO 1 I = 1 ,NS
      VOL(I) = PCNT(I) * DV
    1 CONTINUE
C
C     COMPUTE WEIGHT OF DUST
      W = DL * VG
C
      TEMP=TEMP+459,
C CALCULATE MEAN FREE PATH
      TDK=TEMP/1,8
      ZMV=8,205E-05*TDK/P
      ZMFP=ZMV/(1,414*PI*(1,6E-19)*(6,02E+23))
      DO 6993 J=1,NS
      CCF(J)=1+(ZMFP/RAD(J))*(1,257+,4*EXP(-1,1*RAD(J)/ZMFP))
 6993 CONTINUE
      NPRINT=0
C
C   COMPUTE VALUE OF EXPONENT IN DEUTSCH EQUATION FOR THE STATED EFF,
C
  305 X=ALOG(100,/(100,-ETAO))
      DO 9 I = 1, NS
      DXS(I)=0,
      XNO(I) = VOL(I)/ ( 4,/3, * PI * RAD(I)**3 )
      ONO(I) = XNO(I)
    9 CONTINUE
C
C
C   COMPUTE EFFICIENCY PER 0,3 METER INCREMENT
C
      ETAPF = 1,-EXP(-0,3*X/PL)
C
C   COMPUTE AMOUNT OF MATERIAL REMOVED PER INCR.ON A TOTAL WEIGHT BASIS
C
      SW = 0,0
C
      DO 700 I=1,NF
      DW(I) = (W - SW) * ETAPF
      SW = SW + DW(I)
  700 CONTINUE
C
C         PRINT THOSE PARAMETERS THAT ARE INDEPENDENT OF SECTION
C
      IF(LK)111,111,160
C
  111 WRITE(3,10)PL,NF,VG
   10 FORMAT(' PPR LENGTH =',E11.4,1X,'METERS',T41,'NO. OF INCREMENTS ='
     $,I3,19X,'GAS FLOW RATE =',E11.4,' M3/SEC')
      WRITE(3,13) DL,VGAS,ETAO
   13 FORMAT(' DUST LOAD =',E11.4,' KG/M3',T41,'GAS VELOCITY =',E11.4,
    $'  M/SEC',9X ,'EST. EFFICIENCY =',F6.2,' PERCENT')
      WRITE(3,14) DD, RHO, DV
   14 FORMAT(' DUST DENSITY =',E11.4,' KG/M3',T41,'DUST RESISTIVTY =',
    $ E11.4,' OHM-M',7X ,'DUST VOLUME =',E11.4,' M3/M3')
      WRITE(3,15) W,TDK,P
   15 FORMAT(' DUST WEIGHT =',E11.4,' KG/SEC',T41,'TEMPERATURE =',F8.3,'
    1 K',18X,'PRESSURE =',F8.3,' ATM')
      WRITE(3,8146) VIS,U,EPS
 8146 FORMAT(' VISCOSITY =',E11.4,' KG/M-SEC',T41,'ION MOBILITY =',E11.4
     1,' M2/VOLT-SEC',4X,'REL. DIELECTRIC CONSTANT =',E11.4)
      WRITE(3,8147) VAVG
 8147 FORMAT(' MEAN THERMAL SPEED =',E11.4,' M/SEC')
C
C
  160 X=ETAPF*100.
      WRITE(3,161)X
  161 FORMAT(/' INPUT EFFICIENCY/INCREMENT=',F6.2)
C***********************************************************************
C
C       START  INCREMENTAL ANALYSIS OF PRECIPITATOR
C
C***********************************************************************
C
        LK=1
        ZWT=0.
        ROVRI=10.
        UROVRI=20.0
        TMFP=ZMFP*2.
        KK=1
        ECHARG=4.8E-10
        RATIO=(EPS-1.)/(EPS+2.)
        BOLTZ=1.38044E-16
        G=EPS+2.
        VC=ECHARG**2/(BOLTZ*TDK)
        FACTHC=(PI*VAVG)/2.
        COEFFC=PI*U*ECHARG*3.E+06
        TINC=0.305/VGAS
        INDEX=0
        NSECT=1
        NCOOP=0
        DO 3000 I=1,NF
        INDEX=INDEX+1
        IF(I.EQ.1) GO TO 761
        IF(INDEX-LSECT(NSECT)) 760,760,761
  761   CONTINUE
        NCOOP=1
        NPRINT=1
        IF(I.EQ.1) GO TO 760
        NSECT=NSECT+1
      INDEX=1
  760 CONTINUE
      A=AS(NSECT)*9.3E-02
      VO=VOS(NSECT)
      TC=TCS(NSECT)
      WL=WLS(NSECT)*0.305
      AC=ACS(NSECT)*2.54E-02
      B=BS(NSECT)*2.54E-02
      SY=SYS(NSECT)*2.54E-02
      NWIRE=NWS(NSECT)
      SX=B
      AX=SX/10.
      NX=11
      NY=SY/AX
      IF(NCOOP.NE.1) GO TO 764
      ERAVG=VO/B
      EZERO=ERAVG/3.E+04
      DO 6989 L=1,NS
      GSAT(L)=(4.*PI*EPSO*(RAD(L)+TMFP)**2)*ERAVG*(1.+2.*((EPS-1.)/
     1(EPS+2.))*(RAD(L)/(RAD(L)+TMFP))**3)*1.2
 6989 CONTINUE
      R=(ECHARG*EZERO)/(BOLTZ*TDK*(EPS+2.))
      RR=(ECHARG*EZERO)/(BOLTZ*TDK)
      RG=R*G
      CALL CMAN(VO,NX,NY,AX,SX,SY,PI,AC,NWIRE,VCOOP)
C
C   COMPUTE CURRENT DENSITY
      CD = TC / A
C
C   COMPUTE ELECTRIC FIELD IN DEPOSIT
      ET = CD * RHO
C
C   COMPUTE CURRENT PER  M. OF CORONA WIRE
C
      CL = TC / WL
C
      NCOOP=0
  764 CONTINUE
      FID=CD/(EMU*ERAVG)
      SUM=0.0
      DO 1300 L=1,NS
 1300 SUM=SUM+GSAT(L)*XNO(L)
      ZC=200.*(DM(I)/W)*(FLOAT(LSECT(NSECT))/TC)*VG
      ROVRI=ZC*SUM+1.0
      AFID=FID/ROVRI
      AVGFID=AFID*1.E-06
      XCD=CD*100000.
C
C   COMPUTE EFFECTIVE MOBILITY
      UEQ=U/ROVRI
      IF(UEQ.LT.1.0E-4)UEQ=1.0E-4
C
      IF(I.EQ.1) GO TO 376
      IF(UEQ.NE.1.0E-4) GO TO 376
      IF(UEQ.EQ.1.0E-4)EPLT=SKIP
      GO TO 375
  376 CONTINUE
      SIGMA=OROVRI-ROVRI
      IF(SIGMA.LT..01) GO TO 375
      CALL FFIELD(UEQ,CD,AC,VO,SX,SY,AEPLT,VCOOP,VERGE,CVERGE)
      VERGE=CVERGE
      EPLT=1,*AEPLT
      SKIP=EPLT
  375 DRDVRI=RDVRI
C
C**********************************************************************
C
C           START PARTICLE SIZE LOOP
C
C**********************************************************************
C
      PROT=0,0
      HI = 0,
      DO 2900 J = 1, NS
C
C    COMPUTE CHARGE ON EACH PARTICLE AFTER ONE INCREMENT OF TRAVEL
      IF(NCALC,EQ,1) GO TO 9323
      IF(I,NE,1) GO TO 426
      IF(J,GT,1) GO TO 428
      TIMEI=0,
      TIMEF=TINC
      XIPC=0,
      H=TINC/NN
      GO TO 428
  426 IF(J,GT,1) GO TO 429
      TIMEI=FLOAT(I-1)*TINC
      TIMEF=FLOAT(I)*TINC
      H=TINC/NN
  429 XIPC=XDC(I-1,J)/1,6E-19
  428 CONTINUE
      RSIZE=RAD(J)*1,E+02
      SCHARG=QSAT(J)/1,6E-19
      DCONST=RATIO*RSIZE**3
      CONST=2,*DCONST*EZERO
      S=3,*RSIZE
      V=VC/RSIZE
      ECONST=S*H
      FCONST=RG*DCONST
      FACTRE=FACTRC*RSIZE**2
      COEFF=COEFFC*SCHARG
      CALL CHARGN(ECHARG,SCHARG,NUMINC,CONST,EZERO,V,RSIZE,ECONST,RR,
     1FCONST,FACTRE,COEFF,AVGFID,RATE,H,TIMEI,XIPC,KK,NN,CTIME,CNUMBR)
      Q(J)=CNUMBR*1,6E-19
      XDC(I,J)=Q(J)
      GO TO 9324
 9323 CONTINUE
      CTIME=FLOAT(I)*0,305/VGAS
      NII=CTIME/,001
      IF(I,EQ,1) GO TO 4290
      IF(I,GT,1) GO TO 4270
 4290 NII1=1
      NII2=NII
      XIPC=0,0
      GO TO 4280
 4270 IF(J,GT,1) GO TO 4260
      NII1=NII2
      NII2=NII
 4260 XIPC=XDC(I-1,J)
 4280 CONTINUE
      CALL CHARGE(NII1,NII2,AFID,XIPC,J)
      Q(J)=XIPC
      XDC(I,J)=XIPC
 9324 CONTINUE
C   COMPUTE MIGRATION VELOCITY FOR EACH SIZE RANGE
C
      EMV=(Q(J)*EPLT)/(6.*PI*RAD(J)*VIS)
      EMV=CCF(J)*EMV
      XMV(J)=EMV
C
C   COMPUTE EFFICIENCY FOR EACH SIZE RANGE
C
      X=(-A*EMV)/(VG*FLOAT(LSECT(NSECT)))
C
      EFF =  1. - EXP( X )
C
C     COMPUTE NUMBER OF PARTICLES REMOVED IN EACH SIZE RANGE
C
C
      DXNO=XNO(J)*EFF
      DXS(J)=DXS(J)+DXNO
      WS(J)=DXNO*(1.33333*PI*RAD(J)**3)*DD
      XNO(J)=XNO(J)-DXNO
      WT=WT+WS(J)
 2900 CONTINUE
      ZWT=ZWT+WT
C
C  CALCULATE MMD AND WEIGHT COLLECTED FOR EACH INCREMENT
      ZTM=0.
      DO 2901 J=1,NS
      ZTM=ZTM+WS(J)
      CZA=ZTM/WT
      IF(CZA-0.5)2901,2901,2902
 2901 CONTINUE
 2902 CZB=(ZTM-WS(J))/WT
      TL1=CZA-CZB
      TL2=0.50-CZB
      KJ=J-1
      IF(KJ)2910,2910,2911
 2910 ZMD=DIAM(J)
      GO TO 2912
 2911 ZMD=DIAM(KJ)+(TL2/TL1)*(DIAM(J)-DIAM(KJ))
 2912 CONTINUE
      IF(NPRINT.NE.1) GO TO 8439
      NPRINT=0
      WRITE(3,7820) NSECT
 7820 FORMAT(' CALCULATION IS IN SECTION NO. =',I2)
      WRITE(3,7715) A,VO,TC
 7715 FORMAT(' COLLECTION AREA =',E11.4,' M2',T41,'APPLIED VOLTAGE =',E1
     11.4,' VOLTS',7X,'TOTAL CURRENT =',E11.4,' AMPS')
      WRITE(3,7716) B,AC,WL
 7716 FORMAT(' WIRE TO PLATE =',E11.4,' M',T41,'CORONA WIRE RADIUS =',E1
     11.4,' M',8X,'CORONA WIRE LENGTH =',E11.4,' M')
      WRITE(3,7717) CL,CD,ET
 7717 FORMAT(' CURRENT/M =',E11.4,' AMP/M',T41,'CURRENT DENSITY =',E11.4
     1,' AMP/M2',6X,'DEPOSIT E FIELD =',E11.4,' VOLT/M')
      WRITE(3,7718) SY
 7718 FORMAT(' 1/2 WIRE TO WIRE =',E11.4,' M')
      WRITE(3,4322)
 4322 FORMAT(//T5,'ROVRI',T16,'ERAVG',T31,'EPLT',T48,'AFID',T63,'CMCD',T
     176,'MMD',11X,'WEIGHT',7X,'INCREMENT NO.'/)
```

Reproduced from
best available copy.

```
 4849 CONTINUE
      WRITE(6,4823)ROWWI,ERAVG,EPLT,AFID,XCD,ZMU,WT,I
 4823 FORMAT(1X,F6.3,I13,E11.4,T27,E11.4,T45,E11.4,T60,F7.1,4X,E11.4,4X,
     1F11.4,4X,I2)
 4000 CONTINUE
C
      ETC=(Z-1/DL)*100.
      DIFF=ETC-ETAO
      DIFF=ABS(DIFF)
      IF(DIFF-0.05)60,300,300
  300 ETAO=ETC
      GO TO 305
C
C         PRINT DIAM., PERCENT, AND EFFICIENCY FOR EACH SIZE RANGE
C
   60 WRITE(3,18)
   18 FORMAT('0PARTICLE SIZE RANGE STATISTICS'/)
      WRITE(3,19)
   19 FORMAT(5X,'DIAMETER-METERS',5X,'PERCENT OF TOTAL',4X,'EFFICIENCY'
     1,7X,'CCF',10X,'W',10X,'W''',10X,'EFF''')
C
C
      ATOTAL=0.
      DO 4985 I=1,NUMSEC
      ATOTAL=ATOTAL+AS(I)*9.3E-02
 4985 CONTINUE
      SCOREF = 0.0
      X = 0.0
      DO 2990 I=1,NS
      EFESR     = DXS(I) / DNO(I)
      IF (EFESR .GT..999999 ) EFESR = .999999
      X = X + EFESR * PCNT(I)
      XY=PCNT(I)*100.
      XEP=EFESR*100.D0
      IF (XEP .GE. 99.9999  ) XEP = 99.9999
      IF(ZIGGY-0.0)4704,4704,4705
 4704 F1=1.
      GO TO 4706
 4705 CONTINUE
      F1=1.+.766*EFESR*ZIGGY**1.786+.0755*ZIGGY*DLOG(1./(1.-EFESR))
 4706 CONTINUE
      IF(SNUCK-0.0)4701,4701,4702
 4701 F2=1.
      GO TO 4703
 4702 F2=DLOG(1.-EFESR)/(ZNUMS*DLOG(SNUCK+(1.-SNUCK)*(1.0-EFESR)**(1./
     1ZNUMS)))
 4703 CONTINUE
      ZNLFF = F1*F2
      IF(EFESR.GT.0.99999)WY=XMV(I)*100.
      IF(EFESR.LT.0.99999)WY=(VG/ATOTAL)*100.*ALOG(100./(100.-XEP))
      WYP=WY/ZNLFF
      COREFF=100.*(1.-EXP(-ATOTAL*WYP/(100.*VG)))
      SCOREF = SCOREF + COREFF*PCNT(I)
      WRITE(3,2291)DIAM(I),XY,XEP,CCF(I),WY,WYP,COREFF
 2291 FORMAT(2X,E17.7,T29,F10.6,T45,F10.6,T61,F7.4,T73,F7.3,
     & 4X ,F7.3,6X ,F7.4)
      SL=(1.0-EFESR)*DNO(I)
      WSL(I)=SL*(1.33333*PI*RAD(I)**3)*DD
 2990 CONTINUE
C
```

```
      X = X * 100.
      WRITE(3,2292) ETAO, X
 2292 FORMAT(1H0,1X,'EFFICIENCY - STATED = ',F5.2,5X,'COMPUTED =' ,F6.2
     *,5X,'CONVERGENCE OBTAINED')
C
C CALCULATE MMD OF EFFLUENT
C
      WTL=(1.-(X/100.))*DL
      ZTM=0.
      DO 2995 I=1,NS
      ZTM=ZTM+WSL(I)
      CZA=ZTM/WTL
      IF(CZA-0.5)2995,2995,2996
 2995 CONTINUE
 2996 CZB=(ZTM-WSL(I))/WTL
      TL1=CZA-CZB
      TL2=0.50-CZB
      KJ=I-1
      IF(KJ)2980,2980,2981
 2980 ZMDL=DIAM(I)
      GO TO 2982
 2981 ZMDL=DIAM(KJ)+(TL2/TL1)*(DIAM(I)-DIAM(KJ))
 2982 WRITE(3,2997)ZMDL
 2997 FORMAT(5X'MMD OF EFFLUENT=',E11.4)
      COREFW=(VG/ATOTAL)*100.*ALOG(100./(100.-SCOREF))
      WZ=(VG/ATOTAL)*100.*ALOG(100./(100.-X))
      WRITE(3,2998)WZ
 2998 FORMAT(5X,'PRECIPITATION RATE PARAMETER =',F7.3//)
      WRITE(3,4615)ZIGGY,SNUCK,ZNUMS
 4615  FORMAT(5X,'SIGMA=',2X,F7.4,2X,'WITH',2X,F7.4,'SNEAKAGE OVER',2X,
     1F7.4,2X,'STAGES')
      WRITE(3,5002) SCOREF
 5002  FORMAT(1X,'CORR. EFF. = ',F8.4)
      WRITE(3,5003) COREFW
 5003 FORMAT(1X,'CORRECTED PRECIPITATION RATE PARAMETER =',F8.2)
C OUTPUT FROM CHARGING ROUTINE
      IF(JLY)1000,360,350
  350 CONTINUE
 9992 FORMAT(1H1)
      WRITE(3,9992)
      WRITE(3,356)
  356 FORMAT(/T3,'CHARGING RATES FOR SUB-MICRON PARTICLES FROM SUBROUTIN
     1E CHARGN'//T2,'INCREMENT NO.',T20,'Q/QSATF FOR INDICATED PARTICLE
     2SIZES')
      WRITE(3,357) (DIAM(J),J=1,JLY)
  357 FORMAT(T4,10(E11.4,2X)/)
      DO 360 I=1,NF
      DO 359 J=1,JLY
  359 YY(J)=XDC(I,J)/QSAT(J)
      WRITE(3,358) I,(YY(J),J=1,JLY)
  358 FORMAT(T3,I2,T6,10(F7.4,6X))
  360 CONTINUE
      WRITE(3,9992)
      WRITE(3,432)
  432 FORMAT(/T5,'CHARGE ACCUMULATED ON SUBMICRON PARTICLES EACH INCREME
     1NT'//T3,'INCREMENT',T20,'CHARGE FOR INDICATED PARTICLE SIZES')
      WRITE(3,425)(DIAM(J),J=1,JLY)
  425 FORMAT(T8,10(E11.4,3X)/)
      DO 431 I=1,NF
      WRITE(3,430)I,(XDC(I,J),J=1,JLY)
      450 FORMAT(I5,I6,I6,10(E13.5,1X))
      451 CONTINUE
          GO TO [illegible]
     9999 STOP [illegible]
          END
[illegible] > 4K
```

```
      SUBROUTINE EFIELD(UEQ,CD,AC,VO,SX,SY,AEPLT,VCOOP,VERGE,CVERGE)
C  EVALUATION OF FIELDS, SPACE CHARGE DENSITY, POTENTIAL , AND
C  CURRENT DENSITY FOR A WIRE-PLATE PRECIPITATOR
      REAL MAXJ,MINJ
      DIMENSION RHO(11,9),VCOOP(11,9),EX(11,9),OLDRO(11,9),OLDV(11,9),
     1CONSTY(11,9),V(11,9),EY(11,9)
      DATA RHO/99*0./,V/99*0./,EX/99*0./,EY/99*0./,OLDRO/99*0./,OLDV/99*
     10./,CONSTY/99*0./
      VO=-1.*VO
      QZERO=VERGE
      PI=3.1416
      EPSO=8.854E-12
      NX=11
      A=SX/10.0
      NY=SY/A
      MAXJ=CD*1.001
      MINJ=CD*.9999
      NX1=NX-1
      NY1=NY-1
      Z=0
      DO 4615 I=1,NX
      DO 4615 J=1,NY
 4615 V(I,J)=VCOOP(I,J)
    1 Z=Z+1
      IZ=Z
      IF(Z.EQ.25) GO TO 700
      RHO(1,1)=QZERO
      DO 201 I=2,NX
      EY(I,1)=0.
      EX(I,1)=(V(I-1,1)-V(I,1))/A
      Q=EPSO/A*EX(I,1)*RHO(I-1,1)
      RHO(I,1)=(-5.)*EPSO/A*EX(I,1)-.5*SQRT((EPSO/A*EX(I,1))**2+
     14.*ABS(Q))
  201 CONTINUE
      DO 202 I=2,NX
      EY(I,NY)=0.
      EX(I,NY)=(V(I-1,NY)-V(I,NY))/A
      R=EPSO/A*EX(I,NY)*RHO(I-1,NY)
      RHO(I,NY)=(-.5)*EPSO/A*EX(I,NY)-.5*SQRT((EPSO/A*EX(I,NY))**2
     1+4.*ABS(R))
  202 CONTINUE
      DO 203 J=2,NY
      EX(1,J)=0.
      EY(1,J)=(V(1,J-1)-V(1,J))/A
      P=EPSO/A*EY(1,J)*RHO(1,J-1)
      RHO(1,J)=(-.5)*EPSO/A*EY(1,J)-.5*SQRT((EPSO/A*EY(1,J))**2
     1+4.*ABS(P))
  203 CONTINUE
      LL=0
  300 LL=LL+1
      DO 301 I=1,NX1
      DO 301 J=1,NY
      OLDV(I,J)=V(I,J)
      OLDRO(I,J)=RHO(I,J)
      IF(I.EQ.1.AND.J.EQ.1) GO TO 302
      GO TO 303
  302 RHO(I,J)=QZERO
      V(I,J)=VO
      EX(I,J)=0.0
      EY(I,J)=0.0
```

Reproduced from
best available copy.

```
      GO TO 301
  303 CONTINUE
      IF(I.EQ.1.AND.J.NE.1) GO TO 304
      IF(I.NE.1.AND.J.EQ.1) GO TO 305
      IF(J.EQ.NY) GO TO 600
      GO TO 306
  600 V(I,NY)=0.25*(V(I-1,NY)+V(I+1,NY)+2.*(V(I,NY-1))+A**2*RHO(I,NY)/EP
     1SO)
      GO TO 301
  304 IF(I.EQ.1.AND.J.EQ.NY)  GO TO 350
      V(1,J)=0.25*(V(1,J+1)+V(1,J-1)+2.*V(2,J)+A**2*RHO(1,J)/EPSO)
      GO TO 301
  350 V(1,NY)=0.5*(V(1,NY-1)+V(2,NY)+0.5*A**2*RHO(1,NY)/EPSO)
      GO TO 301
  305 V(I,1)=0.25*(V(I-1,1)+V(I+1,1)+2.0*V(I,2)+A**2*RHO(I,1)/EPSO)
      GO TO 301
  306 V(I,J)=0.25*(V(I,J+1)+V(I-1,J)+V(I,J-1)+V(I+1,J)+A**2*RHO(I,J)/
     1EPSO)
  301 CONTINUE
      DO 307 I=1,NX
      DO 307 J=1,NY
      IF(I.EQ.1.AND.J.EQ.1) GO TO 402
      GO TO 403
  402 RHO(I,J)=RZERO
      V(I,J)=V0
      EX(I,J)=0.0
      EY(I,J)=0.0
      GO TO 307
  403 CONTINUE
      IF(I.EQ.1.AND.J.NE.1) GO TO 310
      GO TO 311
  310 EX(I,J)=0.0
      EY(I,J)=(-1.)*(V(I,J)-V(I,J-1))/A
      GO TO 314
  311 IF(I.NE.1.AND.J.EQ.1) GO TO 312
      GO TO 313
  312 EY(I,J)=0.0
      EX(I,J)=(-1.)*(V(I,J)-V(I-1,J))/A
      GO TO 314
  313 EX(I,J)=(-1.)*(V(I,J)-V(I-1,J))/A
      EY(I,J)=(-1.)*(V(I,J)-V(I,J-1))/A
      IF(J.EQ.NY) EY(I,J)=0.0
  314 C=(-1.)*(EPSO/A)*(RHO(I-1,J)*EX(I,J)+RHO(I,J-1)*EY(I,J))
      D=EPSO/A*(EX(I,J)+EY(I,J))
      D1=(D/2.)**2
      RHO(I,J)=(-1.)*(D/2.)-SQRT(ABS(D1)+ABS(C))
  307 CONTINUE
      IF(IT.EQ.2000) GO TO 700
      DO 320 I=1,NX1
      DO 320 J=1,NY1
      IF(ABS(V(I,J)-OLDV(I,J)).LT.1.) GO TO 320
      GO TO 300
  320 CONTINUE
      CONSTY(NX,1)=EX(NX,1)*UEQ*RHO(NX,1)
      ACONTY=CONSTY(NX,1)
  400 DO 450 J=2,NY
      CONSTY(NX,J)=EX(NX,J)*UEQ*RHO(NX,J)
      ACONTY=ACONTY+CONSTY(NX,J)
  450 CONTINUE
      ACONTY=ACONTY/NY
      IF(ACDNTY.GT.MAXJ) GO TO 910
      IF(ACDNTY.LT.MINJ) GO TO 920
      GO TO 980
  910 QZERO=MINJ/ACDNTY*QZERO
      GO TO 1
  920 QZERO=MAXJ/ACDNTY*QZERO
      GO TO 1
  980 EPLT=EX(NX,1)
      DO 1000 J=2,NY
      EPLT=EPLT+EX(NX,J)
 1000 CONTINUE
      AEPLT=EPLT/NY
  700 CONTINUE
      CVERGE=QZERO
      VO=-1.*VO
      RETURN
      END
      SUBROUTINE CHAN(VO,NX,NY,AX,SX,SY,PI,AC,NWIRE,VCOOP)
C
C**********************************************************************
C    COOPERMAN SERIES DETERMINATION FOR VOLTAGE WIRE TO PLATE
C    FOR SUBROUTINE EFIELD
      REAL NUM,M,NWIRE
      DIMENSION VCOOP(11,9)
      VO=-1.*VO
      DO 402 I=1,NX
      DO 430 J=1,NY
      X=(I-1)*AX
      Y=(J-1)*AX
      IF(X.EQ.0.0.AND.Y.EQ.0.0) GO TO 440
      GO TO 450
  440 VCOOP(I,J)=VO
      GO TO 430
  450 CONTINUE
      M=-NWIRE
      NUM=0.0
      DENOM=0.0
  490 E1=PI*(Y-(2.*M*SY))/(2.*SX)
      F1=PI*X/(2.*SX)
      G1=PI*M*SY/SX
      H1=PI*AC/(2.*SX)
      E2=(EXP(E1)+EXP(-E1))/2.
      F2=COS(F1)
      G2=(EXP(G1)+EXP(-G1))/2.
      H2=COS(H1)
      TT=(E2-F2)/(E2+F2)
      TA=(G2-H2)/(G2+H2)
      F=ALOG(TT)
      G=ALOG(TA)
      NUM=NUM+F
      DENOM=DENOM+G
      IF(M.LT.NWIRE) GO TO 408
      GO TO 410
  408 M=M+1.0
      GO TO 490
  410 VCOOP(I,J)=VO*NUM/DENOM
  430 CONTINUE
  402 CONTINUE
      VO=-1.*VO
      RETURN
      END
      SUBROUTINE CHARGN(ECHARG,SCHARG,NUMINC,CONST,EZERO,V,RSIZE,ECONST
     *,RR,FCONST,FACTOR,COEFF,AFID,RATE,H,XI,YI,KK,NN,X,Y)
      H2=H/2.
      Y=YI
      X=XI
      DO 2 I=1,NN
      DO 1 J=1,KK
      T1=H*RATE(ECHARG,SCHARG,NUMINC,CONST,EZERO,V,RSIZE,ECONST,RR,
     *FCONST,FACTOR,COEFF,AFID,X,Y)
      T2=H*RATE(ECHARG,SCHARG,NUMINC,CONST,EZERO,V,RSIZE,ECONST,RR,
     *FCONST,FACTOR,COEFF,AFID,X+H2,Y+T1/2.)
      T3=H*RATE(ECHARG,SCHARG,NUMINC,CONST,EZERO,V,RSIZE,ECONST,RR,
     *FCONST,FACTOR,COEFF,AFID,X+H2,Y+T2/2.)
      T4=H*RATE(ECHARG,SCHARG,NUMINC,CONST,EZERO,V,RSIZE,ECONST,RR,
     *FCONST,FACTOR,COEFF,AFID,X+H,Y+T3)
      Y=Y+(T1+2.*T2+2.*T3+T4)/6.
    1 X=X+H
    2 CONTINUE
      RETURN
      END
```

Reproduced from
best available copy.

```
      FUNCTION RATE(ECHARG,SCHARG,NUMINC,CONST,EZERO,V,RSIZE,ECONST,
     *RR,FCONST,FACTOR,COEFF,AFID,NTIME,NUMBER)
      REAL INTGHL,NE,NUMBER,NTIME
      NE=-NUMBER*ECHARG
      IF(NUMBER-SCHARG)7005,7006,7006
 7005 CALL ARCCOS(NUMBER,SCHARG,THZERO)
      IF(THZERO.LE.1.E-05) GO TO 7006
      IF(1,57-THZERO) 7011,7011,7015
 7015 CONTINUE
      GO TO 7007
 7006 THZERO=0.
 7007 DELTAX=(1,57-THZERO)/FLOAT(NUMINC)
      THETA=THZERO-DELTAX
      SUMODD=0.
      RSTART=RSIZE
      DO 7000 I=1,NUMINC,2
      THETA=THETA+DELTAX*2.
      TCONST=CONST*COS(THETA)
      ECOS=EZERO*COS(THETA)
      CALL ZERO(ECOS,0,,NE,TCONST,RSTART,RZERO)
      ARG1=-(NUMBER*V*(RZERO-RSIZE)/RZERO+(ECONST-RR*RZERO+FCONST/RZERO*
     1*2)*COS(THETA))
      IF(ABS(ARG1),GT,100,) GO TO 7025
      YVAL=EXP(ARG1)*SIN(THETA)
      GO TO 7026
 7025 YVAL=0.
 7026 CONTINUE
      SUMODD=SUMODD+YVAL
      RSTART=RZERO
 7000 CONTINUE
      THETA=THZERO
      SUMEVN=0.
      RSTART=RSIZE
      DO 7001 J=2,NUMINC,2
      THETA=THETA+DELTAX*2.
      TCONST=CONST*COS(THETA)
      ECOS=EZERO*COS(THETA)
      CALL ZERO(ECOS,0.,NE,TCONST,RSTART,RZERO)
      ARG1=-(NUMBER*V*(RZERO-RSIZE)/RZERO+(ECONST-RR*RZERO+FCONST/RZERO*
     1*2)*COS(THETA))
      IF(ABS(ARG1),GT,100,) GO TO 7027
      YVAL=EXP(ARG1)*SIN(THETA)
      GO TO 7028
 7027 YVAL=0.
 7028 CONTINUE
      SUMEVN=SUMEVN+YVAL
      RSTART=RZERO
 7001 CONTINUE
      IF(THZERO,EQ,0.) GO TO 7051
 7050 RZERO=RSIZE
      GO TO 7052
 7051 CONTINUE
      TCONST=CONST*COS(THZERO)
      ECOS=EZERO*COS(THZERO)
      CALL ZERO(ECOS,0.,NE,TCONST,RSIZE,RZERO)
 7052 CONTINUE
      ARG2=-(NUMBER*V*(RZERO-RSIZE)/RZERO+(ECONST-RR*RZERO+FCONST/RZERO*
     1*2)*COS(THZERO))
      IF(ABS(ARG2),GT,100,) GO TO 7029
      ZVAL=EXP(ARG2)*SIN(THZERO)
      GO TO 7030
 7029 ZVAL=0,
 7030 CONTINUE
      INTGRL=DELTAX/3,*(4,*SUMODD+2,*SUMEVN+ZVAL)
      RATE1=INTGRL*FACTOR*AFID
      GO TO 7012
 7011 RATE1=0,
 7012 CONTINUE
      ARG3=-V*NUMBER
      IF(ABS(ARG3),GT,100,) GO TO 7031
      RATE2=FACTOR*EXP(ARG3)*AFID
      GO TO 7032
 7031 RATE2=0,
 7032 CONTINUE
      IF(NUMBER-SCHARG)7008,7009,7009
 7008 RATE3=COEFF*(1,-NUMBER/SCHARG)**2*AFID
      GO TO 7010
 7009 RATE3=0,
 7010 CONTINUE
      RATE=RATE1+RATE2+RATE3
      RETURN
      END
      SUBROUTINE ARCCOS(A,B,ACOS)
      RATIO=A/B
      T=1.
      SUM=0.
      TERM=RATIO
    1 U=2.*T-1.
      V=2.*T
      W=2.*T+1.
      TERM=TERM/V*U**2/W*RATIO**2
      SUM=SUM+TERM
      T=T+1.
      IF(TERM-5.E-05)3,3,1
    3 ACOS=1.5707963-SUM*RATIO
      RETURN
      END
      SUBROUTINE ZERO(A,B,C,D,R,X)
      Y=R
      Z=0.1*R
      W=Y+Z
      P1=A*Y**3+B*Y**2+C*Y+D
      GO TO 1
    3 Y=W
      P1=P2
      W=W+Z
    1 P2=A*W**3+B*W**2+C*W+D
      SUMA=ABS(P1)+ABS(P2)
      ASUM=ABS(P1+P2)
      IF(SUMA.NE.ASUM) GO TO 2
      GO TO 3
    2 X=(W*(P2-P1)-P2*(W-Y))/(P2-P1)
      GO TO 5
    6 X=(W*(P2-P)-P2*(W-X))/(P2-P)
    5 CONTINUE
      E=A*X**3
      F=B*X**2
      G=C*X
      E1=ABS(A*X**3)
      F1=ABS(B*X**2)
      G1=ABS(C*X)
      D1=ABS(D)
      IF(E1.GE.F1) GO TO 10
      H=F1
      GO TO 11
   10 CONTINUE
      H=E1
   11 CONTINUE
      IF(H.GE.G1) GO TO 12
      H=G1
   12 CONTINUE
      IF(H.GE.D1) GO TO 13
      H=D1
   13 CONTINUE
      H1=ALOG10(H)
      H2=ABS(H1)+1.
      N=IFIX(H2)
      P=E+F+G+D
      T=P*10**N
      IF(ABS(T).LE.1.E-04) GO TO 4
      GO TO 6
    4 RETURN
      END
      SUBROUTINE CHARGE(NII1,NII2,AFID,Q1,J)
      COMMON RAD(20),QSAT(20),U,E,EPSO,PI,ERAVG,BC,TEMP,EPS
      VRMS=4.4E2
      DELTT=.001
      F=TEMP-459.
      TEMQ=5./9.*(F-32.)
      TEMQ=TEMQ+273.
      DO 401 K=NII1,NII2
      DELTQ1=((AFID*E*U*QSAT(J)/(4.*EPSO))*(1.-Q1/QSAT(J))**2)*DELTT
      ARG=-Q1*F/(4.*PI*EPSO*RAD(J)*BC*TEMQ)
      IF(ABS(ARG).GT.100.)GO TO 402
      DELTQ2=PI*RAD(J)**2*E*VRMS*AFID*EXP(ARG)*DELTT
  402 CONTINUE
      IF(Q1-QSAT(J))410,411,411
  410 DELTQ=DELTQ1+DELTQ2
      GO TO 412
  411 DELTQ=DELTQ2
  412 CONTINUE
      Q1=Q1+DELTQ
  401 CONTINUE
      RETURN
      END
```

APPENDIX 3

Conversion Factors

To Convert From	To	Multiply By
lbs	Kg	0.454
grains/cf	grams/m^3	2.29
cfm	m^3/sec	0.000472
lbs/in.^{2}	Kg/m^2	703
°F	°C	(°F - 32) x 5/9
ft^2/1000 cfm	$m^2/(m^3/sec)$	0.197
inches w. g.	mm Hg	1.868
gallon	liter	3.785
ft	m	0.3048
inches	m	0.0254